STOCHASTIC MODELING AND ANALYSIS OF PLANT MICROTUBULE SYSTEM CHARACTERISTICS

A Dissertation

by

EZGI CAN EREN

Submitted to the Office of Graduate Studies of
Texas A&M University
in partial fulfillment of the requirements for the degree of

DOCTOR OF PHILOSOPHY

May 2012

Major Subject: Industrial Engineering

Stochastic Modeling and Analysis of Plant Microtubule System Characteristics

STOCHASTIC MODELING AND ANALYSIS OF PLANT MICROTUBULE SYSTEM CHARACTERISTICS

A Dissertation

by

EZGI CAN EREN

Submitted to the Office of Graduate Studies of
Texas A&M University
in partial fulfillment of the requirements for the degree of

DOCTOR OF PHILOSOPHY

Approved by:

Chair of Committee,	Natarajan Gautam
Committee Members,	Guy L. Curry
	Richard M. Feldman
	Salih Yurttas
	Ram Dixit
Head of Department,	César O. Malavé

May 2012

Major Subject: Industrial Engineering

ABSTRACT

Stochastic Modeling and Analysis of Plant Microtubule System Characteristics.

(May 2012)

Ezgi Can Eren, B. S., Bogazici University

Chair of Advisory Committee: Dr. Natarajan Gautam

In this dissertation, we consider a complex biological system known as cortical microtubule (CMT) system, where stochastic dynamics of the components (i.e., the CMTs) are defined in both space and time. CMTs have an inherent spatial dimension of their own, as their length changes over time in addition to their location. As a result of their dynamics in a confined space, they run into and interact with each other according to simple stochastic rules. Over time, CMTs acquire an ordered structure that is achieved without any centralized control beginning with a completely disorganized system. It is also observed that this organization might be distorted, when parameters of dynamicity and interactions change due to genetic mutation or environmental conditions. The main question of interest is to explore the characteristics of this system and the drivers of its self-organization, which is not feasible relying solely on biological experiments. For this, we replicate the system dynamics and interactions using computer simulations. As the simulations successfully mimic the organization seen in plant cells, we conduct an extensive analysis to discover the effects of dynamics and interactions on system characteristics by experimenting with different input parameters. To compare simulation results, we characterize system properties and quantify organization level using metrics based on entropy, average length and number of CMTs in the system. Based on our findings and conjectures from simulations, we develop analytical models for more generalized conclusions and

efficient computation of system metrics. As a first step, we formulate a mean-field model, which we use to derive sufficient conditions for organization to occur in terms of input parameters. Next, considering the parameter ranges that satisfy these conditions, we develop predictive methodologies for estimation of expected average length and number of CMTs over time, using a fluid model, transient analysis, and approximation algorithms tailored to our problem. Overall, we build a comprehensive framework for analysis and control of microtubule organization in plant cells using a wide range of models and methodologies in conjunction. This research also has broader impacts related to the fields of bio-energy, healthcare, and nanotechnology; in addition to its methodological contribution to stochastic modeling of systems with high-level spatial and temporal complexity.

To the memory of my Dad, Ali Eren (1954 - 1995)

ACKNOWLEDGMENTS

I would like to express my deepest gratitude to my advisor, Dr. Natarajan Gautam, for giving me the opportunity to work with him, and for his continuous support and encouragement during my PhD studies. His guidance has been an invaluable asset to not only the completion of this dissertation but also my overall PhD education as I have learned so much from his wisdom and experience.

I would like to thank to Dr. Ram Dixit for his close collaboration and guidance during this study and for patiently providing the biological information and data that are a part of this dissertation.

I am grateful to our departmental graduate advisor Dr. Guy L. Curry, who has also served as my committee member, for his invaluable advice on several matters. I would also like to sincerely thank to Dr. Richard M. Feldman and Dr. Salih Yurttas for agreing to serve in my committee and their encouragement. I would like to also mention my appreciation towards Dr. Richard J. Mayer, Dr. Rodger J. Koppa., Dr. Andrew Jonhson, Dr. Sergiy Butenko, Dr. Abhijit Deshmukh, Dr. Ibrahim Karaman, and Dr. Tahir Cagin.

I am indebted to Ms. Judy Meeks for all her help, attention to detail and patience; and continuously being there when needed with a friendly face and comforting smile. I would like to also recognize Mark Hopcus, Dennis Allen and Mark Henry for their help with technical problems and putting up with my endless code running in the computer lab.

My PhD studies would be much less fun without my friends. I would like to recognize them all for their support and making my College Station years more meaningful: Benat Kockar, Burcu B. Keskin, Yakut Gazi, Arzu Karaer, Can Attila, Dilhan Ilk, Ahmet Ugursal, O. Ozgu Ozsoy, Olcay Aykac, Cem Sevik, Ceki Halmen, Cansin Y.

Evrenosoglu, Feyza Berber, Mert Dogan, Elif Alper, Gokhan Ozturk, Alper Kinaci, Simge Andolsun, Marie des Neiges Léonard, and finally my dear friend in Houston, Aysegul Dastan Fidaner... I would like to also mention my friends with whom I shared the same department, Homarjun Agrahari, Gopalarishnan Easwaran, Hui Lin, Liqing Zhang, Bahadir Aral, Fatih Mutlu, N. Onur Bakir, Gokhan Memisoglu, Zeynep Ertem, Samyukta Sethuraman, Cesar Rincon-Mateus, Hiram Moya, Jaime Luna, Baski Balasundaram, Piyush Goel, Hoda Parvin, Arupa Mohapatra, and Young Myoung Ko... I feel lucky to have met these wonderful people and many others during my years at Texas A&M. Finally, a special thank you to my dear friend Selen Ustun for her indispensable friendship and comforting words even at the hardest times.

I would not be the same person that I am today without the unconditional love and support from my family members. I am so blessed to have my mom, Emine Kaya Eren, as she sets a great example with her hardwork, and has always been empathetic, understanding and supportive during my studies and my whole life. I am proud of my younger sister, Bestecan R. Eren, for the person that she is and I feel so lucky to have her. My grandmother, Namiye Kaya, has always inspired me with her dedication to life and was always there for me and my sister. I would like to also thank my uncle, Ertugrul Kaya, for his great support and encouragement together with the rest of his family, my precious aunt, Iclal Kaya, my cousins Emre and Kerem Kaya. My large and loving family that I cannot fit in here, thank you for believing in me and giving me confidence.

Finally, my other half, Omer Izgec whom I met during my studies and became my husband along the way, has gone through every step with me, all the ups and downs of my studies and my life, and made everything much more meaningful than it could have ever been. Thanks for sharing the life with me and filling it with love and joy.

TABLE OF CONTENTS

CHAPTER Page

LIST OF TABLES

LIST OF FIGURES

FIGURE Page

FIGURE Page

CHAPTER I

INTRODUCTION

In this chapter, we introduce the research problem studied in this dissertation. We begin with a discussion of the underlying motivation and background followed by a definition of the problem in detail.

I.1. Motivation and Background

Since mathematical and computational methodologies began to be employed to study biological systems and their dynamics, biosciences have significantly benefited from quantitative modeling applications and their use in conjunction with experimental studies. Mathematical and computational techniques can be broadly classified as two types: simulation and analytical. Simulation techniques have been widely used as they can replicate real systems to a great detail. Analytical efforts often rely on stronger assumptions to describe the system in mathematical equations and get closed-form solutions or generalized conclusions. Together, these mathematical and computational methodologies enable efficient analysis of biological systems which would take enormous time and efforts - or even would be infeasible in most cases - relying only on biological experiments. As a result, they help better understand and explore mechanisms in living things.

Modeling and analysis of mechanisms in biology and life sciences in general creates a potential for development of novel techniques and new technologies in quantitative sciences and engineering. It has recently been realized that some engineered complex systems such as Internet and computer chips possess many features of molec-

---

The journal model is *IIE Transactions*.

ular interaction networks within a living cell (Skjeltrop and Belushkin, 2005). In a way, nature has inherent mechanisms that are worth mimicking in artificially manufactured systems. Sensory functions, adaptability to environmental conditions, and atomic-level distributed autonomic control of self-assembled structures are a few examples of intriguing properties of biological systems that are leveraged for emerging technologies. Developing structures without centralized control, such as carbon nanotubes, sensor dust, etc., is a major objective in manufacturing of very small scale systems. Further innovations in nano-technology, sensor development and other related areas rely highly on the discovery and better understanding of processes in living organisms.

Having made a case for the use of mathematical and computational methods for bio-systems, as well as the use of bio-systems in developing artificially engineered systems, there are several challenges to consider. For example, it is not possible to study living systems just by analyzing their components individually. A systems approach is required to take into account the interactions between the components that are highly nonlinear in nature. These interactions together with dynamics defined in the system lead to emergence of complex functionality which is critical for survival of living organisms. Although several methods have been applied to analyze complex physical systems such as the atmosphere and oceans, living cells present an unprecedented complexity due to significant molecular mechanisms, which creates a continuing challenge for discovery and analysis as well as opportunities to engineer similar systems. Such systems typically exhibit inherent complexity at both spatial and temporal levels, where randomness and organization coexist in an intriguing manner. A basic common example would be pattern formation on animal coats, such as zebra stripes and leopard spots. The coat patterns are specific to the species, they would help identify the type of the animal with certainty in most cases. However, it

would not be possible to find the exact replica of prints of an animal on another individual of the same type. Plants also exhibit similar pattern formation in their leaves and flowers. Systems biology has recently developed an understanding that the complexity of biological systems begins at the cellular level (Ghosh *et al.*, 2006). Thus, discovering the mechanisms of the cellular activities are essential in understanding higher level biological systems, including humans.

Our work is motivated by a special system in living cells, namely the cortical microtubule (CMT) system, which serves as the skeleton of plant cells (see Figure 1). They are essential for development of the cell shape, maintenance of the cell structure, and other critical functions including cellular transportation and division. Microtubules are fiber-like structures that are formed by the polymers inside the cell and appear in clusters or arrays according to the cell type and function. Cortical microtubules form ordered arrays that are similarly aligned to each other on the plant cell wall. They are observed to acquire this ordered structure by self-organizing from a completely disorganized system of tiny CMTs that are distributed randomly over the cell surface (cortex) growing in random directions. This organization is achieved despite the lack of any central control mechanism, relying only on the individual dynamics of CMTs and interactions among them.

In addition to the spatial and temporal complexity of the whole CMT system, inherent dynamics of CMTs introduce an additional spatial dimension to the problem. Both the dynamics and interactions in the system are governed by stochastic rules and processes. Traditional modeling approaches are unsuitable for modeling such complex stochastic distributed systems with spatio-temporal properties. Our objective is to develop methods to model and analyze this complex system that will answer questions related to its characteristics including organization and other performance measures of CMT length and number in the system. We first develop a computer simulation

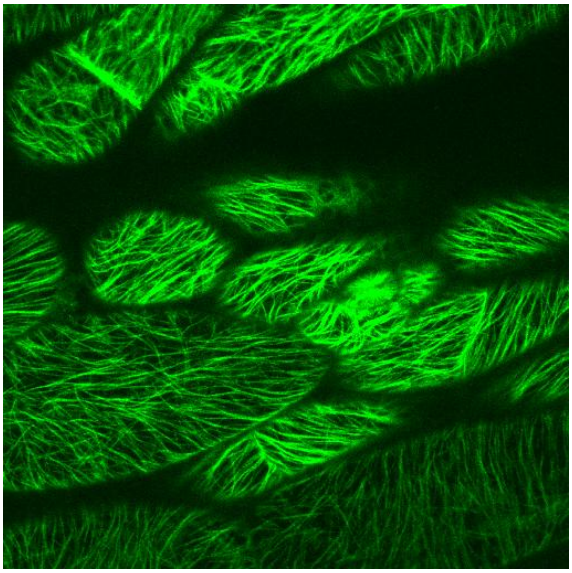

Fig. 1. Plant Cell Microtubules

model to replicate the dynamics and interactions of CMTs based on the data from biological experiments, that is microscopic studies of live plant cells. Simulations provide a means to characterize system properties including CMT organization and develop related metrics as well as identify possible types of system behavior. Using the quantification metrics, we test the impacts of CMT dynamics and interactions (input parameters) on system characteristics (output measures). Based on our conjectures from the simulations that we conduct, our next objective is to formulate analytical techniques that are more efficient and will lead to more generalized results and conclusions in terms of the relations between input parameters and output measures. First, we theoretically determine the conditions for organization in terms of system parameters. Finally, focusing on that region, we develop predictive methodologies to estimate certain system metrics (expected average CMT length and number) and their evolution in time based on a given set of inputs. Overall, we build a frame-

work using computational and analytical methods all together for a comprehensive quantitative modeling of the system characteristics.

In addition to its short-term objective of studying self-organization and other characteristics of plant CMTs, this research also has some broader reaching impacts. It contributes to our understanding of similar microtubule arrays that are generated without any central control in specialized animal cells such as neurons and muscle cells, where ordered arrays are critical for the specialized morphology and functions. This research is also related to the field of biofuel engineering, as CMT organization directly influences the ordered deposition of cellulose microfibrils, the most abundant biopolymer on the planet. Finally, as we mentioned above, the complex structure of living systems exhibit unique mechanisms that can be harnessed in manufacturing of artificial systems. In this context, there are current studies that relate self-organization of microtubules to design and assemble of nanostructures for the directional transport or delivery of materials at the nanoscale (Goel and Vogel, 2008).

I.2. Problem Definition

In this dissertation, we consider a CMT system with dynamics and interactions defined over time and space. We describe system properties based on experimental data from relevant literature (Dixit and Cyr, 2004; Shaw *et al.*, 2003). We begin by describing the dynamics for a single CMT, and subsequently consider interactions between CMTs. CMTs are fiber-like structures that have an approximately linear shape. They are formed by head-to-tail assembly of tubulin dimers which are the building blocks (see Figure 2). Their formation results in distinct dynamics at both ends. One end is highly dynamic and "grows" on average, which is designated as the "leading end";

whereas the other end is less dynamic, "shortening" on average and accordingly called the "lagging end". More specifically, the leading end stochastically switches between *growth* (G), *shortening* (S) and *pause* (P) phases, whereas the lagging end alternates only between *shortening* (S) and *pause* (P) phases. Growth occurs by assembling more dimers to the leading end, and shortening occurs by breaking down into the dimer level on either end. The length of the CMT at time t, $L(t)$, changes according to its state at time t, $M(t)$, which is defined as a two-tuple of leading and lagging end phases. A sample path for the state of a CMT with the corresponding length graph is plotted in Figure 3. Note that while in a state, the length of the CMT changes with a constant velocity.

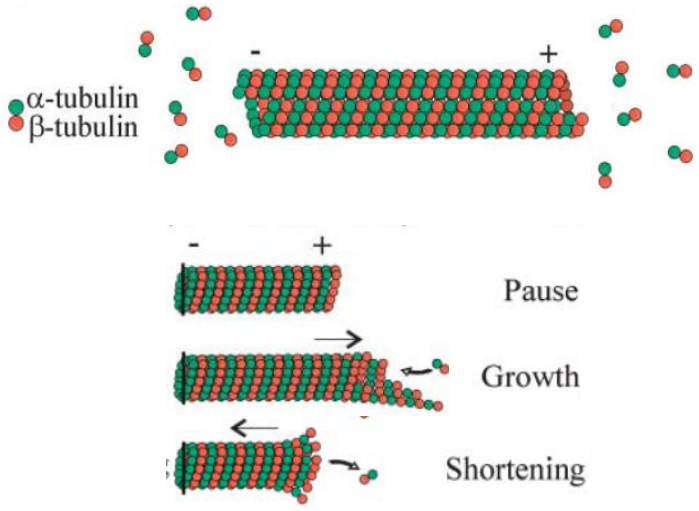

Fig. 2. Structure of a CMT with Leading (+) and Lagging (-) Ends and Leading End Dynamics

Having described the dynamics of a single CMT briefly, we now put this in the context with other CMTs in a plant cell. CMTs appear randomly over time at random locations over the cell wall with an arbitrary orientation that is determined by the

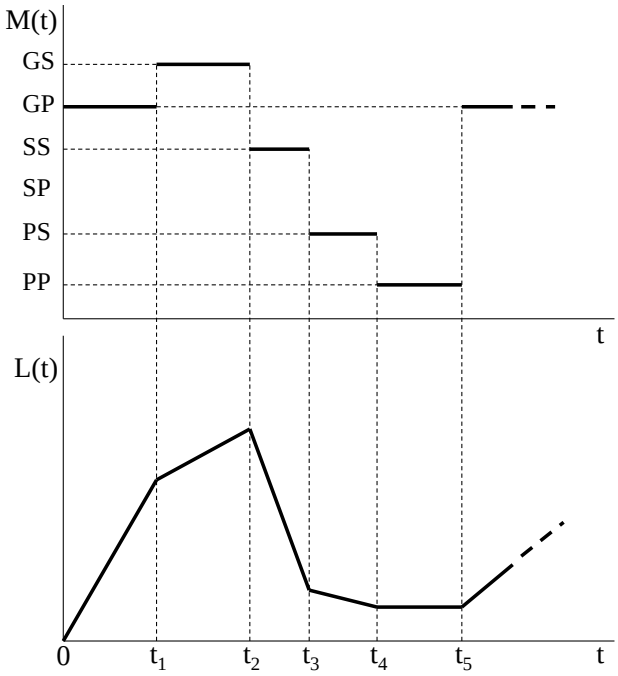

Fig. 3. Realization of the Length Process, $L(t)$ of a CMT Based on Its State, $M(t)$

growth direction of the leading end. As a result of the distinct dynamics at both ends, a CMT moves in the direction that its leading end grows. Hence, it runs into other CMTs in the system, which results in CMT interactions. These interactions occur on an approximately planar area as CMTs are attached to the cell surface (cortex) tightly and potentially result in a change in the dynamics and orientation of the CMT. According to experimental data, there are three possible outcomes when a CMT runs into another one that we call the "barrier". We use Figure 4 to describe events that can occur as a result of a CMT interaction. The CMT can bend in the direction of the barrier and continue to grow along it forming a bundle at the point of collision. This "bundling" would happen with a curvature, however we are approximating it by a linear shape in the figure. Another possibility is that facing the barrier, the

leading end of the CMT immediately leaves the growth phase and transitions into the shortening phase, which is called a (collision-induced) "catastrophe". Finally, the CMT can cross over the barrier neither changing its dynamics nor orientation. These events are experimentally observed to be dependent on the collision angle between the two CMTs and plant cell type, which we will explain in more detail in Chapter III.

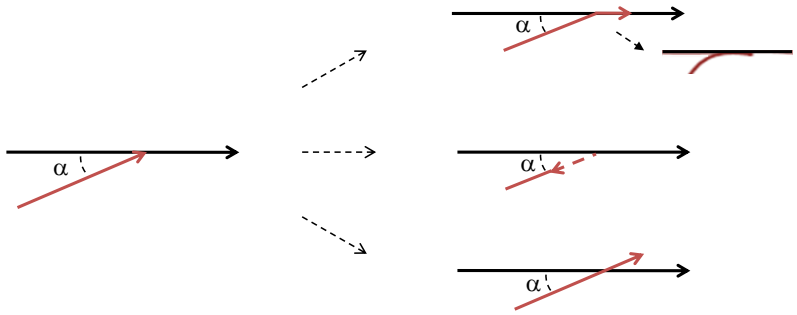

Fig. 4. Events Induced by CMT Interactions

It is observed in plant cells that over the course of time disorganized CMTs with random orientations get organized to be aligned with similar orientations as seen in Figure 5. What is remarkable is that there is no centralized control and this organization emerges purely by the dynamics and interactions of individual CMTs that we described. This motivates the question of whether it would be possible to replicate this self-organization by simulating CMT dynamics and interactions. It turns out that using simulations that start with a disorganized set of CMTs, they indeed evolve similarly, self-organizing into ordered arrays as seen in the simulated example in Figure 5, which we will discuss in Chapter III. Having confirmed that, our main point of interest is that CMT organization can be distorted by genetic mutations or environmental conditions that alter dynamics and interactions in plant

cells. Hence, certain CMT systems might stay disorganized, which has significantly adverse effects on the functionality of the cell. Our objective in this dissertation is to quantitatively characterize this complex system and particularly its organization, to develop predictive methodologies for its characteristics, and explore underpinnings of self-organization in terms of system parameters. For this, we next describe a framework of our approach.

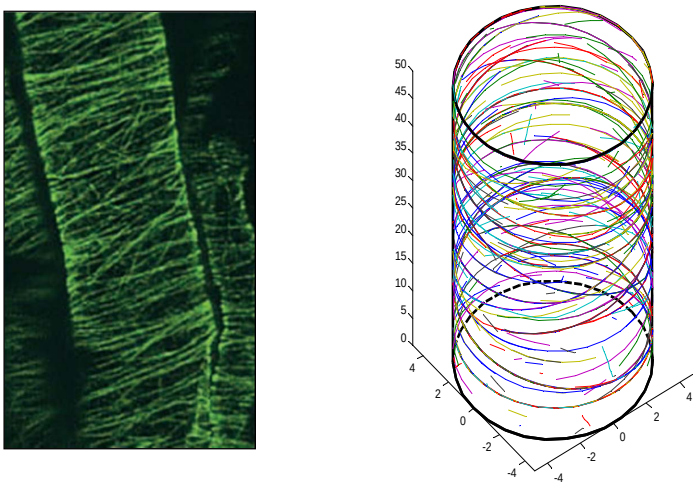

Fig. 5. CMT Organization in a Plant Cell and Replication in a 3D Simulation Model

I.3. Objectives and Framework

In summary, the crux of this research is in the development of computational and analytical models and methodologies for the CMT system that will answer questions such as:

- Can we replicate the system using computational and analytical models, by mimicking the CMT dynamics and interactions observed in real cells to obtain similar behavior?

- How can properties related to the length, number and orientation of CMTs including organization in the system be characterized?
- What are the effects of CMT dynamics and interactions on organization and other system characteristics such as average CMT length and number?
- Is it possible to predict organization, average CMT length and number in time for a given system?

Primarily, we are interested in developing methods to explore the effects of parameters related to CMT dynamics and interactions on the properties of the whole system as well as predicting evolution of system characteristics in time. A representative diagram for the implementation of such methods outlining their inputs and outputs is given in Figure 6. A related objective is to develop measures that characterize system properties (outputs) to be able to conduct a quantitative comparison of results.

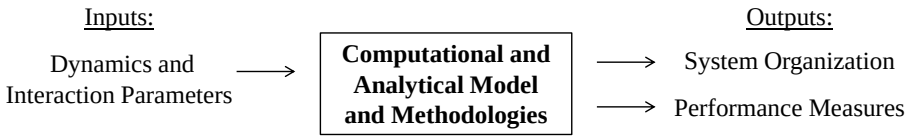

Fig. 6. Input-Output Diagram for Computational and Analytical Methods

This dissertation takes a systematic approach to the problem considered. A detailed framework of the derivation of models and analysis is presented in Figure 7. First, we use computer simulations to replicate the dynamics and interactions of CMTs based on data from biological experiments. We test different scenarios changing input parameters of the simulation algorithm. We compare simulation results based on certain performance measures including organization, length and number of CMTs,

which are the major determinants of the system structure. For system organization, we use a metric that characterizes the distribution of CMT orientations, which we also employ on real cell pictures via imaging techniques in order to compare simulated and real systems more quantitatively. Based on simulation results and conjectures, we develop a mean-field model for CMT dynamics and interactions; and use it to derive sufficient conditions for system organization in terms of problem parameters. Finally, considering the parameter regions that guarantee organization, we develop predictive methodologies for other system metrics such as expected number and average length of CMTs over time. This final step of research brings a unified approach including a fluid model for CMT dynamics, approximation algorithms and simulations applied in conjunction to derive an estimation method that is well-suited for the considered system. We verify results of our analytical methodologies using simulations.

I.4. Organization of the Dissertation

This dissertation is organized as follows. In Chapter II, we review the related literature by classifying it into two major areas: i) computational and mathematical biology, and ii) complex system dynamics and self-organization. In this chapter, we also present a detailed discussion of papers that focus specifically on modeling of CMTs. In Chapter III, we introduce a mathematical framework for the developed models, quantification of system properties and a discussion of the simulation model with its validation and results. Chapter IV describes the mean-field model for system organization together with its analysis and results. In Chapter V, we present the fluid model for single CMT dynamics and related methodologies for estimation of system metrics. We include a numerical comparison of outputs to simulation results. Finally, we conclude in Chapter VI with a summary of contributions and ideas for

future research.

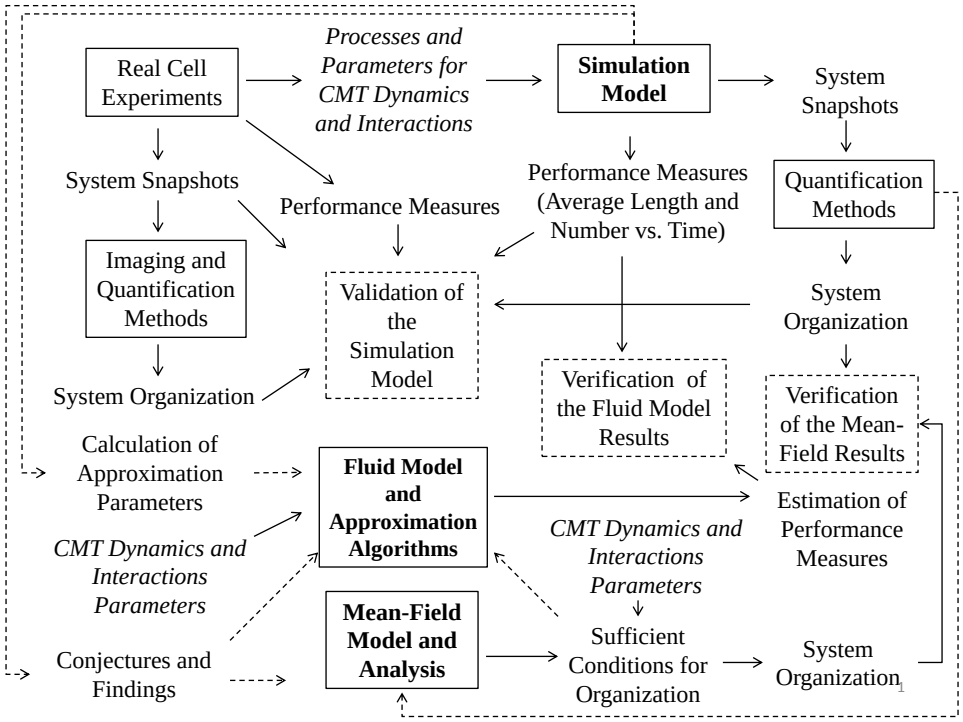

Fig. 7. A Framework of the System Analysis Approach

CHAPTER II

LITERATURE REVIEW AND BACKGROUND RESEARCH

Having described our problem and its underlying motivation, we review in this chapter two related research areas. We first summarize relevant computational and mathematical biology literature, and next briefly discuss the area of complex systems with an emphasis on emergent behavior such as self-organization observed in the CMT system that we consider. Note that those two areas are major fields that we review here very concisely to establish the connections and differences of our problem with respect to some prior studies. Finally, we devote a separate section for the studies under the category of computational and mathematical biology literature that particularly focus on CMT systems.

II.1. Computational and Mathematical Biology

Computational and mathematical biology is an active fast-growing research field which requires an interdisciplinary approach. A compilation of computational studies in the field of systems biology can be found in Kriete and Eils (2006), including a discussion of information technologies that enable computational analysis of biological data. Murray (1993) presents a detailed discussion of several models developed in the broad area of the mathematical biology. A significant portion of research in this area focuses on ecological and epidemiological models. In addition to discrete models, continuous approximations are widely used to model population dynamics, which generally yields to so-called "reaction-diffusion" equation systems. In this approach, the entities are considered as particle-like structures where their interaction frequencies are formulated as functions of the spatial densities of their species and others. Cantrell and Cosner (2003) specifically focus on modeling of ecological systems using

reaction-diffusion equations. Curry and Feldman (1987) develop stochastic models of population dynamics in agricultural ecosystems and provide a comparison to the deterministic approaches in terms of estimation of mean performance measures. They also study derivation of optimal control policies for insect populations. Other major phenomena considered in mathematical biology include travelling wave-like motion of chemicals and organisms, such as spreading epidemics; analysis of biological oscillators with time-periodic dynamics, examples of which can be listed as the breathing process and the pacemaker of the heart. Another widely studied topic is spatial pattern formation in living organisms, which is also related to the concept of emergent behavior seen in complex systems (and will be discussed in Section II.2). The problem that we consider in this research distinguishes itself from prior studies in general, as we consider micro-level dynamics in time and space, where the components (CMTs) have an inherent spatial dimension of their own (as CMT length changes in time) and interact with each other accordingly. Hence, they are not suitable to be modeled as particle systems and do not exhibit any spatial or temporal periodicity in their dynamics.

Among quantitative methodologies, operations research techniques have been fairly applied to the area of genomics and molecular biology. Waterman (1995) includes applications of several combinatorial and statistical tools such as graph theory, integer programming, heuristics and renewal theory for modeling biological data as sequences and maps. There have been introductory efforts to employ network theory for the study of interactions between components of biological systems (Palsson, 2006), in line with the transition from reductionist approaches to a systems perspective for analysis of bio-systems. Still it is a perceived fact that operations research techniques, including especially stochastic modeling approaches, have been underused to study biological mechanisms. Our objective in this research is to develop method-

ologies that account for both the stochastic dynamics and spatio-temporal nature of the biological system that we consider, making use of the best-suited techniques.

There are a few studies that specifically focus on microtubule systems, which fall under the category of computational and mathematical biology. We review these models in Section II.3 in the end of this chapter. Here, we continue with a discussion of the relevant literature in complex systems area in the following section.

II.2. Complex System Dynamics and Self-Organization

The study of complex systems is an emerging field that focuses on systems with inter-connected parts where the aggregate behavior can not be described by the single components but depends highly on their interactions (Bar-Yam, 1997). It can be defined as the "ultimate of the inter-disciplinary fields" as it brings a seemingly limitless number of disciplines together. In biology, it is possible to find infinitely many examples of complex systems. One fundamental phenomenon related to complexity is structuring and differentiation of a large variety of functions and systems from similar cells.

Having established the relation between the complex systems field and biosciences in general, we discuss some major characteristics of complex systems that are related to the problem that we consider. Self-organization is an emergent property seen in several complex systems, where the components gain an ordered structure in time through local interactions among themselves despite the absence of a central control mechanism. One of the major research topics at the intersection of mathematical biology and complex systems literature is the spatio-temporal pattern formation in living things. A standard application is the study of patterns in animal coats, wings etc. (Chaplain *et al.*, 1999), although there exists a wider range of domains

from the structures observed in skin, hair (Nagorcka and Adelson, 1999) and capillary networks (Chaplain and Anderson, 1999) to the pattern formation in cancerous cells (Sherratt *et al.*, 1999). A review and classification of mathematical models used in biological pattern formation can be found in Murray (1993) and Maini (1999). For a more recent and methodology-based review of modeling and analysis of pattern formation, the reader is referred to Hoyle (2006) and Desai and Kapral (2009).

Another type of self-organization seen in living systems is ordered motion where organisms change their active movement in response to the local interactions with other members, which leads to an harmonious motion of the whole group, as seen in fish schools and insect societies. Mikhailov and Calenbuhr (2002) study several topics in this area including dynamical clustering, synchronization of motion, and hierarchical organization of living systems. Schieve and Allen (1982) compile studies on uncovering the mechanisms of this type of self-organization in chemical, biological and social systems.

Another emergent property seen in complex systems is chaos, which is the irregular behavior in systems that are defined by simple rules; doesn't repeat itself; and is unpredictable because of its sensitivity to the initial conditions which are never exactly known (Ott, 1993). The analysis of unpredictable chaotic behavior is mainly based on investigation of the attractors of the system, i.e. the sets of states toward which the dynamical system evolves over time. Chaos exhibited in biological complex systems is a result of interactions between components and generally observed at both spatial and temporal dimensions. Kaneko and Tsuda (2001) study analysis of deterministic chaotic behavior in complex systems with applications to the life sciences (some of the examples include the immune system and chaotic information processing in the brain). Bifurcation is an important concept in the analysis of complex chaotic behavior as it establishes relations between system parameters and stabil-

ity. A compilation of recent studies of bifurcation in nonlinear systems can be found in Sun and Luo (2006). Crauel and Gundlach (1999) present studies that focus on stochastic analysis of similar dynamical systems.

The problem studied in this research is related to both concepts in the complex systems theory that are mentioned above. The system that we consider is an example of a self-organized system with spatio-temporal properties. Moreover, unlike the self-organizing systems mentioned above, CMTs also possess inherent spatial structure that affects their interactions with the rest of the system. That is, their length, which changes as a result of their stochastic dynamics, adds another dimension to the problem. CMT system exhibits also chaotic properties, as system behavior and organization in plant cells is quite unpredictable although the dynamics and interactions are defined by simple rules. Moreover, there is a high variability of output measures observed in simulations under similar conditions, which will be discussed in Chapter III. Thus, an analysis of this potentially chaotic behavior and system stability is required to better understand system dynamics.

In summary, the problem that we study has distinct characteristics among the common self-organized and chaotic systems considered in the related literature. We believe that the analysis of CMT system will lead to development of novel techniques for study of stochastic processes with high-level spatial and temporal complexity, in addition to contributing to the area of mathematical and computational biology.

II.3. Computational and Analytical Models for Microtubules

Having discussed some major fields related to the considered problem, in this section we focus on studies of CMT and other microtubule systems in more detail. We mainly include properties related to modeling and results, and refer the reader to

Eren *et al.* (2012) for more biological details. We first begin by reviewing a few papers that consider only the dynamics of microtubules with no interactions. This types of microtubule systems are mainly found in animal cells and form an aster-like structure centered at a compartment of the cell (centrosome). Unlike CMT systems, the organization is typically controlled by this central mechanism rather than being generated by interactions of microtubules. Such microtubule systems have been generally modeled by formulating their dynamics in terms of continuum differential equation systems and using computer simulations. Cytrynbaum *et al.* (2003) present a quantitative model of microtubules which is numerically simulated in one-dimensional and two-dimensional surfaces to study generation of aster-like arrays. In Cytrynbaum *et al.* (2006), they also provide an asymptotic solution of the problem for the one-dimensional case. Maly (2002) develops a diffusion approximation for the stochastic dynamics of a single microtubule that switches between states of growth, shortening and pause. Finally, extending the microtubule dynamics model by Dogterom and Leibler (1993), Yarahmadian *et al.* (2011) develop a generalized convection-diffusion model where the transition rates between growth and shortening phases are dependent on the concentration of tubulin (which is the raw material for CMTs), and conduct an analysis to investigate existence and stability of steady-state solutions.

CMT organization in plant cells is one intriguing example of self-organization mechanisms widely seen in living things. There is rising interest in modeling the CMT system, particularly its organization into ordered arrays and the mechanisms that facilitate this organization. Most of the studies so far focus on self-organization of CMT arrays starting from a randomly oriented population and investigate answers to questions such as:

- Are simple dynamics and interactions between CMTs sufficient to result in organization? How does this self-organization occur? What are the necessary conditions for emergence of ordered CMT arrays?

- What are the effects of altering dynamics, interactions, and properties of cell edges on the CMT self-organization? What are the relative contributions of these different mechanisms on organization?

There is also an even more recent line of research which models molecular and mechanical behavior of CMTs to understand the mechanisms that govern their interactions as well as their individual tendencies for orientation based on cell geometry. In other words, these models delve into the details of events that are induced by interactions of CMTs with other CMTs and the constraints of the space that they are confined in. More specifically, the objective of such studies might be answering one or more of the following questions:

- How do interactions such as CMT bundling and collision- induced catastrophe occur? Why are those events dependent on the collision angle?

- How does the attachment (anchoring) of CMTs to the cell surface (cortex) occur and what are its effects on CMT interactions?

- How do the interactions with the space and geometry constraints occur?

It is worth noting that our classification is inspired by the cell-level vs. molecular-level questions in Allard *et al.* (2010b), although we extend their definition to include mechanical models which focus on bending mechanisms of CMTs based solely on their elasticity and geometric constraints -which include interactions with the cell boundaries as well as the parameters that determine the size of the system- without considering their interactions with other CMTs. In this section, we refer to the

first class of models as the "organization-oriented" models and the second class of models as the "interaction-oriented" models. In the following, we begin by reviewing organization-oriented models leaving a few interaction-oriented studies for later discussion.

II.3.1. CMT Organization-Oriented Models

There have been both computational and analytical approaches to address CMT self-organization emerging due to the interactions in the system. Simulation techniques offer the advantage of replicating real systems to a great detail and conducting computational experiments to test different scenarios easily by modifying the input parameters. On the other hand, analytical efforts often rely on stronger assumptions to get closed-form solutions or more general conclusions while enabling even more efficient analysis. There are certain properties common to both analytical and simulation studies of CMT organization in general, such as modeling CMTs as line segments and considering their dynamics as being identical in the absence of interactions. As a result, CMTs can be roughly modeled similar to interacting particles although with a certain length and orientation. In simulations, coordinates of CMTs are updated according to the dynamics and interactions in accordance with the assumptions of the particular model. Analytical efforts usually rely on spatial homogeneity assumption, which allows ignoring coordinates and formulation based on average density of CMTs over the whole area. For both types of models, bundling mechanism results in the possibility of multiple segments with different orientation for a single CMT. Having described some general characteristics of CMT models, we continue with a discussion of some fundamental simulation studies and their major findings related to the impact of interactions on array organization.

To the best of our knowledge, the first published attempt to model CMT orga-

nization computationally is by Dixit and Cyr (2004). They developed a Monte Carlo simulation with a limited number of CMTs in the system where the appearance of new CMTs is not considered. Their simulations show that simple rules for CMT interactions extracted from biological experiments can result in a parallel CMT array from a randomly arranged population. They found that bundling and catastrophes are both necessary and sufficient for CMT organization, although this conclusion might be related to the restricted size of the simulations, as stated by the authors. As a matter of fact, more complex models distinguish between the relative significance of those two mechanisms, which we will address in the following subsection. Baulin *et al.* (2007) model a CMT system where they incorporate the appearance process of new CMTs. However, in their simulations, interaction mechanisms and dynamics are simplified as follows. Dynamics of a single CMT are assumed to be deterministic where the leading end grows and lagging end shortens continuously with their corresponding time-averaged velocities. When a CMT runs into another one, it pauses for the duration that it is blocked by the barrier, which is called *stalling*. Their simulations show that even these overly simplified interaction mechanism and dynamics are enough to achieve self-organization. However, their model is limited in the sense that only growth-prone dynamics with a positive net velocity can be studied due to exclusion of multiple states. Shi and Ma (2010) consider similar interaction mechanism with stalling -that they call *steric* interactions- and model the CMT dynamics at both ends. They particularly focus on analyzing the effects of dynamicity parameters on the organization of CMTs by conducting an extensive simulation study. Tindemans *et al.* (2010) consider bundling and catastrophe interactions as well as possibility of growth and shortening (a two-state model) at the leading end, complementing their analytical model in Hawkins *et al.* (2010). According to their models, CMT lagging end is always static, which reduces the dimensional complexity of the problem. Allard

Table 1. Summary of CMT Models in the Literature

	Leading End	Lagging End	Interactions	Appearance
Dixit and Cyr (2004)	G, S	Static	C*, B**	-
Baulin *et al.* (2007)	G	S	Stalling	Y
Shi and Ma (2010)	G, S	S	Stalling	Y
Tindemans *et al.* (2010)	G, S	Static	C, B	Y
Hawkins *et al.* (2010)	G, S	Static	C, B	Y
Allard *et al.* (2010b)	G, S, P	S	C, B	Y
Our models	G, S, P	S, P	C, B	Y

* "Catastrophe" is abbreviated as "C"
** "Bundling" is abbreviated as "B"

et al. (2010b) consider a model with three states by incorporating the possibility of pausing at the leading end. They also consider a continuously shortening lagging end with the time-averaged velocity based on the data from biological experiments. In our simulation model, we consider stochastic dynamics at both ends in addition to bundling and catastrophe interactions, which we will discuss in Chapter III. Table 1 summarizes certain properties of CMT organization models in the literature. Note that the table lists the phases considered for each end of a single CMT according to the notation in Section I.2, in addition to the type of interactions modeled. Finally, the last column stands for whether the appearance of new CMTs is considered in the model. Different scenarios might be tested using each model, however we roughly list the properties that correspond to the baseline scenario for each study.

In addition to the simulation studies, there are also a few analytical efforts to model the CMT organization. In general, analytical models of CMT organization are complementary to the respective simulation models to provide further insights and more efficient analysis. They usually consider a spatially homogeneous system and model CMT densities per unit area according to their dynamics and interactions. Baulin *et al.* (2007) formulate the average densities of CMTs as a function of length and orientation using diffusion equations. The impact of interactions are approxi-

mated inspired by the kinetic theory of gases based on the average length, velocity and density of CMTs in the system. Interaction (stalling) frequency is orientation-dependent to account for the fact that CMTs with similar angles run into each other less frequently. This relation is not considered while modeling the rescue frequency for a blocked CMT (frequency of being released for a stalling CMT), which is a function of the average length of the blocking CMT. This average length (and, accordingly, the rescue frequency) is assumed to be independent of orientation, which might be the reason for the disagreement between the results of simulations and the analytical model especially for the time after ordered CMT domains start to emerge. However, it is worth noting that authors relate this disagreement to the homogeneity assumption which conflicts with the emergence of locally ordered domains observed in their 2D simulations. Hawkins *et al.* (2010) develop a stronger model with a similar approach, where they consider bundling and catastrophe interactions instead of stalling and consequently the possibility of CMTs with multiple segments. Considering static lagging ends, they call the segment of a CMT with the leading end as the active segment and the rest of the segments as the inactive ones (if any). There is some history dependence in their model introduced by the bundling event as the inactive segments can be reactivated by the shortening and elimination of previously bundled segments. However, they eliminate this history dependence for the isotropic solution, where CMT densities are uniformly distributed with respect to their angles. They conduct a bifurcation study around this isotropic solution to investigate parameter regions where stable ordered solutions may potentially exist, implying possibility of organization. Further, they relate this to a control parameter that they develop, which is a function of the input parameters of the model. In Tindemans *et al.* (2010), they show that the predictions of this model agree well with their simulations, although there is certain discrepancy from the simulations with bundling. Finally, Shi

and Ma (2010) conduct a similar bifurcation analysis for their model, in which they formulate interactions using a mean-field theory approach. Although their interaction mechanism is quite simplistic similar to that of Baulin *et al.* (2007), their formulation results in fairly well predictions in agreement with their simulations. Using both theory and simulations, they provide further insights into the dependence of emergent behavior of the system on the competition between dynamics and interactions.

In summary, there are a few diverse modeling efforts for the microtubule systems, particularly CMTs. Due to the computational and analytical challenges associated with the complexity of the considered system, there are certain assumptions considered by each study to facilitate modeling and analysis. In addition to the varying properties of the models, different studies seem to give different weights to the impacts of certain parameters or mechanisms related to either interactions or dynamics during the analysis, which might be one of the reasons for contradictory results. Our objective in this research is to use simulation and analytical models in conjunction to develop a methodology well-suited to the characteristics of the considered CMT system. We take into account the stochastic nature of both the dynamics and interactions. Further, we employ a systematic approach beginning with a replication of the dynamics and interactions using simulations, and characterization of system behavior and properties accordingly. This provides a means to observe relations between parameters and performance measures related to both the whole system and its components. Based on our conjectures and observations of the simulated system, we select and employ analytical techniques that aid in more efficient and generalized analysis and results. We develop two different analytical approaches which are tuned according to the particular objective considered and properties of which are verified using simulations. Before discussing the methodologies that we develop, we continue to review the papers in the literature presenting further details systematically

according to different types of results and analysis.

II.3.1.1. Relative Contribution of Bundling vs. Catastrophe Interactions

Necessity of interactions for organization is commonly agreed upon among different modeling studies (Allard *et al.*, 2010b; Baulin *et al.*, 2007; Dixit and Cyr, 2004; Hawkins *et al.*, 2010; Tindemans *et al.*, 2010). However, there are varying results regarding the relative contribution of bundling vs. catastrophes. Tindemans *et al.* (2010) conclude that catastrophes are sufficient to induce organization even in the absence of bundling, in line with their theoretical result in Hawkins *et al.* (2010). They show that bundling has only a minor contribution on organization beyond the bifurcation point (see Subsection II.3.1 for details). On the contrary, Allard *et al.* (2010b) find bundling as the main contributor of organization and conclude that catastrophes are neither necessary nor sufficient to organize CMTs into ordered arrays. These differing conclusions might be due to different choice of dynamicity parameters and assumptions, which is not addressed thoroughly in any of the studies. Tindemans *et al.* (2010) and Hawkins *et al.* (2010) consider only the dynamicity parameters in the region of *bounded growth* with a negative average net velocity, where CMTs have finite length even in the absence of interactions. They model CMT lagging ends as static in both their analytical and simulation studies. It is possible that the impact of bundling on organization is underestimated due to combination of these factors. A static lagging end assumption would be expected to reduce the impacts of the bundling mechanism as it does not allow shortening of unbundled (previously existent) segments of bundled CMTs. In such a setting, considering a negative average net velocity for the leading end would hypothetically make the bundling process pretty much reversible by favoring pre-existing segments over the newly formed ones that contain the active leading ends, thus reducing its contribution to array organization.

On the other hand, Allard *et al.* (2010b) might be overlooking the indirect effect of catastrophes on organization by regulating the CMT density in the system especially for the region of *unbounded growth* dynamics with a positive average net velocity. Although their inputs seem to include dynamicity parameters that result in both negative and positive average net velocity values; the mean CMT length seems to stay bounded in all their simulations that they present. They conclude that an extensive random sweep of dynamicity parameters shows that catastrophes are only effective in the limit where the shortening velocity and the transition rate from growth to shortening are approximately zero, and the rate of transition from shortening to growth is relatively much larger. Note that in the limit, this scenario approaches to the setting considered in Baulin *et al.* (2007) with continuously growing leading end.

II.3.1.2. Effect of Dynamicity Parameters on Organization

Shi and Ma (2010) is the only study which thoroughly analyzes the effects of dynamicity parameters on organization. They classify the CMT organization into three phases: *isotropic* state, where the CMTs are disorganized with roughly uniform orientation, *nematic I* state where ordered long CMTs are distributed in a narrow orientation (high level of organization), *nematic II* state where ordered short CMTs are distributed in a broad orientation (lower level of organization). They explore the CMT phase behavior by extensive computational experiments based on a wide range of dynamicity parameters. Their results show that self-organization can be regulated by controlling solely CMT dynamics. They obtain similar results with their analytical model. However, as we mentioned in Subsection II.3.1, they consider only the stalling mechanism, which does not capture the range of CMT interactions that occur in cells. As a result, none of the models conduct a thorough analysis of the effects of CMT dynamics and different types of interactions on organization simultaneously.

II.3.1.3. Quantification of CMT Array Organization

There are a diverse number of techniques used to quantify CMT organization in different studies. Baulin *et al.* (2007) use a cost function that measures the overall proximity of CMT angles to the dominant orientation based on the cosine of angle differences. The dominant orientation is derived quantitatively by maximizing this cost function. They also introduce an alternative version of this metric where the contribution of each CMT is weighted by its length. Shi and Ma (2010) employ a completely different method that relies on computation of eigenvalues of a standard nematic order matrix (Chaikin and Lubensky, 1995). Hawkins *et al.* (2010) and Tindemans *et al.* (2010) employ another nematic liquid crystal order parameter based on the orientation and length densities of CMTs. Allard *et al.* (2010b) use a modified version of the cost function in Baulin *et al.* (2007) that represents the difference between total projected CMT length in the dominant direction and its perpendicular direction. Despite the diversity of methodologies used to measure CMT organization, it is worth noting that Allard (2010) found that the metrics used by Shi and Ma (2010), Tindemans *et al.* (2010), Allard *et al.* (2010b) and Baulin *et al.* (2007) are equivalent.

While all of the available metrics for measuring CMT organization rely on the orientation of the CMTs in the models, a systematic comparison of the performance of these metrics is lacking. In addition, these metrics need to be applied to data obtained from living cells to determine if they can robustly distinguish between different stages/types of CMT organization seen in plants.

II.3.1.4. Effects of Boundary Conditions on Orienting the CMT Array

Despite the varying conclusions related to the relative contributions of different interaction mechanisms and dynamics, CMT modeling studies reveal that there is heuristically no need for a complicated system to get parallel arrangement of CMTs. Still, these mechanisms fail to explain how cells orient the whole array in a particular orientation in the absence of a central control mechanism, as observed in plant cells at certain stages. The net orientation of the CMT array in a cell can change depending on developmental and environmental cues. For example, in rapidly elongating cells of the root, the CMT array is typically arranged transverse to the cell elongation axis (see Figure 5). When these cells stop elongating, the CMT array is typically longitudinally or obliquely arranged with respect to the long axis of the cell.

One potential mechanism to orient the entire CMT array in the cell in a particular orientation is introducing two *catastrophe-inducing edges* that oppose each other. According to this, if a CMT encounters one of those edges, it immediately switches from growth to shortening. Allard *et al.* (2010b) show that this mechanism of catastrophe-inducing edges is sufficient to bias the dominant orientation. They observe that even in the complete absence of CMT interactions, those edges lead to a certain amount of ordering near them. CMT interactions allow this edge-induced orientation to propagate further into the center. However, Allard *et al.* (2010b) also found that presence of catastrophe interactions with catastrophe-inducing edges is still not enough to result in organization.

The recent paper by Ambrose *et al.* (2011) conducts an extensive study of effects of different edge behavior induced by a certain protein on CMT orientation. By live-cell imaging, they first determine the effects of this particular protein on different types of edges in terms of facilitating the growth around the edge. Based on their

observations, they develop a simulation model approximating the cell shape as a cube and considering varying catastrophe inducing impacts for different edges. In addition to employing variable catastrophe probabilities among distinct edges, they also consider non-uniform behavior along an edge, such as permitting passage only through the center. Overall, their simulations show that the geometric constraints of the cell, specifically differential catastrophe-inducing effects of surface edges, are sufficient to bias CMT array orientation. Extending this line of research to more realistic cell shapes is an intriguing subject matter that is open to further investigation.

II.3.1.5. Microtubule-Dependent Appearance (Nucleation) of New CMTs and Array Organization

As noted in Chapter I, new CMTs are introduced into the cell randomly in time with an arbitrary growth direction. These appearances (so-called *nucleations*) occur from multiple sites that are almost uniformly distributed over the cell surface. In addition to this regular type of nucleation, it is also observed that new CMTs can originate in a microtubule-dependent manner. In that case, the newly formed CMT grows either at an acute angle to the mother CMT (called branch-form nucleation) or parallel to the mother CMT (Ambrose and Wasteneys, 2008; Chan *et al.*, 2009; Murata *et al.*, 2005). In Allard *et al.* (2010b), they considered only branch-form nucleation in their simulations, implementing it with and without regular nucleation. Incorporation of branch-form nucleation in their simulations is not observed to have a significant effect on the degree and rate of CMT organization. However, branch-form nucleation by itself results in unrealistic CMT organization with highly sparse arrays (Allard *et al.*, 2010b).

A recent study by Deinum *et al.* (2011) more completely analyzes the effects of branch-form nucleation on CMT organization by considering different branching

processes and dynamicity parameters. They extend their simulations in Tindemans *et al.* (2010) to include the shortening of the lagging end along with the microtubule-dependent nucleation. The authors keep the overall appearance rate constant, while the fraction of microtubule-dependent nucleation increases as a function of the total CMT length in the system. Under these conditions, all CMT nucleations are regular ones at the beginning of the simulations and the ratio of microtubule-dependent nucleation keeps increasing as the system becomes more crowded. They modify their control parameter in Hawkins *et al.* (2010) to incorporate the shortening velocity of the lagging end along with the other dynamicity parameters. It is worth noting that their results are again limited to the range where the control parameter is negative, which implies bounded growth dynamics with a negative average net velocity. For this range, they estimate the critical control parameter which represents the point beyond which system will show at least some degree of order, and quantify the degree of organization using simulations. Their results show that microtubule-dependent nucleation improves parallel CMT organization and widens the range of parameters for which organization occurs. The authors test different scenarios with more weight given to either branch-form or parallel nucleation. To be able to compare these mechanisms quantitatively, they use a co-alignment factor based on the *second Fourier coefficient* of the branch angle distribution. Based on this, they show that this factor, which is a measure of the co-alignment with the mother CMT during nucleation, is the main determinant of the effect of microtubule-dependent nucleation on organization. In fact, the critical control parameter seems to be similar for different nucleation mechanisms with the same dynamicity parameters and co-alignment factor. In particular, they found parallel CMT nucleation to have a strong impact on CMT array organization. In general, greater co-alignment of newly appearing CMTs to their mother CMT was found to enhance parallel array organization as expected. In their simulations, the

authors observed that branch-form nucleation had only a modest effect on enhancing array organization, consistent with the results of Allard *et al.* (2010b) discussed above. Deinum *et al.* (2011) note that the main contribution of branch-form nucleation was to result in spatially more homogeneous arrays than achieved by parallel nucleation alone.

II.3.1.6. Factors That Result in CMT Array Skewing

Some CMT arrays are observed to orient obliquely with respect to the elongation axis in plant cells. To discover the conditions that result in such *skewed* arrays, Deinum *et al.* (2011) test the impact of distorting the symmetry of branch-form nucleation so that more weight is given to nucleation from a particular side of the mother CMTs. They report that skewing of ordered CMTs occurs only for an extreme degree of bias towards one particular side of branching from mother CMT and for a limited range of parameter sets. The only settings that yields skewing was parameter sets that guaranteed too fluid and weakly ordered systems, which still failed to produce consistent results. CMT skewing and its driving factors form a research topic that needs further focus.

II.3.2. CMT Interaction-Oriented Models

In addition to the efforts to discover the mechanisms underpinning CMT self-organization by using computational and analytical models, there have been some recent studies that address the CMT interactions in more detail. The paper by Allard *et al.* (2010a) is the first attempt to model CMT interactions at a molecular level isolated from the rest of the system. These authors first model CMT anchoring, which is the process that keeps CMTs attached to the cell surface (cortex) and is essential to facilitate their interactions by confining them to an approximately two-dimensional space. The

CMT anchoring is modeled as a Poisson process in space, where the distance between anchors on a CMT is exponentially distributed. Based on this, the authors derive the free CMT length distribution, i.e. the distribution of the distance from the leading end of the CMT to the first anchor. This anchoring model is later used to study the interactions between CMTs based on the competition between *cross-linker*-based CMT bundling, CMT flexural rigidity, and CMT growth (Allard *et al.*, 2010a). Probabilities for catastrophe vs. crossover are derived using a dimer-level (building-block-level) model incorporating the linear elastic rod energy of CMTs, which is a function of the free length distribution. However, this model fails to explain the angle dependence of catastrophe events observed experimentally in plant cells (Dixit and Cyr, 2004). The effect of the collision angle is considered while modeling the bundling mechanism. The relative probabilities of bundling vs. crossover are derived for each encounter angle based on the minimization of energies associated with each event. For the bundling mechanism, this includes the chemical energy associated with cross-linker proteins, in addition to the mechanical energies based on the bending elasticity of CMTs. Their results show that bundling probability decreases monotonically with collision angle, in line with the experimental data in Dixit and Cyr (2004).

There are also studies that focus solely on the mechanical properties of CMTs, particularly their elasticity. Lagomarsino *et al.* (2007) studied microtubules grown within microfabricated chambers of cellular dimensions and characterized their organization based on microtubule length, elasticity and the geometric constraints imposed by the chamber. Although their objective is to discover the effects of these factors on array orientation, we classify their model as an interaction model that practically considers a single CMT represented by its length and elasticity confined in an area with a certain geometry and size. They compare the theoretical bending energies corresponding to transverse vs. longitudinal orientations and estimate the preferred

orientation with respect to the CMT length and size of the cylindrical surface of the cell. Their results show that longitudinal helices are favored for long filaments and large aspect ratios of the cell, whereas transverse helices may be favored for shorter microtubules. However, the minimal energy configuration is found to be neither a helix nor a transverse array, but rather an oscillating one where the CMTs cross back and forth between the two end walls of the cylinder. This result holds regardless of the edge properties at the end walls. Overall, the authors conclude that microtubule elasticity and cell geometry fail to explain the typical CMT transverse orientation, indicating the need for active mechanisms such as CMT interactions for the emergence of standard CMT organization. In general, incorporation of the mechanical aspects of CMTs into organization-oriented models might provide further insights that neither type of modeling currently does.

CHAPTER III

MATHEMATICAL FRAMEWORK AND SIMULATION MODEL

As discussed in Chapter II, CMT system is a complex system that exhibits properties that can not be described from its interconnected individual parts. Due to highly nonlinear interactions in addition to multi-dimensionality of the problem considered with its spatio-temporal properties, it is challenging to build a theory that will directly result in a mathematical model and closed-form solutions. As a result, we employ computational techniques to model and simulate the system according to the mechanisms and parameters derived by biological experiments.

Another challenge related to the analysis of the CMT system is regarding the interpretation of simulation results. For this, we develop methods to characterize different system properties, particularly organization. Using these system metrics, we compare the results for different scenarios by varying input parameters of the simulation. A framework of the approach taken for development of the simulation model, quantification methods and related analysis is provided in Figure 8. Note that this is a part of the general framework provided in Figure 7 of Chapter I that corresponds to the scope of the current chapter.

We begin by developing a mathematical notation and framework for the CMT system which is employed in the rest of the dissertation. We present it in its most generalized form, however we will note when we use different versions of this notation for the sake of simplicity while formulating different models. We also include some modeling details of the processes defined in Chapter I based on experimental data.

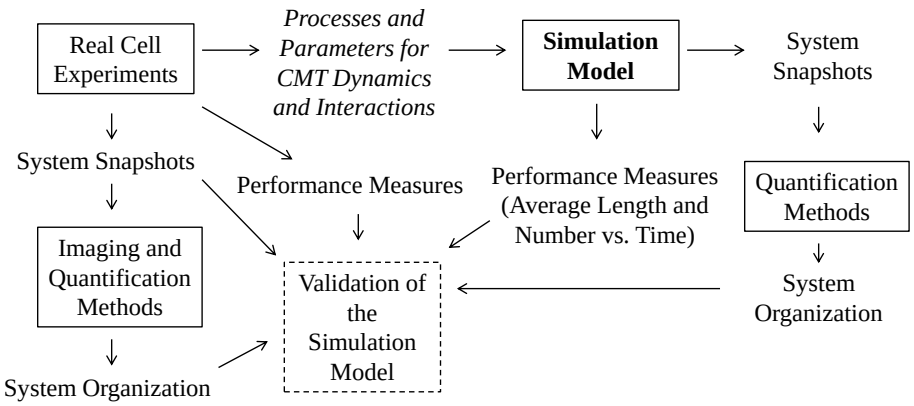

Fig. 8. A Framework of the Simulation and Quantification Methodologies

III.1. Mathematical Framework and Notation

Let us indicate CMTs by $i = 1, ..., I(t)$, where $I(t)$ is the total number of CMTs in the system at time t. Note that a CMT can have more than one segment as a result of bundling with other CMTs. Let $N_i(t)$ be the number of segments of CMT i at time t, for all $i = 1, 2, ..., I(t)$. We denote the orientation and length of n^{th} segment of the i^{th} CMT at time t by $\theta_i^n(t)$ and $l_i^n(t)$ respectively, where $\theta_i^n(t) \in \Phi^{360} = \{0^o, 1^o, ..., 359^o\}$ (see Figure 9 for a representative sketch). Note that the segments of CMTs are counted according to the order they appear. Hence, the leading end of CMT i is located at its $N_i(t)^{th}$ segment at time t, whereas the lagging end is always at the first segment. The total length for CMT i at time t is given by $L_i(t) = \sum_{n=1}^{N_i(t)} l_i^n(t)$. Note that a CMT i disappears and departs the system if it shrinks to length zero. It is worth noting that we renumber the indices every time a CMT departs or when a segment disappears due to shortening of the lagging end, which does not affect our analysis.

Dynamics of CMT i is modeled as governed by the environment process $\{M_i(t) :$

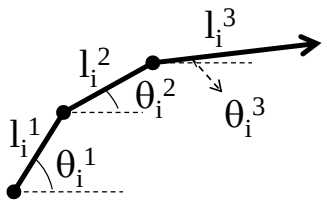

Fig. 9. Sketch of a CMT with Multiple Segments and the Corresponding Variables

$t \geq 0\}$, which corresponds to its state that includes the phases of leading and lagging ends as defined in Chapter I. Experimental data suggests that both ends spend an exponentially distributed amount of time in each phase and switch to one of the other possible phases. Since the transitions are Markovian, the state process can be modeled as a continuous-time Markov chain (CTMC) with an infinitesimal generator matrix $Q = [q_{m,n}]$, $m, n \in \{GS, GP, SS, SP, PS, PP\}$.

We define the individual velocities for each phase of both ends in addition to the net velocities for each state, as they are all required for modeling. The absolute velocities corresponding to each phase are given by the matrix $v^+ = diag(v_{G^+}, v_{S^+}, v_{P^+})$ for the leading end, and by the matrix $v^- = diag(v_{S^-}, v_{P^-})$ for the lagging end, where $diag(\cdot)$ stands for a diagonal matrix with its corresponding diagonal entries starting in the upper left corner. Note that $v_{P^+} = v_{P^-} = 0$, since the velocity is zero in the pause phase. As a result, we can define a diagonal net velocity matrix $V = diag(v^m) = diag(v_{G^+} - v_{S^-}, v_{G^+}, -v_{S^+} - v_{S^-}, -v_{S^+}, -v_{S^-}, 0)$ that composes of the net velocities for each state $m \in \{GS, GP, SS, SP, PS, PP\}$, which are generated according to Q.

We next present CMT interactions in more detail and define the related parameters. It is possible to state some basic rules to explain the CMT interactions based on the experimental data. The outcome of any interaction depends on the collision

angle, α, and a critical interaction angle specific to the system, θ^c. If a CMT runs into another one (barrier) with a collision angle that is less than the critical interaction angle, i.e. $\alpha \leq \theta^c$ (see Figure 10), bundling occurs with probability p_b and results in generation of an additional segment with a parallel orientation to that of the barrier. As a result, the leading end is located at the tip of the new segment, whereas the lagging end stays at its original location on the already existing segment. If the collision angle is greater than the critical interaction angle, i.e. $\alpha > \theta^c$, the CMT undergoes catastrophe with probability p_c. For both cases, if the probabilities do not hold, i.e. with probability $(1 - p_b)$ for the $\alpha \leq \theta^c$ case and with probability $(1 - p_c)$ for the $\alpha > \theta^c$ case, the CMT crosses over the barrier neither changing its orientation nor state (see Figure 10).

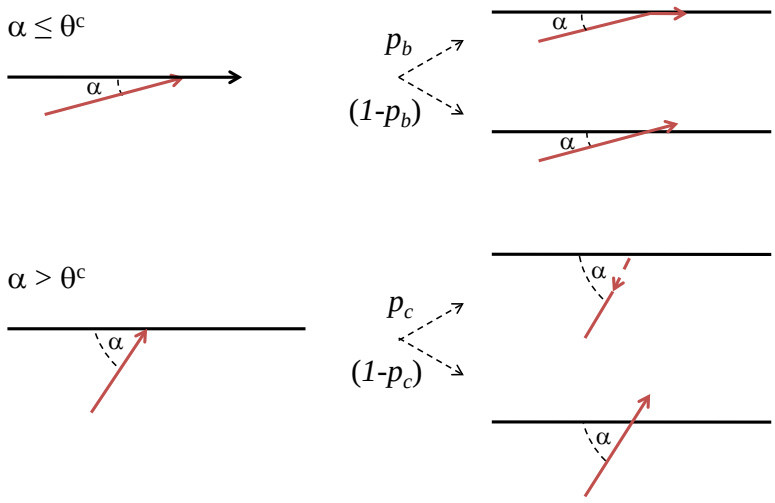

Fig. 10. Events Induced by CMT Interactions

In summary, the matrices Q and V are the parameters related to single CMT dynamics, and the interaction parameters include θ^c, p_b, and p_c. Additionally, new

Table 2. Problem Parameters

Notation	Parameter
Dynamicity Parameters	
$Q = [q_{m,n}]$	infinitesimal generator for the state process
$V = diag(v^m)$	velocity matrix for the CMT states
Interaction Parameters	
θ^c	critical interaction angle
p_b	bundling probability
p_c	catastrophe probability
Parameters Related to the Arrival Process and Initial Conditions	
λ_a	appearance rate for new CMTs
l_0	initial length of an appearing CMT
$I(0)$	initial number of CMTs in the system

CMTs are introduced into the system following a Poisson process with an appearance rate of λ_a. The initial length of any CMT, l_0, is typically tiny and the initial angle (orientation) assigned to it belongs to the set Φ^{360}. Initially there are $I(0)$ CMTs in the system with a length of l_0, and orientation for each CMT sampled from a discrete uniform distribution. The complete set of input parameters including the ones for the initial conditions of the system is given in Table 2. These parameters can take on different values depending on the plant type, genetics and environmental conditions.

Having described the properties and notation for the system that we consider as well as the input parameters, our main objective is to develop methodologies to discover the effects of these simple parameters on characteristics of the whole system. In other words, given the parameters for dynamics and interactions of CMTs as well as the initial conditions at time $t = 0$, we are interested in predicting properties of

the set of CMTs in time such as

- whether they achieve self-organization in time,
- the expected number of CMTs in the system at time $t > 0$,
- the expected average length of CMTs in the system at time $t > 0$.

Having defined the input parameters of the problem considered, next we discuss some metrics that are used to quantify system properties, which will be the output measures of the developed methods.

III.2. Metrics for Quantification of System Properties

In order to characterize system organization, we first describe angular distributions of CMTs weighted with respect to their length. We weigh this measure with respect to the CMT length as a longer CMT plays a more important role in the system dynamics and structure compared to relatively shorter ones. We classify CMT segments according to their orientation, so that each segment belongs to one of the classes θ' $\in \Phi^{180} = \{0, ..., 179\}$. For this, each segment with $\theta_i^n(t)$ in $\{0^o, ..., 179^o\}$ is assigned to the same class as its angle, whereas each segment with $\theta_i^n(t)$ in $\{180^o, ..., 359^o\}$ is mapped to class $\theta_i^n(t) - 180$. In other words, we distinguish CMT segments by their slopes rather than their exact orientations, as their alignment is the actual determinant of the organization level. For each $\theta' \in \Phi^{180}$, we calculate

$$k(\theta', t) = \frac{\sum_{i=1}^{I(t)} \sum_{n=1}^{N_i(t)} l_i^n(t) 1_{\{\theta_i^n(t) \to \theta'\}}}{\sum_{i=1}^{I(t)} \sum_{n=1}^{N_i(t)} l_i^n(t)}, \tag{1}$$

where $1_{\{\theta_i^n(t) \to \theta'\}}$ stands for the indicator function of whether the angle $\theta_i^n(t)$ belongs to class θ'. Note that Equation (1) represents the ratio of the total length of segments which belong to class θ' to the total length of all CMT segments in the system at

time t.

In order to characterize the angular distribution of CMTs, we employ Shannon's entropy formula (Martin *et al.*, 2006; Shannon, 1948), which quantifies the diversity or uniformity level of a system for any property of interest (Gray, 1990; Lu *et al.*, 2008). Applying the entropy metric on the angle distributions of CMTs given by Equation (1), entropy of the system at time t, $H(t)$, is given by

$$H(t) = -\sum_{\theta'=0}^{179} k(\theta', t) ln\left(k(\theta', t)\right). \tag{2}$$

Note that the entropy value would approach its maximum value of $-\ln(1/180) = 5.19$ if CMTs were perfectly uniformly distributed with respect to their alignment and a minimum value of 0 if all CMTs had the same alignment. As entropy scale is logarithmic, relatively small changes in larger values of entropy imply relatively large changes in CMT organization.

Some other performance measures that we use to characterize the set of CMTs are the total number of CMTs in the system and the average CMT length over time. Total number of CMTs present in the system at time t is given by $I(t)$ as described in Section III.1, and the average CMT length at time t is given by

$$\bar{L}(t) = \frac{\sum_{i=1}^{I(t)} \sum_{n=1}^{N_i(t)} l_i^n(t)}{I(t)}. \tag{3}$$

Those two metrics can also be used to define the total CMT length in the system by

$$\sum L(t) = I(t)\bar{L}(t), \tag{4}$$

which also gives a measure of the crowdedness (or density) of CMTs for a given area.

We utilize these metrics to quantify organization, characterize system behavior and properties for the outputs of the simulation model that we develop. The entropy

metric is also used as a Lyapunov function for the stability analysis of the proposed mean-field model equations, that we will discuss in Chapter IV. Further, we develop methodologies to predict expected values of some of these metrics efficiently utilizing simulation and analytical approaches based on some fluid models, which is the subject of Chapter V.

III.3. Simulation Model and Results

Based on the system description in Section I.2, we developed a simulation model that replicates the dynamics and interactions between CMTs. We consider dynamics of all CMTs as being stochastically identical in the absence of any interactions. A CMT is modeled as a line segment that can grow multiple segments as a result of bundling. On the other hand, a CMT segment can be eliminated as a result of shortening to zero length.

We model a setting where the CMTs reside on a planar area, as they are attached to the cell surface. This two-dimensional surface corresponds to the lateral surface of a cylinder, which is closest to the shape of a plant cell (see Figure 5), although our methodology would not be affected by the shape considered. We model the edges of this surface as *periodic* edges which are defined as follows: Any CMT that encounters a periodic edge appears from the opposite edge continuing its original dynamics. This also results in formation of an additional segment for simulation purposes, although this new segment is only a continuation of the original one. In certain simulations, we additionally model *catastrophe-inducing* edges in line with the cylindrical cell shape considered (see Figure 5). In that case, two opposite edges of the planar surface that correspond to the circumference of the top and bottom of the cylinder induce catastrophe such that any CMT leading end encountering one of

those edges immediately switches from growth phase to shortening.

III.3.1. Derivation of Input Parameters

We derive input parameter values based on experimental data from plant cell studies. Table 3 lists raw data used, including the frequency of transitions between phases (K_{i-j}, $i, j \in \{G, S, P\}$), the percentage of time spent and velocity in each phase of the leading and lagging ends. We use "Time in Phase" data to estimate steady-state probabilities in phases, π_G^+, π_S^+, π_P^+ for the leading end; and π_S^-, π_P^- for the lagging end. The elements of the Q matrix are estimated according to

$$K_{i-j}^+ = \pi_i^+ q_{ij}^+$$
$$K_{i-j}^- = \pi_i^- q_{ij}^-$$

where K_{i-j}^+, q_{ij}^+ are used to denote the transition rates for the phases of the leading end; and K_{i-j}^-, q_{ij}^- stand for the rates of the lagging end. The Q matrix is constructed using q_{ij}^+ and q_{ij}^- values.

The first two columns of Table 3 include the data set that we refer to as the *baseline* scenario (shown as I) which is based on Shaw *et al.* (2003). It leads to a Q matrix given by

$$Q = \begin{bmatrix} -8.925 & 6.72 & 1.485 & 0 & 0.72 & 0 \\ 2.427 & -4.632 & 0 & 1.485 & 0 & 0.72 \\ 3.537 & 0 & -11.192 & 6.72 & 0.935 & 0 \\ 0 & 3.537 & 2.427 & -6.898 & 0 & 0.935 \\ 5.05 & 0 & 2.376 & 0 & -14.1 & 6.72 \\ 0 & 5.05 & 0 & 2.376 & 2.427 & -9.85 \end{bmatrix}.$$

Note that the velocities for each phase are given as intervals $A_i \pm B_i$ median of

Table 3. Raw Data for CMT Dynamics

	Lagging End	**Leading End**				
	I	I	II	III	IV	V
Transitions (events per min.)						
K_{G-S}	0.52	0.97	0.17	1.59	0.38	0.82
K_{G-P}	0.28	0.47	0.2	0.38	0.2	0.96
K_{P-G}	0.26	0.51	2.01	1.4	1.56	0.7
K_{P-S}	1.3	0.24	1.02	0.7	0.56	0.62
K_{S-P}	1.09	0.23	0.31	0.44	0.59	1.21
K_{S-G}	0.59	0.87	1	1.99	1.18	0.61
Time in phase						
Growth	8.4%	65.3%	72.0%	68.0%	71.0%	35.0%
Pause	66.3%	10.1%	8.0%	16.0%	10.0%	45.0%
Shorten	25.3%	24.6%	20.0%	16.0%	19.0%	20.0%
Velocities (μm/min.)						
Growth	-	3.69±1.9	3.5±1.9	6.5±3.5	2.5±1.5	2±1.5
Shortening	2.78±2.13	5.88±5.07	9±5.8	12.4±9.3	6.2±4.3	3.8±3.1

which is taken as the average value. In fact, experimental data shows that phase velocities are distributed normally. Accordingly, we sample the velocities for each phase i from a normal distribution with mean $\mu_i = A_i$ and standard deviation $\sigma_i = B_i/3$ every time one of the ends of a CMT transitions into a new phase in our simulations. However, it is worth noting that we disregard the standard deviation values in our analytical models, as they are relatively small compared to their mean values resulting in an ignorable squared coefficient of variation ($\ll 1$). It is also verified by simulations that their omittance do not cause any remarkable changes. Hence, we use only the mean values of the velocities which results in the velocity matrix $V = diag(0.91, 3.69, -8.66, -5.88, -2.78, 0)$.

The interaction parameters for the baseline scenario are given by $\theta^c = 40^o$; $p_b = 1$; $p_c = 0.3$. That is, all the collisions with an angle less than 40^o result in a bundling event, whereas the collisions with an angle greater than 40^o result in a catastrophe with 0.3 probability and a crossover with 0.7 probability.

There are no exact data for the initial conditions of the CMT system as well as the appearance rate of new CMTs. We determine these parameters based on trials with several different values and assessing the proximity of simulation outputs to the properties seen in living cells. According to this, the appearance rate is set as 100 CMTs per min. and the initial length for newly appearing CMTs is 0.1 μm; i.e. $\lambda_a = 100$, $l_0 = 0.1$. Simulations are started with 100 CMTs ($I(0) = 100$) of length l_0 at state PP where both ends are pausing.

The last four columns of Table 3 include data for leading end dynamics corresponding to different mutants and different environmental conditions from relevant literature (Kawamura and Wasteneys, 2008). The corresponding input parameters are listed in Appendix A. Having described derivation of input parameters, we next discuss the configuration and algorithm for simulations.

III.3.2. Configuration and Algorithm

We developed a simulation algorithm that was implemented in MATLAB. CMTs are introduced into the system as tiny line segments with a random orientation at an arbitrary location over a planar surface of 30 μm by 50 μm, which falls in the range for a typical plant cell size. The simulation works iteratively by considering each CMT in a sequential order at each time step. According to the state of the CMT, its coordinates and segments are updated considering the possibility of interactions, if its leading end is at the growth phase. As a result, the snapshot and metrics of the system are updated and recorded at each time step, which is set as a minute.

An outline of the main steps of the simulation is given in Algorithm III.1.

Algorithm III.1. *(Simulation Algorithm)*

0: FOR t FROM 0 TO MAXTIME BY Δt DO

1: FOR i FROM 1 TO I(t) DO

2:$t2 = t$*;*

3: WHILE $t_2 < (t + \Delta t)$ *DO*

//Leading end dynamics:

4: IF $M_i(t_2) = GS$ *OR* $M_i(t_2) = GP$ *THEN //in growth phase*

5: Update the coordinates of CMT i according to its growth velocity and time;

//Interactions with other CMTs:

6: FOR j FROM 1 TO I(t) DO

7: IF $j \neq i$ *THEN //a CMT cannot interact with itself*

8: FOR n FROM 1 TO $N_j(t_2)$ *DO //consider all segments*

9: IF $\tan(\theta_i^{N_i(t_2)}) \neq \tan(\theta_j^n)$ *THEN //eliminate the segments that have the same slope as CMT i*

10: IF the segments are intersecting inside the surface limits THEN

11: Calculate the collision angle, α*;*

12: IF $\alpha \leq \theta^c$ *THEN*

13: $p = RAND()$*; //generate a random variable in* $(0, 1)$

14: IF $p < p_b$ *THEN //bundling occurs*

15: Calculate the collision time t_c *according to the positions of the segments;*

16: Update the coordinates of CMT i to form the new segment;

17: $N_i(t_c) = N_i(t_c) + 1$*; //segment number of CMT i is increased by 1*

18: END IF

19: ELSE //$\alpha > \theta^c$

20: $p = RAND()$*; //generate a random variable in* $(0, 1)$

21: IF $p < p_c$ *THEN //catastrophe occurs*

22: Calculate the collision time t_c *according to the positions of the segments;*

23: $M_i(t_c) = SS$ *or* $M_i(t_c) = SP$ *//update state by changing the phase of the leading*

end while keeping the lagging end at its original phase

24: Assign a time for shortening;

25: END IF

26: END IF

27: END IF

28: END IF

29: END FOR

30: END IF

31: END FOR

32: Update t_2*;*

33: Check interactions with surface edges, and update the coordinates accordingly;

34: END IF

35: IF $M_i(t_2) = SS$ *OR* $M_i(t_2) = SP$ *THEN //leading end in shortening phase*

36: Calculate the shortening distance until $\min\{t + \Delta t,$ *end of shortening phase*$\}$*;*

37: Calculate $l_i^{N_i(t_2)}(t_2)$*;//the length of the segment that contains the leading end*

38: IF shortening distance > segment length THEN //shortening distance exceeds the segment length

39: WHILE $N_i(t_2) > 1$ *AND shortening distance > segment length DO*

40: Eliminate segment;

41: $N_i(t_2) = N_i(t_2) - 1$*; //segment number of CMT i is decreased by 1*

42: Update t_2*;*

43: Update shortening distance and $l_i^{N_i(t_2)}(t_2)$*;*

44: END WHILE

45: IF $N_i(t_2) == 1$ *THEN*

46: IF shortening distance > segment length THEN

47: Eliminate CMT completely;

48: Update t_2;

49: $I(t_2) = I(t_2) - 1$; //number of CMTs is decreased by 1

50: ELSE

51: Update the coordinates of CMT i according to the shortening distance;

52: END IF

53: END IF

54: END IF

55: END IF

56: //If in pause phase, do nothing.

57: If the phase is ending before time t_2, assign new state and sojourn time, and update velocities;

58: Update t_2;

59: END WHILE

60: Consider the dynamics of the lagging end similarly (shortening and pause phases);

61: END FOR

62: Introduce new CMTs that appear between time t and time $t + \Delta t$ at an arbitrary location; assign a random orientation; implement their dynamics and interactions;

63: Record system snapshot and system metrics, $I(t)$, $\bar{L}(t)$, and $H(t)$;

64: Update $t = t + \Delta t$;

65: END FOR

III.3.3. Results

Using simulations with the baseline scenario, we were able to replicate the CMT organization seen in the plant cells. Snapshots of the system at different time points (from 0 to $500^t h$ minute) for a sample simulation run are provided in Figure 11.

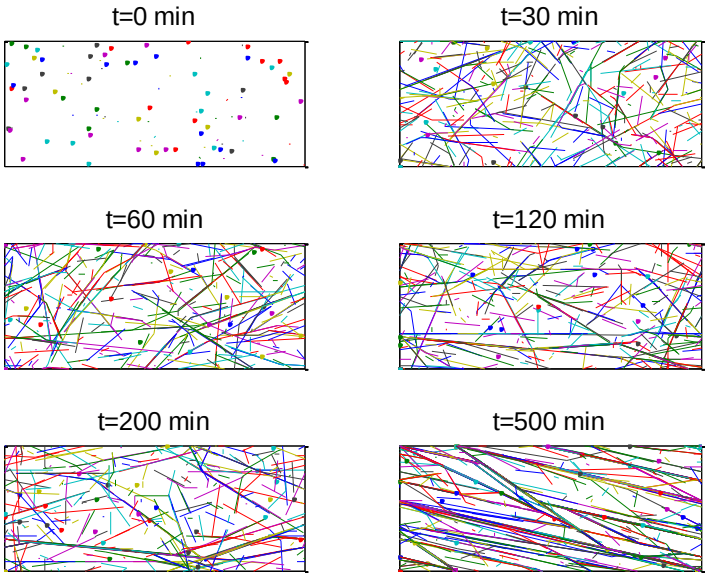

Fig. 11. Snapshots of the Simulated CMT System at Different Time Points

The course of organization observed in simulations is as follows: The system begins with a certain amount of tiny CMTs growing at random directions. They grow into a highly disorganized array early in the process. However, over time, they become more crowded and longer on average, and as a result they start to interact with each other, continuously transforming into better ordered arrays as seen in living cells.

An analysis of the angle distributions over time shows similar course of organization (see Figure 12) as seen in the snapshots. In the beginning, CMT angles are scattered akin to a uniform distribution. As time passes, they cluster around a few dominant orientations. Those dominant angles subsequently become more pronounced although they can fluctuate to some degree. These observations are also supported by the entropy plots, which show a continuous decrease in value (followed by a small increase early in the simulations), indicating increased organization over

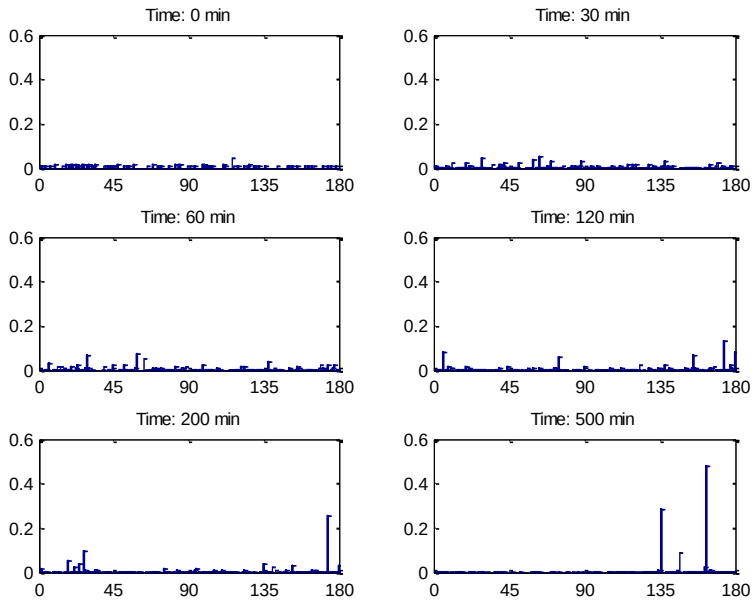

Fig. 12. Angle Distribution Plots for the Simulated CMT System

time. Figure 13 shows entropy plots for ten independent runs of the simulation model for the baseline scenario. Note that the time units are in minutes unless otherwise stated.

Having observed CMT organization and related metrics produced by baseline simulations, we next discuss results for other system metrics that we defined in Section III.2. It is observed that both total number and average length of CMTs begin to increase quickly early in simulations (see Figure 14). This is quite intuitive as input parameters of the baseline scenario suggest a positive net growth on average, and the appearance rate of new CMTs in the system is set to a relatively high value. However, as CMTs grow longer and begin to interact with each other, the rate of increase for $I(t)$ and $\bar{L}(t)$ start to decrease. It is observed that those metrics *temporarily stabilize* such that they tend to stay roughly constant beginning around the time the interaction frequencies reach their peak. After stabilizing for a limited amount of time, as

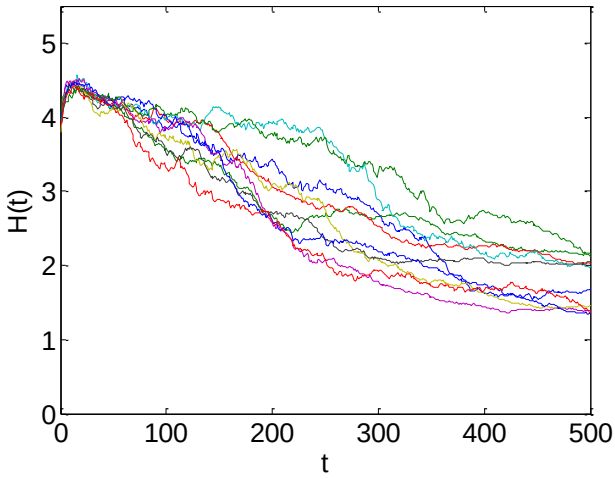

Fig. 13. $H(t)$ vs. t for Multiple Independent Runs of the Simulation

the organization is settled to a certain degree, they continue to increase indefinitely. We will refer to this notion as "pseudo-stabilization" of system metrics. This trend can be explained in a relation to the frequency of interactions among CMTs, particularly that of catastrophes. The catastrophe frequency in the system keeps varying over time according to the course of organization and has a direct effect on regulating length and number of CMTs in the system by controlling the transition rate from growth to shortening in a dynamic manner. As seen in Figure 15, catastrophe frequency per CMT, $c(t)$, initially keeps increasing until it reaches a peak, and stays around this high value, after which it starts decreasing. The eventual decline is a result of the fact that CMTs encounter catastrophe much less frequently as the system gets better organized in time.

Having tested the simulation model with a baseline scenario, we next try different parameter sets to analyze effects of dynamics and interactions on system properties and organization. These include altering dynamicity parameters; eliminating impacts

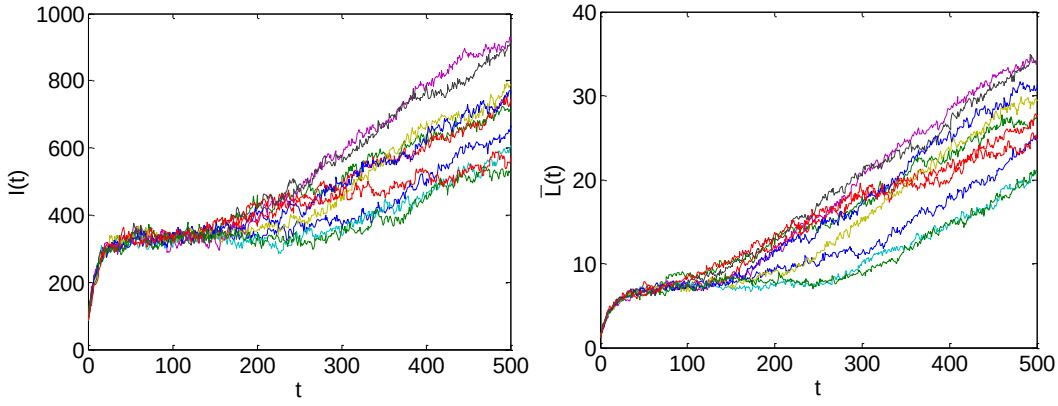

Fig. 14. $\bar{L}(t)$ vs. t and $I(t)$ vs. t for Multiple Independent Runs of Simulation

of interactions, i.e. bundling and/or catastrophe events, via setting $p_b = 0$ and/or $p_c = 0$; changing impacts of interactions by selection of a different critical angle, θ^c, or p_b, p_c. In the following we discuss major results and observations that are mostly relevant for the entirety of this dissertation. Remainder of the analysis is presented in Appendix B. For some further details and biological interpretation of results, the reader is referred to Eren *et al.* (2010).

III.3.3.1. Effects of Interactions on System Metrics

In order to assess the role of interactions on CMT array organization, we modeled a scenario where CMT interactions are eliminated. In other words, all bundling and catastrophic collisions are replaced by cross-over events ($p_b = p_c = 0$). We observed that CMTs fail to self-organize into ordered arrays in the absence of interactions as seen in Figure 16. Unlike simulations with interactions, entropy values do not decrease but rather increase and approach the maximum suggesting a uniform distribution of CMT orientations and accordingly a disorganized system (see Figure 17).

A side effect of elimination of interactions is that CMTs become more crowded

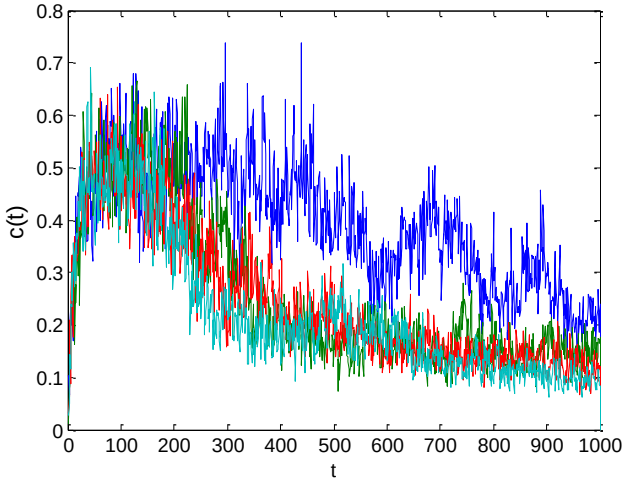

Fig. 15. Graph of $c(t)$ vs. t for Multiple Independent Runs of Simulation

and longer in time as long as the parameters for CMT dynamics fall under the region of unbounded growth with a positive average net velocity (see Figure 18). Also, simulation runs with no interactions show much less variability among system metrics of independent runs compared to the simulations with interactions. Interactions are observed to increase the variation between system metrics, pronounced especially after CMTs grow long enough to interact with each other (see Figures 13 and 14).

We have also investigated relative contributions of bundling vs. catastrophe events to CMT organization by setting $p_c = 0$ and $p_b = 0$ in relative order. That is, each mechanism is replaced by "crossover" when eliminated. Simulations with no bundling show much less ordering compared with simulations that have both interaction mechanisms present. Eliminating catastrophic collisions have a less significant impact on CMT organization relative to the bundling as suggested by the entropy plots (see Figure 19). However, results show that catastrophes have a major role in regulating the number and length of the CMTs in the system, which in turn con-

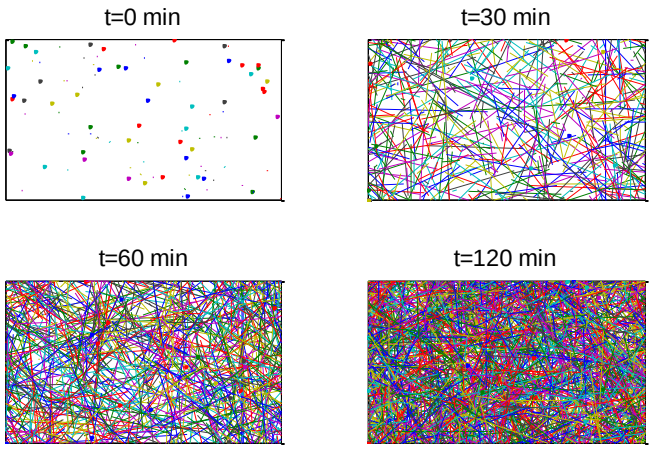

Fig. 16. Snapshots of the Simulated CMT System without Interactions

tributes to the characteristics of the system including organization. In fact, simulations with no catastrophes result in average length and number values quite similar to the case with no interactions as seen in Figure 20 (compare with Figure 18). On the other hand, when only bundling is eliminated, the average length and number values stay even lower than those in the baseline case, as catastrophes continue to occur at a relatively high frequency when the CMTs stay oriented dissimilarly due to the lack of bundling (see Figure 21, compare to Figures 14 and 20).

We observed that the system organization is mostly robust to the values of p_b and p_c as long as they are not set to zero and dynamicity parameters ensure a growing system on average. That can be explained by the fact that, CMTs would continue colliding with each other and encounter the impact of interactions eventually as long as they keep growing regardless of interaction parameters. Small changes in the critical interaction angle (in the range of 0^o to 10^o) also does not affect CMT organization. However, larger changes in θ^c lead to weaker organization, although organization is still achieved. Setting θ^c to 20^o results in relatively shorter CMTs and poor organi-

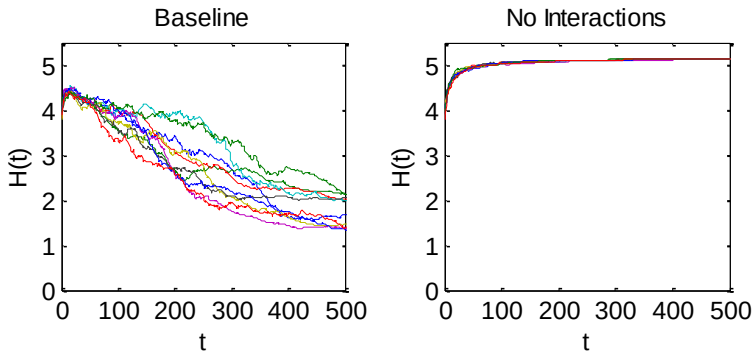

Fig. 17. Comparison of Entropy Plots for Simulations with and without Interactions

zation compared to the control simulations (Figure 22). On the other hand, a larger θ^c (such as 60^o) caused CMTs grow longer on average. Although these simulations with larger θ^c initially show faster organization, they eventually stabilize at a higher entropy value than the control simulations (compare Figure 22 with Figure 13). In these experiments that we alter the critical interaction angle, we adjusted the catastrophe frequency so that it is similar to the baseline scenario in order to more reliably evaluate the impacts of changing the angle.

III.3.3.2. Effects of CMT Dynamics on System Metrics

We also tried changing dynamicity parameters in simulations, where we used data from biological experiments that correspond to different mutants tested at different temperatures (Kawamura and Wasteneys, 2008). The input parameter sets are provided in the Appendix A based on the data from Table 3 (II-V). We have another parameter set corresponding to another mutant (Mutant VI) which alters the CMT dynamics such that the lagging end remains static at all times (Burk *et al.*, 2001; Burk and Ye, 2002). Among these cases, only Mutant V failed to achieve organization as CMTs remain too short to interact enough. All other cases resulted in ordered

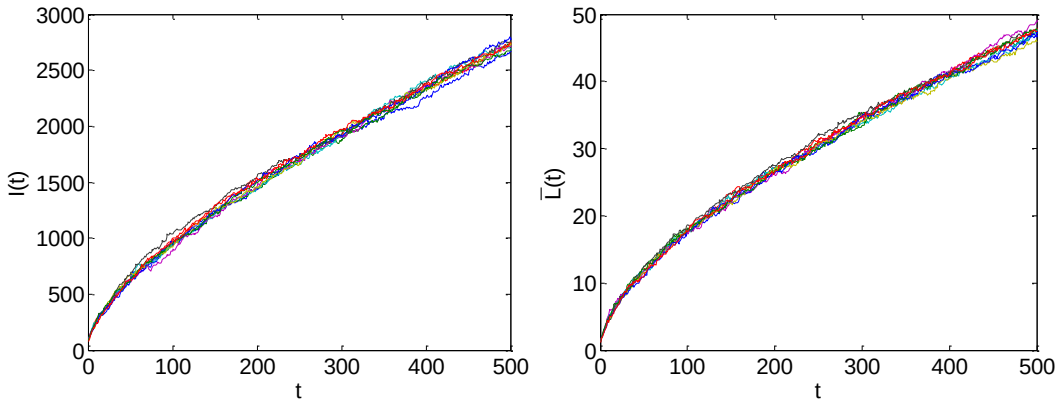

Fig. 18. $\bar{L}(t)$ vs. t and $I(t)$ vs. t for Simulations with No Interactions

arrays although the degree of organization showed variety (Figure 23). The structure seen in each snapshot shows close similarity with the images of CMTs in living cells corresponding to the data set.

It is worth noting that we have also tested different appearance rate parameters in our simulations. Appearance rate has a significant impact on the rate of organization. Overall, having a greater arrival rate of new CMTs into the system speeds up organization, whereas setting it too high distorts the degree of organization achieved.

III.3.3.3. Effects of Surface Edges on System Metrics

As mentioned above, we also model catastrophe-inducing surface edges in line with the cylindrical shape of the plant cell. In that case, the two opposite walls of the planar surface that correspond to the circumference of the top and bottom of the cylinder are assigned as catastrophe-inducing edges. That is, if the leading end of a CMT encounters one of those edges, it immediately switches from growth phase

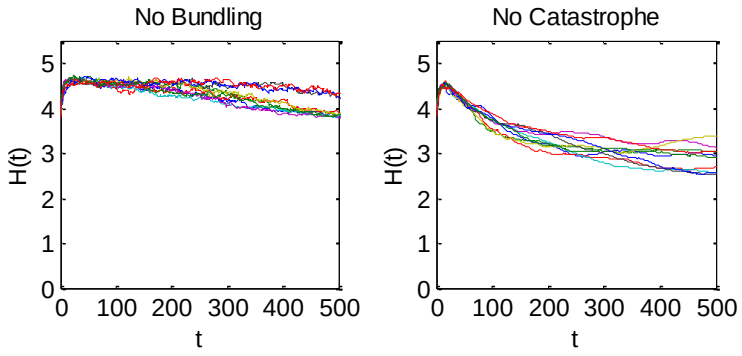

Fig. 19. Comparison of Entropy Plots for Simulations without Bundling and Catastrophes

to shortening. Although this change does not affect the level of organization in the system significantly as long as the simulation area is not set too small, it results in ordering of the overall CMT array in a particular dominant orientation rather than an arbitrary dominant angle. This emergent orientation is selected such that the frequency of running into catastrophe-inducing edges is minimized. A sample snapshot for this setting with the corresponding 3D picture is provided in Figure 24. Figure 25 presents plots of the average angle weighted by the CMT length in time for multiple independent simulations of this case and the baseline scenario. Note that the average angle values are adjusted to fall in the set Φ^{180} instead of Φ^{360} as in quantification of organization so that averaging works properly. As the edge properties are not observed to have a significant effect on the level of organization reached as well as other system metrics that we are interested in, we consider only periodic edges in the rest of the dissertation as described for the baseline scenario.

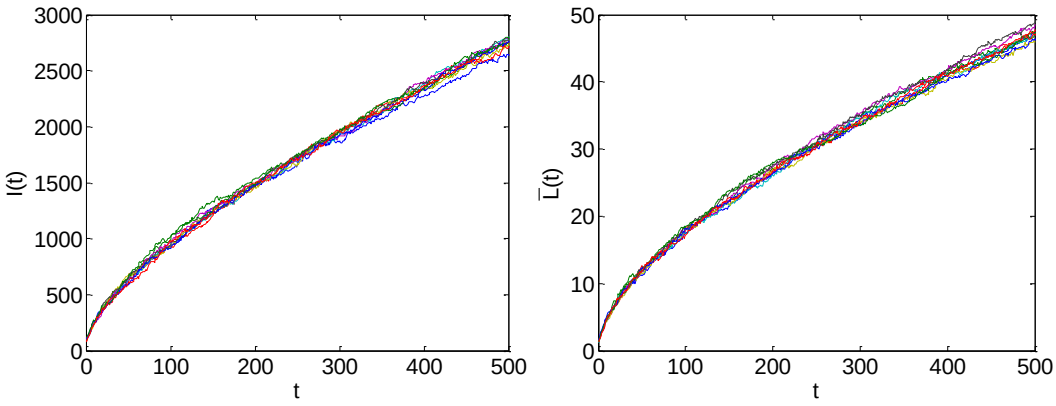

Fig. 20. $\bar{L}(t)$ vs. t and $I(t)$ vs. t for Simulations with No Catastrophe

III.3.4. Validation

Using the simulation algorithm that we developed, it was possible to replicate organization observed in CMT arrays. This is supported by the fact that snapshots from the simulations look similar to the live cell images; and input parameters corresponding to mutant data result in similar output as seen in plant cells. Moreover, the average length metric around the time organization is achieved ($\sim 10\ \mu m$) in the simulations of baseline scenario matches well with the experimentally reported values (8.6-12.4 μm). Finally, the timing around which organization emerges in simulations and plant cells are quite similar (around 120-150 min.).

In order to compare the organization achieved in simulations to that in living cells more quantitatively, we employ the entropy metric introduced in Section III.2 to the live cell images with organized and disorganized CMT arrays and compare the obtained values to the ones in simulations. For this, we implement some imaging techniques in MATLAB, using built-in functions to detect the line segments on a given image. The algorithm that we use and the related functions can be summarized

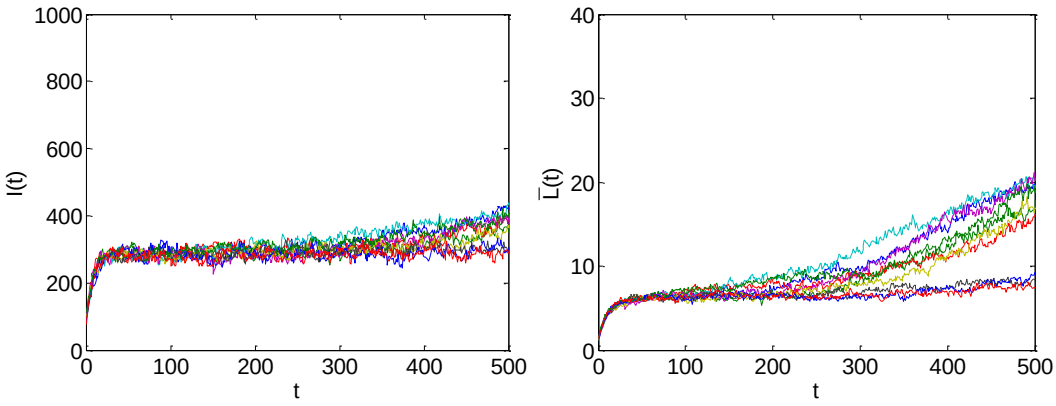

Fig. 21. $\bar{L}(t)$ vs. t and $I(t)$ vs. t for Simulations with No Bundling

as follows:

1. Read the given CMT photo using "imread" function.
2. Convert the image to grayscale using "rgb2gray" function.
3. Detect the edges in the image using "edge" function.
4. Use the "houghpeaks" and "houghlines" functions to form a matrix of the line segments with their coordinates (Shapiro and Stockman, 2001).
5. Calculate the entropy corresponding to the extracted array of line segments.

We calibrate the parameters used for the functions in the algorithm to best capture the CMT arrays in the microscopy images of plant cells. Parameters used for different functions can be listed as follows:

- For the "edge" function, we use "Canny" method (Canny, 1986), as this method is the one that is most robust to noise among different alternatives.
- For the "houghpeaks" function, we set number of peaks as 100.

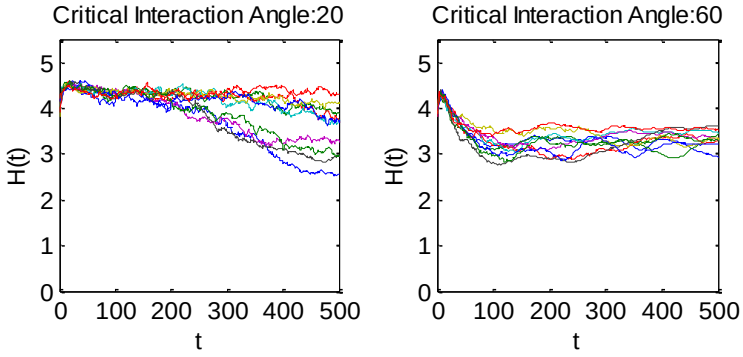

Fig. 22. Comparison of Entropy Plots for Simulations with Different θ^c

- For the "houghlines" function, we set "FillGap" parameter as 4 units, and "MinLength" parameter as 1 unit. That is, the line segments with a distance of less than 4 units are merged together; and merged lines shorter than 1 unit are discarded.

Figures 26 through 29 present CMT snapshots from live cells and their processed images used to calculate corresponding entropy metrics. Figures 26 and 27 show organized CMT arrays with entropy values lower than 3. Studying snapshots and entropy plots of the baseline scenario carefully, CMT entropies corresponding to live cell images are found to be similar to the entropy values seen in simulations after organization is achieved to a significant degree (around $t = 200$) with similarly structured CMT arrays. Figures 28 and 29 correspond to poorly organized CMTs, which match well to the entropy values and CMT snapshots early in baseline simulations (around $t \in [30, 60]$).

III.3.5. Conclusions

Due to the complexity of the problem considered, we first began by developing a detailed simulation algorithm of the CMT system where all the dynamics and interactions in living cells were replicated based on experimental data. Simulations showed similar course of organization as observed in plant cell CMT arrays, ending up with emergence of a dominant orientation where most of the CMTs are aligned according to it. We introduced metrics to quantitatively compare organization and other system characteristics seen in different scenarios. Simulations were also able to reproduce similar structure observed in plant cell experiments corresponding to parameter sets of different mutants, etc. We investigated effects of dynamicity and interaction parameters on system organization and other properties such as CMT number and length. Overall, our results suggest that:

- Interactions between CMTs are necessary for the self-organization to occur.
- CMTs need to grow long enough to interact for the organization to be achieved. In fact, when the dynamics ensure that the average net velocity for a single CMT is strictly positive, it is observed that interactions are facilitated and organization is achieved independent of interaction and appearance parameters, as long as they are not completely eliminated.
- For organized systems, it is observed that certain metrics such as average length and total number of CMTs *temporarily stabilize* such that they fluctuate around a constant value for a limited amount of time until organization settles to a certain degree, after which they keep increasing ("pseudo-stabilization" of system metrics).
- System organization is robust to small changes in critical interaction angle,

θ^c. However significant changes result in weaker organization, although it still occurs. System organization is also mostly robust to the other interaction parameters, p_b and p_c, as long as they are not set to zero, especially for cases that guarantee a positive net growth on average.

- Bundling mechanism seems to contribute to the organization more directly by reorienting CMTs, whereas catastrophe mechanism is observed to be more effective in regulating average length and number of CMTs by controlling transition rate of the leading ends from growth to shortening.

- Interactions, especially catastrophes, are observed to increase the variation between system metrics of independent runs with the same parameter set. This variation is significantly pronounced after CMTs grow long enough to interact with each other.

- It is observed that CMTs align in a way parallel to the catastrophe-inducing edges (if any) so that they minimize the frequency of running into them. In the case where all surface edges are periodic (baseline scenario), the dominant orientation attains an eventual random value which is roughly uniformly distributed over the range of $[0, 180)$.

Finally, we conducted a comparison of the system generated by simulations to the plant cell CMTs using imaging techniques and metrics developed to the extent possible with the available data. The quantitative analysis of live cell images supported the reliability of simulations in line with qualitative comparisons.

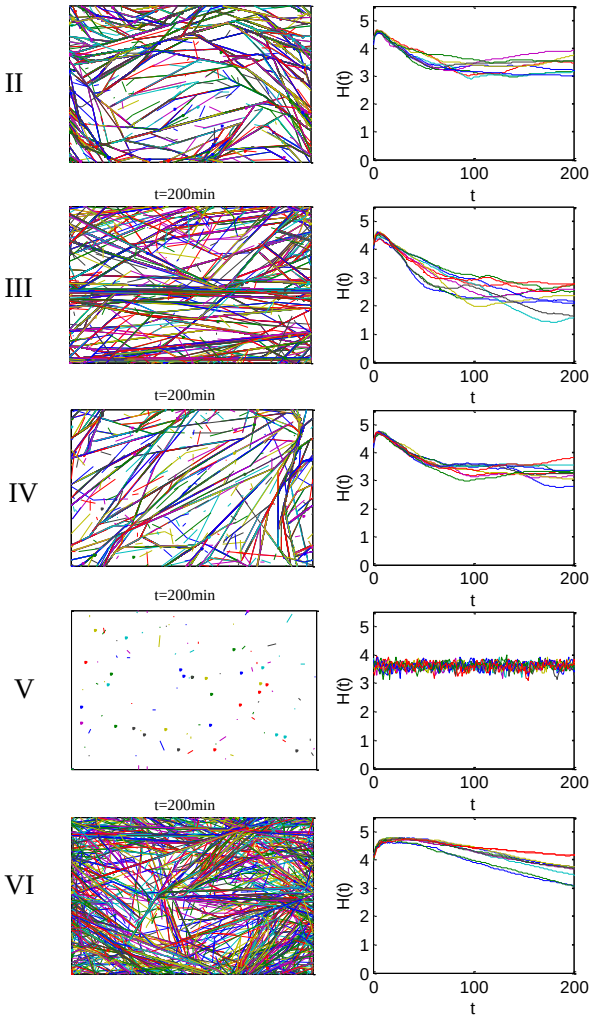

Fig. 23. Snapshots and Entropy Plots for Different Dynamicity Parameters

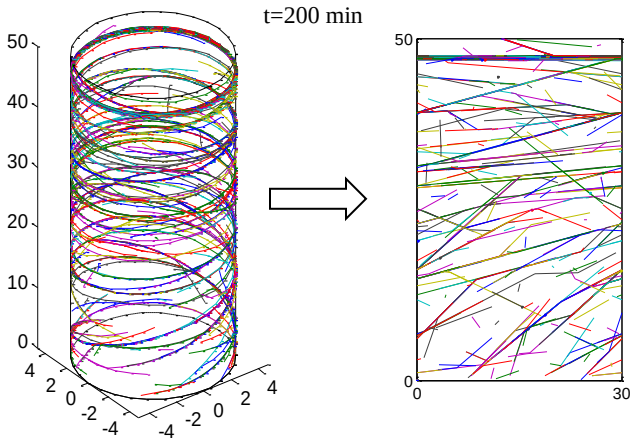

Fig. 24. A Sample Snapshot for a Simulation with Catastrophe-Inducing Edges and Its Corresponding 3D Plot

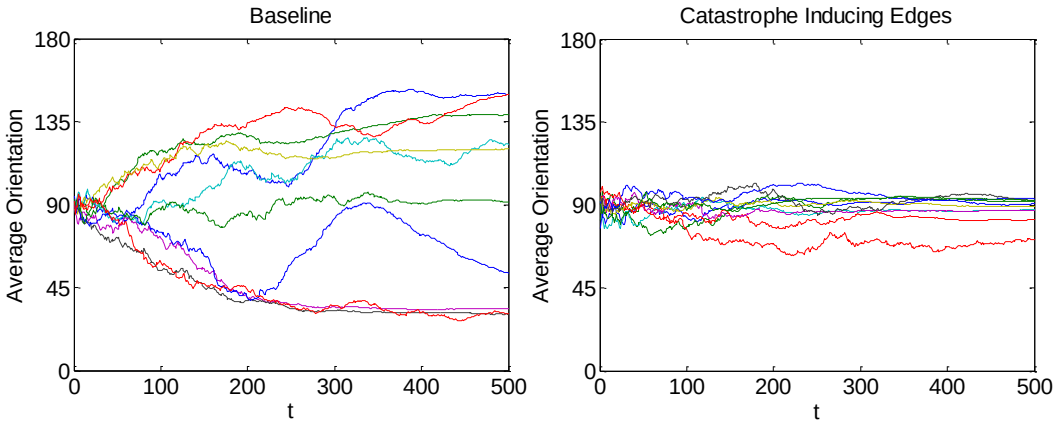

Fig. 25. Average Weighted Angle for Baseline Simulations and Simulations with Catastrophe-Inducing Edges

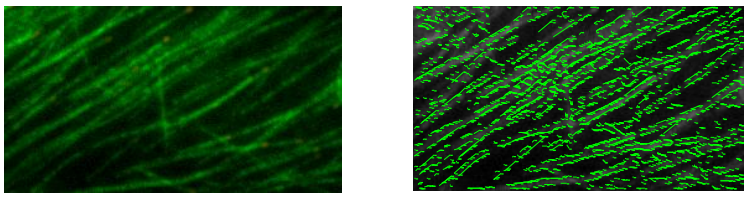

Fig. 26. Real and Processed Image of an Organized CMT Array (Entropy=2.6)

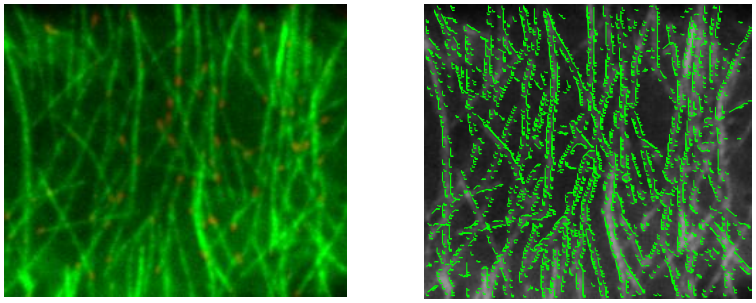

Fig. 27. Real and Processed Image of an Organized CMT Array (Entropy=2.25)

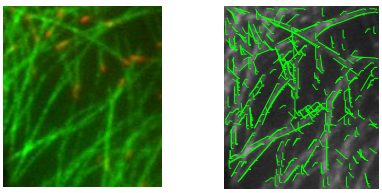

Fig. 28. Real and Processed Image of a Poorly Organized CMT Array (Entropy=3.9)

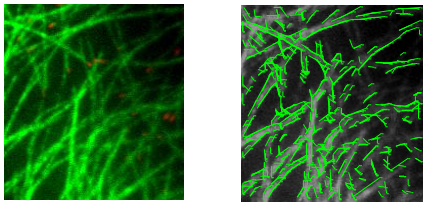

Fig. 29. Real and Processed Image of a Poorly Organized CMT Array (Entropy=4.24)

CHAPTER IV

MEAN-FIELD MODEL FOR CMT ORGANIZATION

Having discussed the simulation model and its major results, we develop more efficient and generalized methodologies to establish relations between input parameters and system characteristics defined in Sections III.1 and III.2. Despite the advantage of incorporating all the details of dynamics and interactions described in Section I.2, and accelerating the tests with different parameters tremendously compared to biological experiments; simulations are still computationally expensive due to the complexity of the system and interaction mechanisms incorporated. Simulating a large number of runs that yields reliably conclusive results requires huge computational time. Therefore, we develop analytical models that aid in development of more efficient techniques as well as generalizing certain results that are conjectured based on simulations. In this chapter, we present a mean-field model for CMT dynamics and interactions, which is used to derive conditions in terms of input parameters that are sufficient to generate organization in the system. We begin by explaining objectives in relation to the observations from the simulation study. The framework corresponding to the analysis in this chapter is provided in Figure 30.

IV.1. Objectives and Relation to the Simulation Results

As explained in Section III.3.3, different system behavior and properties are observed in CMT simulations for varying parameters of dynamicity and interactions. We roughly classify these as three distinct cases. Before introducing this classification of the system structure, we introduce the related terminology that we use in Definitions 1 and 2.

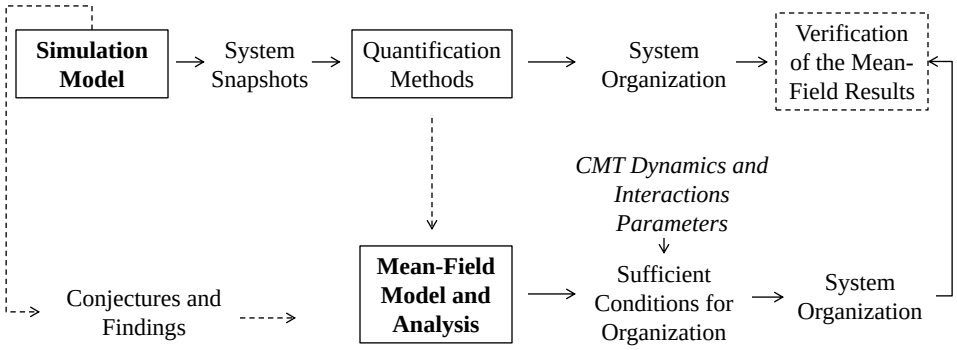

Fig. 30. A Framework of the Mean-Field Model and Analysis

Definition 1. *A CMT system is defined as disorganized if the entropy metric given by Equation (2) satisfies*

$$\lim_{t\to\infty} H(t) = 5.19;$$

and it is defined as organized if the following condition holds

$$\lim_{t\to\infty} H(t) = 0.$$

Definition 2. *A deterministic system metric $G(t)$ (particularly, $I(t)$ or $\bar{L}(t)$) is defined to be stable if*

$$\lim_{t\to\infty} G(t) < \infty;$$

and it is defined to be unstable otherwise, i.e.

$$\lim_{t\to\infty} G(t) = \infty.$$

Our classification of possible system behavior based on simulation results is as follows:

1. *Organized, pseudo-stable* case, where angle distributions of CMTs are biased

towards a dominant angle in time and accordingly entropy values are continuously decreasing; and system metrics such as average length and number of CMTs temporarily stabilize around a constant value after an initial increase. These system metrics tend to increase indefinitely, once a certain degree of organization is achieved.

2. *Disorganized, stable* case, where CMTs stay disorganized with non-decreasing entropy values and a corresponding angle distribution close to uniform; and system metrics stay finite around a rather low value. In such systems, CMTs do not grow long and crowded enough to interact.

3. *Disorganized, unstable* case, where CMTs stay disorganized and system metrics keep increasing indefinitely. In such systems, CMTs do not interact enough to generate organization despite running into each other.

Note that by stability here we refer to the system metrics such as length and number remaining finite over time as described in Definition 2. In fact, each case is stable in terms of angle distributions corresponding to an organized or disorganized system. Sample plots of independent simulation results for all three cases are presented in Figure 31 for better comparison. The plots show realizations of average length of CMTs vs. time, however the realizations for number of CMTs vs. time show quite similar characteristics. Corresponding entropy plots that give a measure of organization level in time are also provided. As a side note, by a queueing analogy to the classical stability conditions for queues, those three cases can be considered roughly similar to $i)\lambda \approx \mu$, $ii)$ $\lambda < \mu$, $iii)$ $\lambda > \mu$, where λ and μ are defined as the arrival rate into the system and the service rate in respective order. Note that for case i, μ would in fact be time-dependent and would approach λ only for a temporary amount of time according to the status of organization. Also, case ii requires λ to be significantly

less than μ, as otherwise the system approaches to a heavy-traffic queue.

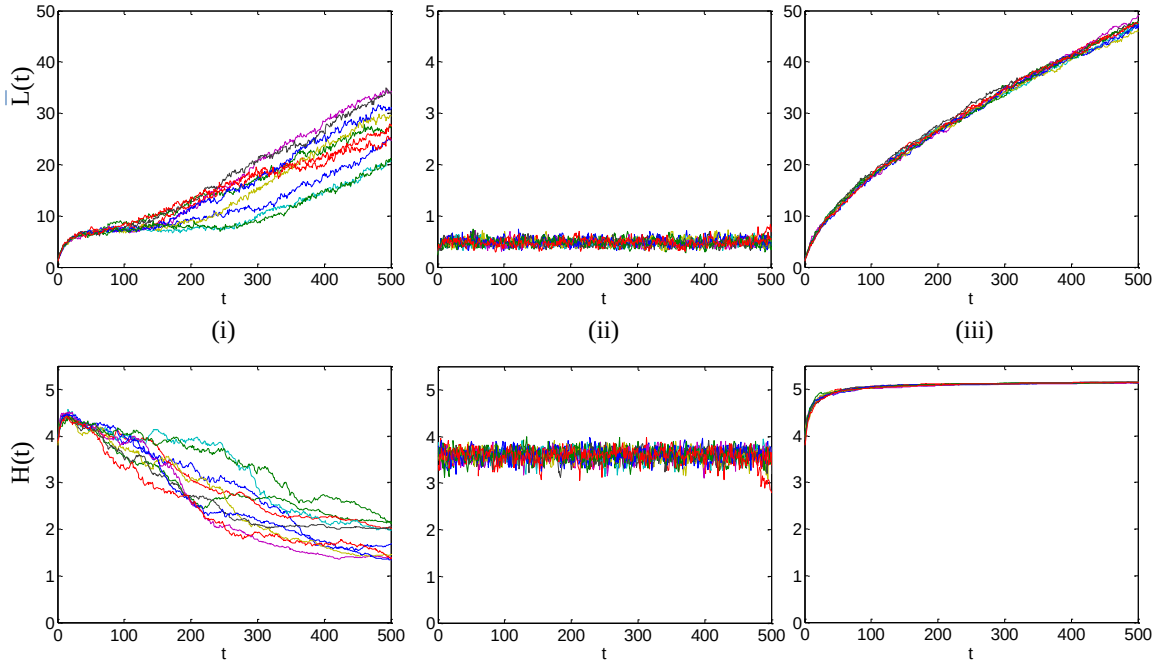

Fig. 31. Sample Average Length and Entropy Plots for Independent Simulations of Cases (i), (ii) and (iii)

Among these three types of systems, the preferred one is case (i). That is in a plant cell, observed system behavior coincides with this case where CMTs exist as organized arrays. This organization may be distorted by a genetic mutation or environmental conditions that cause a change in system parameters, which results in one of the other cases. We are particularly interested in exploring conditions for case (i) to be guaranteed, which would facilitate engineering of settings that will maintain or generate organization in plant cells. Building on our observations from simulations, we continue to establish stronger analytical relations between problem parameters and system properties. Next, we present the mean-field model that we use to derive sufficient conditions for organization to be achieved.

IV.2. Model Equations and Analysis

In this section, we present the formulation for a mean-field model of CMT dynamics and interactions (Section IV.2.1) followed by an equilibria analysis of model equations (Section IV.2.2). We derive sufficient conditions for organization using Lyapunov stability concepts.

IV.2.1. Problem Formulation

We consider a mean-field model where CMTs are distributed around the surface homogeneously. We alter the bundling mechanism for modeling purposes as follows: In case of a bundling event, the colliding CMT of length l completely aligns with the barrier CMT with probability $p_b(l)$ rather than forming a new segment. That is, with a certain probability which is a function of length, the CMT changes its orientation parallel to that of the barrier. As a result, each CMT has only a single segment throughout its lifetime. The bundling probability is considered as a decreasing function of the CMT length to account for the fact that bundling is more likely to be reversible for relatively longer CMTs due to different dynamics at the leading and lagging ends. It is worth noting that this mechanism was tested using simulations and verified not to change the overall system characteristics. Based on these and other properties and notation described in Section I.2, we derive an integro-differential equation system as follows. We define $p_m(l, \theta, t)$ as the density of CMTs with length l and angle θ that are at state m at time t, where $m \in \{GS, GP, SS, SP, PS, PP\}$. For example, $p_{GS}(l, \theta, t)$ stands for the density of CMTs with length l, angle θ that has a growing leading end and shortening lagging end at time t. Recall that $q_{m,n}$ for $m, n \in \{GS, GP, SS, SP, PS, PP\}$ correspond to the elements of the infinitesimal generator matrix, Q; and v^m stands for the velocity in state m. Based on these, model equations

can be stated as:

$$
\begin{aligned}
\frac{\partial p_{GS}(l,\theta,t)}{\partial t} &= -v^{GS}\frac{\partial p_{GS}(l,\theta,t)}{\partial l} + p_{GS}(l,\theta,t)q_{GS,GS} \\
&\quad + p_{SS}(l,\theta,t)q_{SS,GS} + p_{PS}(l,\theta,t)q_{PS,GS} + p_{GP}(l,\theta,t)q_{GP,GS} \\
&\quad - C_s(l,\theta,t) - B_s(l,\theta,t) + B_s^*(l,\theta,t), \\
\frac{\partial p_{GP}(l,\theta,t)}{\partial t} &= -v^{GP}\frac{\partial p_{GP}(l,\theta,t)}{\partial l} + p_{GP}(l,\theta,t)q_{GP,GP} \\
&\quad + p_{SP}(l,\theta,t)q_{SP,GP} + p_{PP}(l,\theta,t)q_{PP,GP} + p_{GS}(l,\theta,t)q_{GS,GP} \\
&\quad - C_p(l,\theta,t) - B_p(l,\theta,t) + B_p^*(l,\theta,t), \\
\frac{\partial p_{SS}(l,\theta,t)}{\partial t} &= -v^{SS}\frac{\partial p_{SS}(l,\theta,t)}{\partial l} + p_{SS}(l,\theta,t)q_{SS,SS} \\
&\quad + p_{GS}(l,\theta,t)q_{GS,SS} + p_{PS}(l,\theta,t)q_{PS,SS} + p_{SP}(l,\theta,t)q_{SP,SS} \\
&\quad + C_s(l,\theta,t) \\
\frac{\partial p_{SP}(l,\theta,t)}{\partial t} &= -v^{SP}\frac{\partial p_{SP}(l,\theta,t)}{\partial l} + p_{SP}(l,\theta,t)q_{SP,SP} \\
&\quad + p_{GP}(l,\theta,t)q_{GP,SP} + p_{PP}(l,\theta,t)q_{PP,SP} + p_{SS}(l,\theta,t)q_{SS,SP} \\
&\quad + C_p(l,\theta,t) \\
\frac{\partial p_{PS}(l,\theta,t)}{\partial t} &= -v^{PS}\frac{\partial p_{PS}(l,\theta,t)}{\partial l} + p_{PS}(l,\theta,t)q_{PS,PS} \\
&\quad + p_{GS}(l,\theta,t)q_{GS,PS} + p_{SS}(l,\theta,t)q_{SS,PS} + p_{PP}(l,\theta,t)q_{PP,PS}, \\
\frac{\partial p_{PP}(l,\theta,t)}{\partial t} &= +p_{PP}(l,\theta,t)q_{PP,PP} \\
&\quad + p_{GP}(l,\theta,t)q_{GP,PP} + p_{SP}(l,\theta,t)q_{SP,PP} + p_{PS}(l,\theta,t)q_{PS,PP},
\end{aligned}
\tag{5}
$$

where $0 < l, t < \infty$ and $\theta \in \Phi^{180} = \{0, 1, ..., 179\}$. Note that we consider only the angles in Φ^{180} as two CMTs with orientation θ and $\theta + 180$ are equivalent in terms of dynamics and interactions (when coordinates are not considered), as well as their contribution to system organization. Formulation of Equation (5) follows considering $p_m(l, \theta, t+\Delta t)$, for each $m \in \{GS, GP, SS, SP, PS, PP\}$, where Δt is a small positive

real number:

$$p_m(l,\theta,t+\Delta t) = p_m(l-v^m\Delta t,\theta,t)(1+q_{m,m}\Delta t)+\sum_{n\neq m} p_n(l-v^n\Delta t,\theta,t)q_{n,m}\Delta t+o(\Delta t). \tag{6}$$

Note that Equation (6) follows from the fact that the length of a CMT in any state n would change by $v^n\Delta t$ in Δt time, and conditioning on the transitions from all states $n \in \{GS, GP, SS, SP, PS, PP\}$ to state m, as the transition probability from state n to m in Δt time is given by $q_{n,m}\Delta t+o(\Delta t)$ if $n \neq m$ and $1+q_{m,m}\Delta t+o(\Delta t)$ if $n = m$, where $o(\Delta t)$ is a collection of terms of higher order than Δt such that $o(\Delta t)/\Delta t \to 0$ as $\Delta t \to 0$. Subtracting $p_m(l,\theta,t)$ from each side of the equation and dividing by Δt, we obtain

$$\begin{aligned}\frac{p_m(l,\theta,t+\Delta t)-p_m(l,\theta,t)}{\Delta t} =& \frac{p_m(l-v^m\Delta t,\theta,t)-p_m(l,\theta,t)}{\Delta t} \\ &+\sum_n q_{n,m}p_n(l-v^m\Delta t,\theta,t)+o(\Delta t)/\Delta t.\end{aligned}$$

Letting $\Delta t \to 0$ yields

$$\frac{\partial p_m(l,\theta,t)}{\partial t} = -v^m\frac{\partial p_m(l,\theta,t)}{\partial l}+\sum_n q_{n,m}p_n(l,\theta,t),$$

which describes part of the equations in (5) that corresponds to CMT dynamics.

The remaining terms in Equation (5) are related to interactions. In particular, $B_s(l,\theta,t)$ denotes the frequency of CMTs with length l and angle θ that has a growing leading end and a shortening lagging end to run into another CMT and bundle with it at time t, whereas $B_p(l,\theta,t)$ stands for similar frequency for CMTs with with length l and angle θ, a growing leading end, and a pausing lagging end. Note that notations are distinguished according to the phase of the lagging end, as the leading ends of CMTs that run into others in the system can only be at growth phase. Similarly, $C_s(l,\theta,t)$ and $C_p(l,\theta,t)$ are the frequencies for CMTs with length l, angle θ to undergo

catastrophe, i.e. collide with another CMT and transition into a new state such that their leading ends leave the growth phase and begins shortening immediately at time t. Finally, $B_s^*(l,\theta,t)$ and $B_p^*(l,\theta,t)$ stand for the frequency of CMTs with angle θ to act as a barrier and result in the bundling of other CMTs of length l by switching their orientation to θ, where the subscripts again stand for the phase of the lagging ends of bundling CMTs. We approximate these interaction frequencies as a function of sine of the difference in angles of the two colliding CMTs similar to the methodology in Hawkins *et al.* (2010). According to this, the interaction frequency for parallel CMTs is zero and it increases as the collision angle increases. The resulting formulation is as follows:

$$C_s(l,\theta,t) = v_G^+ p_{GS}(l,\theta,t) \sum_{\theta' \in \Theta} p_c |sin(\theta - \theta')| \int_{l'} dl'l'(\bar{p}_G(l',\theta',t) + \bar{p}_S(l',\theta',t) + \bar{p}_P(l',\theta',t)),$$

$$C_p(l,\theta,t) = v_G^+ p_{GP}(l,\theta,t) \sum_{\theta' \in \Theta} p_c |sin(\theta - \theta')| \int_{l'} dl'l'(\bar{p}_G(l',\theta',t) + \bar{p}_S(l',\theta',t) + \bar{p}_P(l',\theta',t)),$$

$$B_s(l,\theta,t) = v_G^+ p_{GS}(l,\theta,t) \sum_{\theta' \in \Theta^*} p_b(l) |sin(\theta - \theta')| \int_{l'} dl'l'(\bar{p}_G(l',\theta',t) + \bar{p}_S(l',\theta',t) + \bar{p}_P(l',\theta',t)),$$

$$B_p(l,\theta,t) = v_G^+ p_{GP}(l,\theta,t) \sum_{\theta' \in \Theta^*} p_b(l) |sin(\theta - \theta')| \int_{l'} dl'l'(\bar{p}_G(l',\theta',t) + \bar{p}_S(l',\theta',t) + \bar{p}_P(l',\theta',t)),$$

$$B_s^*(l,\theta,t) = \left(\int dl'l'(\bar{p}_G(l',\theta,t) + \bar{p}_S(l',\theta,t) + \bar{p}_P(l',\theta,t)) \right) \sum_{\theta' \in \Theta^*} v_G^+ p_{GS}(l,\theta',t) p_b(l) |sin(\theta - \theta'),$$

$$B_p^*(l,\theta,t) = \left(\int dl'l'(\bar{p}_G(l',\theta,t) + \bar{p}_S(l',\theta,t) + \bar{p}_P(l',\theta,t)) \right) \sum_{\theta' \in \Theta^*} v_G^+ p_{GP}(l,\theta',t) p_b(l) |sin(\theta - \theta'),$$

where

$$\Theta = \{\theta + \theta^c + 1, ..., \theta + (180 - \theta^c) - 1\} \ mod \ 180 \ ,$$

$$\Theta^* = \{0, 1, ..., 179\} - \Theta - \{\theta\} \ mod \ 180,$$

where the "mod" function is to adjust all the negative degrees and degrees that are equal to or greater than 180 in Θ and Θ^* to fall in the set Φ^{180}; and $\bar{p}_G(l,\theta,t)$, $\bar{p}_S(l,\theta,t)$, $\bar{p}_P(l,\theta,t)$ denote the total density of CMTs with length l and angle θ that has a growing, shortening and pausing leading end in respective order. That is,

$$\bar{p}_G(l,\theta,t) = p_{GS}(l,\theta,t) + p_{GP}(l,\theta,t),$$

$$\bar{p}_S(l,\theta,t) = p_{SS}(l,\theta,t) + p_{SP}(l,\theta,t),$$

$$\bar{p}_P(l,\theta,t) = p_{PS}(l,\theta,t) + p_{PP}(l,\theta,t).$$

The limits of summations are defined according to the critical interaction angle and the rules explained in Section I.2. Note that the interaction frequencies are functions of the velocities of the leading ends rather than the net velocities of growing CMTs, as collisions are directly generated by the dynamics of the leading end. Finally, the boundary condition is given as a function of the appearance rate:

$$p_{GS}(0,\theta,t) = \frac{\lambda_a}{180A}, \tag{7}$$

were A is the area of the surface that CMTs reside on. The boundary condition

indicates that CMTs appear with a 0 length in the GS state (rather than a length of 0.1 in PP state as in simulations in order to not have a discontinuity at $l = l_0 > 0$). Note that Equation (7) is just given for the sake of completeness and does not affect the analysis and results that we discuss next.

IV.2.2. Equilibria Analysis

Having derived an integro-differential equation system for the dynamics and interactions of CMTs, we use Lyapunov stability concepts to characterize its solutions (Long *et al.*, 2008). It is worth noting that by stability, here we imply the convergence of solutions in time to an equilibrium point considered rather than the stability notion used to characterize system properties in Section IV.1. One of the equilibrium points of (5) given by

$$\begin{aligned}
\frac{\delta p_{GS}(l,\theta,t)}{\delta t} = 0, \frac{\delta p_{GP}(l,\theta,t)}{\delta t} = 0, \\
\frac{\delta p_{SS}(l,\theta,t)}{\delta t} = 0, \frac{\delta p_{SP}(l,\theta,t)}{\delta t} = 0, \\
\frac{\delta p_{PS}(l,\theta,t)}{\delta t} = 0, \frac{\delta p_{PP}(l,\theta,t)}{\delta t} = 0
\end{aligned}$$

is

$$\begin{aligned}
P^* = \{&(p_{GS}(l,\theta,t),\ p_{GP}(l,\theta,t),\ p_{SS}(l,\theta,t),\ p_{SP}(l,\theta,t),\ p_{PS}(l,\theta,t),\ p_{PP}(l,\theta,t)) \\
&s.t.\ \ k(\theta^*,t) = 1,\ k(\theta,t) = 0\ \ \forall \theta \neq \theta^*\},
\end{aligned} \tag{8}$$

where $k(\theta,t)$ is given by Equation (1) in Chapter III. Note that Equation (8) corresponds to an ideally organized solution where all CMTs in the system are aligned with the same orientation. We employ the entropy metric defined in Equation (2) as a Lyapunov function to establish conditions for its stability. Use of entropy as a Lyapunov function is rarely seen in the related stability literature. Here, it is very ap-

propriate as organization is directly characterized by the entropy metric. Rearranging Equation (2) in terms of model variables, we obtain

$$H(t) = -\sum_{\theta'=0}^{179} k(\theta', t) ln\left(k(\theta', t)\right), \tag{9}$$

where for all θ, t,

$$k(\theta, t) = \frac{\int_0^\infty l(\bar{p}_G(l,\theta,t) + \bar{p}_S(l,\theta,t) + \bar{p}_P(l,\theta,t))dl}{\sum_{\theta=0}^{179}\int_0^\infty l(\bar{p}_G(l,\theta,t) + \bar{p}_S(l,\theta,t) + \bar{p}_P(l,\theta,t))dl}, \tag{10}$$

where $\bar{p}_G(l,\theta,t)$, $\bar{p}_S(l,\theta,t)$, $\bar{p}_P(l,\theta,t)$ denote the CMT densities with respect to the phase of the leading end as defined in Section IV.2.1. For the solution given by Equation (8), since $k(\theta^*, t) = 1$ and $k(\theta, t) = 0 \ \forall \ \theta \neq \theta^*$, the entropy of the system is zero, which we will denote by $H(t) \mid_{P=P^*} = 0$. For all other solutions $P \neq P^*$, the entropy is positive, i.e. $H(t) \mid_P > 0$. Hence, Equation (9) can be used as a Lyapunov function to prove the asymptotic stability of P^*, or in other words, the convergence of the system towards P^* (hence organization) eventually starting at any other solution. Prior to stating our main result of this section in Proposition 1, we provide a lemma which is used in its proof.

Lemma 1. *Given two different sequences* $(x_1, x_2, ...x_N)$ *and* $(y_1, y_2, ...y_N)$ *with* $x_i > 0$, $i = 1, ..., N$ *and* $\sum_{i=1}^N x_i = 1$, $\sum_{i=1}^N y_i = 1$*; assume that for any two pairs of* x_i, y_i *and* x_j, y_j, $i, j = 1, ..., N$, $x_i \geq x_j$ *if and only if* $y_i \geq y_j$ *and* $(y_i - x_i) \geq (y_j - x_j)$, *i.e. sequences and their difference increase and decrease in the same order. Let* $f(x) > 0$ *be a decreasing function of* x. *Then the following inequality holds*

$$\sum_{i=1}^N f(x_i)(y_i - x_i) < 0. \tag{11}$$

Proof: Let us define $z_i = (y_i - x_i)$ $i = 1, ..., N$. We group z_i values in three sets

as follows:

$$I_+ = \{i \in \{1, N\} : z_i > 0\}$$

$$I_0 = \{i \in \{1, N\} : z_i = 0\}$$

$$I_- = \{i \in \{1, N\} : z_i < 0\}.$$

As $\sum_{i=1}^{N} y_i - \sum_{i=1}^{N} x_i = 0$, it follows that

$$\sum_{i=1}^{N} z_i = \sum_{i \in I_+} z_i + \sum_{i \in I_-} z_i = 0. \tag{12}$$

Let us divide z_i values into infinitesimal pieces of the same size, denoted by $\Delta_z > 0$, such that for each $i \in I_+$, $z_i = w_i \Delta_z$ and for each $i \in I_-$, $z_i = -w_i \Delta_z$, $i = 1, ..., N$, where $\Delta_z > 0$ and w_i are positive real numbers. Equation (12) can be rewritten as

$$\sum_{i \in I_+} w_i - \sum_{i \in I_-} w_i = 0. \tag{13}$$

Hence, we have an equal number ($\sum_{i \in I_+} w_i = \sum_{i \in I_-} w_i := W$) of Δ_z pieces that belong to sets I_+ and I_-. Note that $\forall$ z_i with $i \in I_+$ and z_j with $j \in I_-$, it follows from the definition of z_i values that $z_i > z_j$, and consequently $x_i > x_j$ from the given ordering relation between the sequences x_i, and z_i; and finally $f(x_i) < f(x_j)$ due to the decreasing property of $f(\cdot)$. Let us redefine the sequence of x_i, $i = 1, ..., N$ such that its values are copied w_i times for each x_i value so that every Δ_z has its corresponding $x'_{i'}$ and $f(x'_{i'})$ values, where $i' = 1, ..., W$. Adjusting I_+ and I_- accordingly as I'_+, I'_-, for each Δ_z value that belongs to set I_+, there is a Δ_z which is multiplied with a larger value in I_- in the following equation:

$$\sum_{i' \in I'_+} f(x'_{i'}) \Delta_z - \sum_{i' \in I'_-} f(x'_{i'}) \Delta_z < 0,$$

which gives the desired result. $\square$

Next, we state the proposition regarding the asymptotic stability of P^* given in Equation (8).

Proposition 1. *For a system with $p_b(l), p_c > 0$, a sufficient condition for the global asymptotic stability of P^* defined in (8) is given by*

$$p_G^+(t)v_{G^+} - p_S^+(t)v_{S^+} - p_S^-(t)v_{S^-} > 0,$$

where $p_G^+(t)$ and $p_S^+(t)$ stand for the total density of CMTs that have a growing and shortening leading end in respective order at time t. Similarly, $p_S^-(t)$ stands for the total density of CMTs that have a shortening lagging end at time t. In other words,

$$\begin{aligned}
p_G^+(t) &:= \sum_\theta \int_0^\infty (p_{GS}(l,\theta,t) + p_{GP}(l,\theta,t))dl, \\
p_S^+(t) &:= \sum_\theta \int_0^\infty (p_{SS}(l,\theta,t) + p_{SP}(l,\theta,t))dl, \\
p_S^-(t) &:= \sum_\theta \int_0^\infty (p_{GS}(l,\theta,t) + p_{SS}(l,\theta,t) + p_{PS}(l,\theta,t))dl.
\end{aligned}$$

Proof: According to Lyapunov's stability theory, a sufficient condition for the global asymptotic stability of an equilibrium point P^* is existence of a Lyapunov function $\mathcal{L}(\cdot)$ such that

- $\mathcal{L}(t) \mid_P > 0$, $\forall P \neq P^*$ and $\mathcal{L}(t) \mid_P = 0$ only for $P = P^*$,
- $\frac{\partial \mathcal{L}(t)}{\partial t} \mid_P < 0$, $\forall P \neq P^*$ and $\frac{\partial \mathcal{L}(t)}{\partial t} \mid_{P=P^*} = 0$.

We set our Lyapunov function as the entropy metric, $H(\cdot)$ in Equation (9). We already know that the first condition holds for $H(\cdot)$, as $H(t) \mid_{P=P^*} = 0$ and $H(t) \mid_P > 0$ $\forall P \neq P^*$. What is left to check is the sign of the derivative of the Lyapunov function with respect to t, which is given by

$$\frac{\partial H(t)}{\partial t} = -\sum_{\theta=0}^{179} k'(\theta,t) ln(k(\theta,t)) + k'(\theta,t), \tag{14}$$

where

$$k'(\theta,t) = \frac{\partial\, k(\theta,t)}{\partial t}. \tag{15}$$

Let us define the total density of CMTs with length l and angle θ at time t by

$$\bar{p}(l,\theta,t) := \bar{p}_G(l,\theta,t) + \bar{p}_S(l,\theta,t) + \bar{p}_P(l,\theta,t).$$

Using Equation (10), we can rewrite Equation (15) as

$$k'(\theta,t) = \frac{\left(\int_0^\infty l\frac{d\bar{p}(l,\theta,t)}{dt}dl\right)\sum_{\theta=0}^{179}\int_0^\infty l\bar{p}(l,\theta,t)dl - \left(\int_0^\infty l\bar{p}(l,\theta,t)dl\right)\sum_{\theta=0}^{179}\int_0^\infty l\frac{d\bar{p}(l,\theta,t)}{dt}dl}{\left(\sum_{\theta=0}^{179}\int_0^\infty l\bar{p}(l,\theta,t)dl\right)^2}.$$

Summing equations in (5) side by side, multiplying both sides with l and integrating with respect to l over $(0,\infty)$, we obtain the derivative of total length of all CMTs with angle θ at time t as

$$\begin{aligned}
L'_\theta(t) &:= \int_0^\infty l\frac{d\bar{p}(l,\theta,t)}{dt}dl \\
&= (v_G^+ - v_S^-)\tilde{p}_{GS}(\theta,t) + v_G^+\tilde{p}_{GP}(\theta,t) \\
&- (v_S^+ + v_S^-)\tilde{p}_{SS}(\theta,t) - v_S^+\tilde{p}_{SP}(\theta,t) - v_S^-\tilde{p}_{PS}(\theta,t) \\
&- v_G^+\int_0^\infty \bar{p}_G(l,\theta,t)ldl\sum_{\theta'\in\Theta^*} p_b|sin(\theta-\theta')|\int_{l'} dl'l'\bar{p}(l',\theta',t) \\
&+ v_G^+\int_{l'} dl'l'\bar{p}(l',\theta,t)\sum_{\theta'\in\Theta^*} p_b|sin(\theta-\theta')\int_0^\infty \bar{p}_G(l,\theta',t)ldl,
\end{aligned}$$

where $\tilde{p}_m(\theta,t) := \int_0^\infty p_m(l,\theta,t)dl$, $m \in \{GS, GP, SS, SP, PS, PP\}$ stands for the total density of CMTs with angle θ at state m at time t. We denote the sum of $L'_\theta(t)$ over all θ by $\sum L'(t) := \sum_{\theta=0}^{179} L'_\theta(t)$, which gives the derivative of total length of all CMTs in the system at time t. Defining total length of CMTs with angle θ at time t as $L_\theta(t) := \int_0^\infty lp(l,\theta,t)dl$, and the total length of all CMTs at time t as

$\sum L(t) := \sum_{\theta=1}^{360} L_\theta(t)$, and plugging these into Equation (14) results in

$$\frac{dH(t)}{dt} = -\sum_{\theta=0}^{179} \frac{L'_\theta(t) \ln\left(\frac{L_\theta(t)}{\sum L(t)}\right) \sum L(t) - L_\theta(t) \ln\left(\frac{L_\theta(t)}{\sum L(t)}\right) \sum L'(t)}{(\sum L(t))^2}.$$

Rearranging terms, we obtain

$$\frac{dH(t)}{dt} = -\sum_{\theta=0}^{179} \frac{\frac{L'_\theta(t)}{\sum L'(t)} \ln\left(\frac{L_\theta(t)}{\sum L(t)}\right) - \frac{L_\theta(t)}{\sum L(t)} \ln\left(\frac{L_\theta(t)}{\sum L(t)}\right)}{\sum L(t) \sum L'(t)}. \tag{16}$$

Let us denote $a_\theta := \frac{L'_\theta(t)}{\sum L'(t)}$ and $b_\theta := \frac{L_\theta(t)}{\sum L(t)}$. By definition, it follows that $\sum_{\theta=0}^{179} a_\theta = 1$, $\sum_{\theta=0}^{179} b_\theta = 1$, and $b_i > 0$. Assuming $\sum L'(t) > 0$, i.e. the net total CMT length change in time is positive, we are interested in the sign of

$$\sum -\ln(b_\theta)(a_\theta - b_\theta). \tag{17}$$

If the sign for Expression (17) is negative, then Equation (16) is negative, i.e. $\frac{dH}{dt} < 0$, and the stability condition is satisfied. A sufficient condition to ensure this follows from Lemma 1 as $-ln(b)$ is a decreasing function of b for $0 < b < 1$. Accordingly, we require the two sequences a_θ and b_θ, and their difference $a_\theta - b_\theta$ to increase and decrease in the same order. This roughly means that if CMTs with an angle θ have a larger total length compared to the total length of CMTs with angle $\theta' \neq \theta$, they also grow larger in ratio in total length on average, and vice versa. This property follows by careful observation of model equations and the property that $p_b(l)$ is decreasing in l.

Finally, in order to fulfill $\sum L'(t) > 0$, it is required that the problem parameters satisfy

$$\sum_\theta (v_G^+ - v_S^-) p_{GS}(\theta,t) + v_G^+ p_{GP}(\theta,t) - (v_S^+ + v_S^-) p_{SS}(\theta,t) - v_S^+ p_{SP}(\theta,t) - v_S^- p_{PS}(\theta,t) > 0, \ , \tag{18}$$

$\forall t$, which can be stated as

$$\sum_{\theta} p_G^+(\theta,t)v_{G^+} - p_S^+(\theta,t)v_{S^+} - p_S^-(\theta,t)v_{S^-} > 0, \tag{19}$$

by rearranging terms.□

Note that Inequality (19) ensures a positive net change in CMT length on average. We conjecture that this condition will be satisfied if

$$\pi_G^+ v_G^+ - \pi_S^+ v_S^+ - \pi_S^- v_S^- > 0, \tag{20}$$

where π_G^+, π_S^+, π_S^- are the long-run probabilities for the phases of the leading and lagging ends of a single CMT with no interactions. In particular, π_G^+ and π_S^+ stand for the long-run probabilities that the leading end is in growth and shortening phases in respective order; and π_S^- is the long-run probability that the lagging end is in shortening phase as described in Section III.3.1 and can also be derived using infinitesimal generator Q.

In fact, Proposition 1 and our related conjecture show that CMT organization is roughly robust to interaction parameters as long as CMTs are growing on average, in line with the simulation results. This outcome is quite intuitive as interactions are easily kept at a high frequency regardless of the particular values of p_b and p_c as long as they are not set to zero, as CMTs keep running into each other in a growing system. In fact, for the case $\sum L'(t) < 0$, following similar procedure as in the proof of Proposition 1, our conjecture is that organization can be achieved especially for values close to zero, but this is heavily dependent on interaction parameters to maintain a certain frequency of bundling and catastrophe.

Table 4. $\pi_G^+ v_G^+ - \pi_S^+ v_S^+ - \pi_S^- v_S^-$ Values for Different Parameter Sets

Parameter Set	Status	$\pi_G^+ v_G^+ - \pi_S^+ v_S^+ - \pi_S^- v_S^-$
I	organized	0.260
II	organized	0.017
III	organized	1.733
IV	organized	-0.106
V	disorganized	-0.763
VI	organized	0.963

IV.3. Conclusions

In this chapter, we developed a model for CMT dynamics and interactions using a mean-field approach, which resulted in a system of integro-differential equations as a function of CMT densities with respect to their state, length and orientation. We conducted a stability analysis using Lyapunov's theorem and was able to derive sufficient conditions that guarantee convergence to an organized solution asymptotically. According to this, if the average net velocity for a single CMT is positive, organization is achieved regardless of interaction parameters as long as they are not eliminated completely. This is in line with our observations from simulations. Table 4 lists the organization results for different parameter sets given in Appendix B according to simulations and the corresponding value of $\pi_G^+ v_G^+ - \pi_S^+ v_S^+ - \pi_S^- v_S^-$ for each case.

As seen in Table 4, cases I, II, III and VI satisfy the sufficient condition for organization given in Equation (20) and result in organized systems accordingly regardless of the interaction parameters, whereas case V fails to get organized as its dynamicity parameters correspond to an average net velocity that is significantly less than zero. On the other hand, case IV achieves organization despite not satisfying the sufficient

condition, however heavily dependent on the interaction parameters as discussed in Section IV.2.2. This is quite intuitive, as the condition we derived is a sufficient one but not necessary, so it is possible to have organization even when it is not satisfied, especially for the cases where the average net velocity is close to zero. If we make an analogy to the queueing systems as in Section IV.1, the condition in Equation (20) corresponds to an unstable system with $\lambda > \mu$, growing on average (although μ is increased to approach λ in time due to interactions); and a setting with λ slightly less than μ, even though theoretically stable, corresponds to a heavy-traffic queue, which is quite close to the required condition.

The relation between dynamicity parameters and system organization established in this chapter is potentially useful for generating and maintaining organization in plant cells by regulation of CMT dynamics. Finally, in addition to deriving sufficient conditions that guarantee CMT organization, this chapter also provides a theoretical explanation for the continuous entropy drop seen in the simulations in the course of organization, by using the entropy metric as a Lyapunov function in the stability analysis.

CHAPTER V

FLUID MODEL FOR SINGLE CMT DYNAMICS AND APPROXIMATION OF SYSTEM METRICS

Having analytically derived sufficient conditions for self-organization of CMTs, in this chapter we develop methodologies to estimate certain system metrics (expected number and average length in time) for the parameter regions that these conditions hold, hence when organization is achieved. Among the cases discussed in the Section IV.1, the *organized pseudo-stable* case is the most challenging to estimate such metrics, due to its complex and chaotic properties, and accordingly high variation between simulation runs. These are systems with time-varying interaction frequencies that are hard to estimate. For systems that stay disorganized, interactions can in general be ignored, and system metrics can be estimated mainly based on single CMT dynamics regardless of their stability. However, in organizing systems, interaction frequencies change dynamically according to the status of organization, and the system metrics typically exhibit *pseudo-stabilization* trend with subsequent time phases that we discussed in Section III.3.3. As a result, we employ a combination of various techniques to develop a predictive methodology that is compatible with the considered problem characteristics. These include a fluid model for single CMT dynamics, Laplace inversion techniques to calculate related distributions, approximation algorithms that are used to estimate impact of interactions, and simulations. A framework for the analysis in this chapter similar to previous chapters of the dissertation is provided in Figure 32.

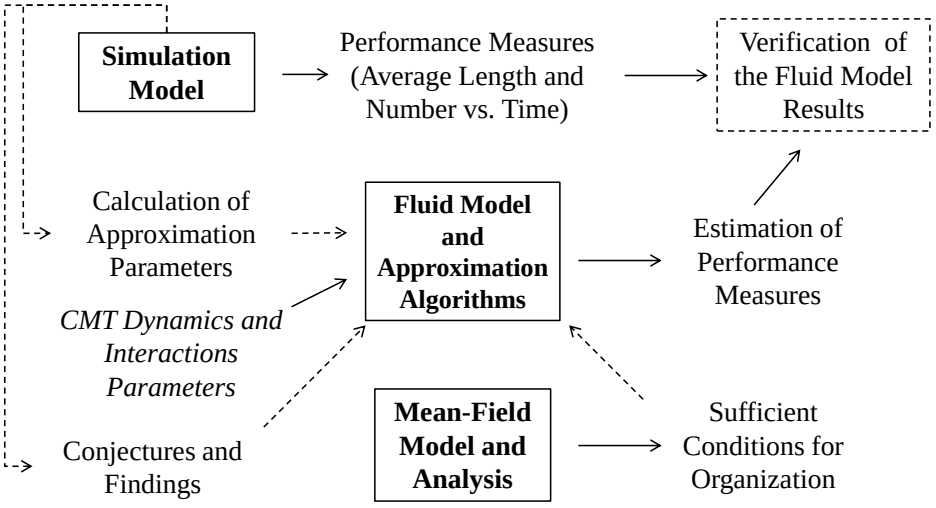

Fig. 32. A Framework of the Fluid Model and Approximation Methodologies

V.1. Objectives and Relation to the Simulation Results

In simulations which result in organization, it's generally observed that around the time the frequency of collision induced catastrophes in the system per unit time reaches its peak, total number and average length of CMTs in the system as well as the total length in the system stays temporarily around a constant value. Once system organization is settled to a certain degree, total number and average length of CMTs continue to grow indefinitely (see Case (i) in Figure 31). Hence, there are three phases of realization of such system metrics in time, associated with an initial increase followed by a roughly *stable* phase and eventually an indefinite increase in time. A sample hypothetical plot for an estimation of expected system metrics for these three phases can be summarized as described in Figure 33. The system initially starts with tiny CMTs where interactions do not have a significant effect until they get long and crowded enough. As a result, metrics begin increasing with a high initial rate, which decreases as frequency of interactions increases and reaches its peak at around

time T_1. Between T_1 and T_2, system metrics roughly fluctuate around a constant value. Hence, T_2 corresponds to a time point that organization has already settled. It is worth noting that we are particularly interested in the region until this time point, as it is already beyond the state experimentally observed in plant cells, and these cells typically move to a completely different set of events (such as cell division, etc.) at some time t, such that $T_1 < t < T_2$. Hence, we develop methodologies to estimate expected values of system metrics up until this time, after which they are considered to remain constant for our purposes. In this chapter, we first introduce a fluid model that considers detailed dynamics of a single CMT at both ends, ignoring the effect of interactions. Based on this model, we develop predictive methodologies for expected realizations of system-wide metrics using a transient analysis and certain approximation techniques tailored to our problem.

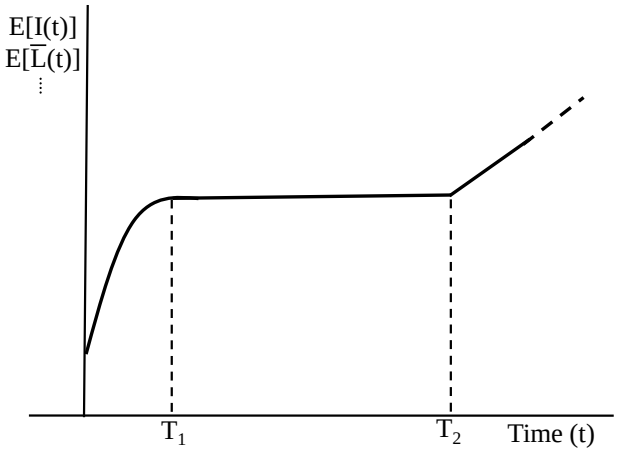

Fig. 33. Sample Plot for Estimation of Expected System Metrics for an Organized Case

V.2. Model Equations and Analysis

In this section, we present the formulation for the fluid model of single CMT dynamics and derive the Laplace transform for the corresponding lifetime distribution (Section V.2.1). Following this, we provide a Laplace inversion algorithm to calculate the lifetime distribution numerically (Section V.2.2).

V.2.1. Problem Formulation

As described in Section III.1, the total length of CMT i at time t is denoted by $L_i(t)$. In the following, we remove index i from our notations, as we are considering single CMT dynamics. As described in Chapter I, the length of a CMT at time t, $L(t)$, changes according to its state at time t, $M(t)$ (see Figure 3). Accordingly, dynamics of the length process, $\{L(t), t \geq 0\}$ is given by

$$\frac{d(L(t))}{dt} = \begin{cases} v_G^+ - v_S^-, & \text{if } M(t) = GS, \\ v_G^+, & \text{if } M(t) = GP, \\ -v_S^+ - v_S^-, & \text{if } M(t) = SS, \text{and } L(t) > 0 \\ -v_S^+, & \text{if } M(t) = SP, \text{and } L(t) > 0 \\ -v_S^-, & \text{if } M(t) = PS, \text{and } L(t) > 0 \\ 0, & \text{if } M(t) = PP \text{ or } L(t) = 0. \end{cases} \tag{21}$$

Note that the "$L(t) = 0$" condition on the last line of Equation (21) follows from the fact that $\{(M(t), L(t)), t \geq 0\}$ is a Markov process with an absorbing barrier at $L(t) = 0$, as a CMT disappears and departs the system if it shrinks to zero length. Considering a CMT that appears at time $t = 0$, its lifetime, τ, is defined as

$$\tau = \inf\{t > 0 : L(t) = 0\}.$$

We next define a slightly different dynamics for the length process, which we will use to derive the lifetime distribution of a CMT.

$$\frac{d(L(t))}{dt} = \begin{cases} v_G^+ - v_S^-, & \text{if } M(t) = GS, \\ v_G^+, & \text{if } M(t) = GP, \\ -v_S^+ - v_S^-, & \text{if } M(t) = SS, \text{and } L(t) > 0 \\ -v_S^+, & \text{if } M(t) = SP, \text{and } L(t) > 0 \\ -v_S^-, & \text{if } M(t) = PS, \text{and } L(t) > 0 \\ 0, & \text{if } M(t) = PP \text{ or } L(t) = 0 \text{ and } M(t) = SS, SP, PS. \end{cases} \tag{22}$$

Equation (22) considers that a CMT stays in the system and continues its dynamics even if it shrinks to zero length. That is, once the CMT transitions into a state with a positive velocity, it resumes growth. As the lifetime of a CMT is actually a first passage time, and Equations (21) and (22) define similar dynamics up until hitting zero length, lifetime distribution implied by both equations are equivalent. We define the joint distribution function for the lifetime of a CMT and its final state conditioned on the initial state and length as

$$F_{ab}(l,t) = P\{\tau \leq t, M(\tau) = b | L(0) = l, M(0) = a\},$$

where $a, b \in \{GS, GP, SS, SP, PS, PP\}$ represent the initial and final states of the CMT in respective order, and l stands for the initial length. We also define the vector, $F_b(l,t) = [F_{GSb}(l,t)\ F_{GPb}(l,t)\ F_{SSb}(l,t)\ F_{SPb}(l,t)\ F_{PSb}(l,t)\ F_{PPb}(l,t)]$ for any final state, b. The following theorem states the partial differential equations for this joint distribution function, in terms of the infinitesimal generator matrix Q, and the velocity matrix V defined in Section III.1,

Theorem 1. *$F_{ab}(l,t)$ is a solution to the following partial differential equation*

$$\frac{\delta F_{ab}(l,t)}{\delta t} - v^a \frac{\delta F_{ab}(l,t)}{\delta l} = \sum_c q_{ac} F_{cb}(l,t), \tag{23}$$

or in the matrix form,

$$\frac{\delta F_b(l,t)}{\delta t} - V \frac{\delta F_b(l,t)}{\delta l} = Q F_b(l,t), \tag{24}$$

where boundary and initial conditions are given by,

$$\begin{aligned}
F_{bb}(0,t) &= 1 \quad for \quad v^b < 0, \\
F_{ab}(0,t) &= 0 \quad for \quad a \neq b, v^a < 0, \\
F_{ab}(l,0) &= 0 \quad for \quad a \neq b, l \geq 0, \\
F_{bb}(l,0) &= 0 \quad for \quad l > 0.
\end{aligned}$$

Proof: Consider $F_{ab}(l, t+h)$, where h is a small positive real number. It can be written as

$$F_{ab}(l,t+h) = P\{\tau \leq t+h, M(\tau) = b | L(0) = l, M(0) = a\}.$$

Conditioning on the first transition from the initial state, we obtain

$$\begin{aligned}
F_{ab}(l,t+h) =& P\{\tau \leq t+h, M(\tau) = b | L(0) = l, M(0) = a\} \\
=& \sum_{c \neq a} P\{\tau \leq t+h, M(\tau) = b | L(0) = l, M(0) = a, M(h) = c\} \\
& P\{M(h) = c | M(0) = a, L(0) = l\} \\
&+ P\{\tau \leq t+h, M(\tau) = b | L(0) = l, M(0) = a, M(h) = a\} \\
& P\{M(h) = a | M(0) = a, L(0) = l\}.
\end{aligned}$$

As $M(t)$ process is independent of $L(0)$, and the length would change by $v^a h$ by time

h, when the CMT is in state a at time 0,

$$
\begin{aligned}
&F_{ab}(l, t+h) \\
=&\sum_{c\neq a} P\{\tau \leq t+h, M(\tau)=b | L(h)=l+v^a h, M(h)=c\} P\{M(h)=c|M(0)=a\} \\
&+ P\{\tau \leq t+h, M(\tau)=b | L(h)=l+v^a h, M(h)=a\} P\{M(h)=a|M(0)=a\} \\
=&\sum_{c\neq a} P\{\tau \leq t, M(\tau)=b | L(0)=l+v^a h, M(0)=c\} P\{M(h)=c|M(0)=a\} \\
&+ P\{\tau \leq t, M(\tau)=b | L(0)=l+v^a h, M(0)=a\} P\{M(h)=a|M(0)=a\}.
\end{aligned}
$$

As the transition probability from state a to c in time h is given by $q_{ac}h + o(h)$ if $c \neq a$ and $1 + q_{aa}h + o(h)$ if $c = a$, where $o(h)$ is a collection of terms of higher order than h such that $o(h)/h \to 0$ as $h \to 0$, it follows

$$F_{ab}(l, t+h) = \sum_{c\neq a} F_{cb}(l+v^a h, t) q_{ac} h + F_{ab}(l+v^a h, t)(q_{aa}h + 1) + o(h).$$

Subtracting $F_{ab}(l,t)$ from each side of the equation, dividing by h and rearranging terms results in

$$\frac{F_{ab}(l,t+h) - F_{ab}(l,t)}{h} = \frac{F_{ab}(l+v^a h, t) - F_{ab}(l,t)}{h} + \sum_c q_{ac} F_{cb}(l+v^a h, t) + o(h)/h.$$

Letting $h \to 0$ yields Equation (23), and rewriting in the matrix form gives Equation (24). Next, we describe the boundary conditions for all a, b and t. As the lifetime would be zero if CMT appeared with zero length at state b such that $v^b < 0$, it follows

$$F_{bb}(0,t) = 1 \quad \text{for} \quad v^b < 0.$$

The second boundary condition,

$$F_{ab}(0,t) = 0 \quad \text{for} \quad a \neq b, v^a < 0,$$

follows from the fact that although the lifetime is zero, the probability that the state is b when the lifetime is reached is zero (since at time $t = 0$ the state is a with $v^a < 0$). Finally, the last two conditions follow from the fact that lifetime cannot be reached at state b at time $t = 0$ if the initial state is $a \neq b$ for any initial length; or if the initial state is b for a positive initial length. □

Let $F_b^*(l, w)$ be the Laplace transform (LT) of $F_b(l, t)$ with respect to t. We denote the LT of $F_b^*(l, w)$ with respect to l by $F_b^{**}(s, w)$. The next theorem gives the equations for $F_b^{**}(s, w)$.

Theorem 2. *The solution to Equation (24) in transform space is given by*

$$F_b^{**}(s, w) = (Vs - wI + Q)^{-1}(w^{-1}(Ve_j)), \tag{25}$$

where I is the identity matrix and e_j is the j^{th} unit vector, with the sizes compatible with V and Q.

Proof: Taking the LT of Equation (24) with respect to t gives

$$(wI - Q)F_b^*(l, w) = V\frac{\delta F_b^*(l, w)}{\delta l}. \tag{26}$$

Taking the LT of Equation (26) with respect to l results in

$$(wI - Q)F_b^{**}(s, w) = V[sF_b^{**}(s, w) - F_b^*(0, w)]. \tag{27}$$

Define e_j as the j^{th} unit vector. Plugging in the boundary condition

$$F_b^*(0, w) = w^{-1}e_j \quad if \quad v^j < 0,$$

we get

$$(Vs - wI + Q)\tilde{F}_b^*(s, w) = w^{-1}(Ve_j).$$

Rearranging terms yields Equation (28). □

Considering the transform of the lifetime distribution independent of the final state of the CMT, we obtain

$$F^{**}(s,w) = (Vs - wI + Q)^{-1}(w^{-1}(Ve_3 + Ve_4 + Ve_5)). \tag{28}$$

Note that the reason we multiply V with e_j, where $j = 3, 4, 5$ is that a CMT can only disappear at one of the corresponding states in the set $\{GS, GP, SS, SP, PS, PP\}$, as SS, SP, and PS are the only ones with a negative net velocity. Finally we are interested in $[0\,0\,0\,0\,0\,1]F^{**}$, as the initial state of CMTs upon appearance is set as PP, i.e. the state at which both ends are pausing.

V.2.2. Numerical Inversion of Laplace Transforms

Having derived the LT of lifetime distribution, we follow the methodology in Kharoufeh and Gautam (2004) to conduct a two-dimensional Laplace transform inversion for numerical computation of $F(l,t)$ for given l and t. Based on the approaches introduced in Choudhury *et al.* (1994) and Moorthy (1995), an approximation for the inverse function $F(l,t)$ is given by

$$F(l,t) \approx (1/2)\exp(c_1 l + c_2 t)(T^{-2})\left\{F^{**}(c_1,c_2)/2 + \sum_{i=1}^{3} k_i\right\} \tag{29}$$

where

$$k_1 = \sum_{m=1}^{\infty} Re\{F^{**}(c_1, c_2 + i\pi m/T)\}\cos(m\pi t/T) - Im\{F^{**}(c_1, c_2 + i\pi m/T)\}\sin(m\pi t/T),$$

$$k_2 = \sum_{n=1}^{\infty} Re\{F^{**}(c_1 + i\pi n/T, c_2)\}\cos(n\pi l/T) - Im\{F^{**}(c_1 + i\pi n/T, c_2)\}\sin(n\pi l/T),$$

$$
\begin{aligned}
k_3 = \quad & \sum_{n=1}^{\infty}\sum_{m=1}^{\infty} Re\{F^{**}(c_1 + i\pi n/T, c_2 + i\pi m/T)\}\cos(n\pi l/T + m\pi t/T) \\
& + Re\{F^{**}(c_1 + i\pi n/T, c_2 - i\pi m/T)\}\cos(n\pi l/T - m\pi t/T) \\
& - Im\{F^{**}(c_1 + i\pi n/T, c_2 + i\pi m/T)\}\sin(n\pi l/T + m\pi t/T) \\
& - Im\{F^{**}(c_1 + i\pi n/T, c_2 - i\pi m/T)\}\sin(n\pi l/T - m\pi t/T),
\end{aligned}
$$

$$
\begin{aligned}
c_1 &= A_1/(2ll_1), \\
c_2 &= A_2/(2tl_2).
\end{aligned}
$$

Note that $Re(\cdot)$ and $Im(\cdot)$ functions stand for the real and imaginary parts of the input complex number respectively, and A_1, A_2, l_1, l_2 are parameters used to control discretization and roundoff errors. We employ the epsilon algorithm (MacDonald, 1964; Wynn, 1966) to compute the infinite series in Equation (29), and set $T = 0.65T_{max}$, where $T_{max} = \max\{l, t\}$.

Our first observation is that the parameter values $A_1 = A_2 = 28.324$ and $l_1 = l_2 = 3$, which are suggested for cumulative probability functions in Choudhury *et al.* (1994), do not work well for our problem. We conjecture the reason for this incompatibility is the ill-conditioned nature of the lifetime distribution ($F(l, \infty) < 1$) when the average net growth rate for a CMT is positive. As recommended in Abate and Whitt (2006), we use multi-precision software and additionally employ varying parameters for different points of the function that we are trying to calculate. It is worth noting that our methodology is related to certain concepts and issues discussed in Abate and Whitt (1992) and Avdis and Whitt (2007), although we are not employing any particular method developed previously. In fact, we have tested some methodologies suggested in those studies on our problem, such as convolution smoothing, probabilistic scaling and different versions of inversion algorithms, none of

which improved results significantly. Instead, we employ a heuristic approach, where initially l_2 parameter is set to a relatively high value, and reduced as the value of t that we are interested in decreases. For the points that still result in stability problems and give divergent results, we make use of single CMT simulations by simplifying the algorithm in Section III.3.2. These simulations have much less computational complexity compared to our original simulations, as they consider a single CMT setting with no interactions. Hence we are able to run thousands of single CMT simulations to obtain a statistically significant data set.

V.3. Estimation of System Metrics

Next, we conduct a transient analysis to derive the expected number of CMTs in the system according to the lifetime distribution calculated. As CMTs appear according to a Poisson process, and there is no external capacity regarding the number of CMTs in the system that we are considering, we can formulate the expected number of CMTs at time t, $E[I(t)]$ similar to the approach in Wolff (1989), where the service time distribution is given by $F(l,t)$. According to this,

$$E[I(t)] = \lambda_a \int_0^t [1 - F(l_0, u)]du, \tag{30}$$

where λ_a is the rate parameter for the appearance (arrival) process, and l_0 is the initial length, as given in Section III.1. Note that this approach would actually work to approximate only the early phase of simulations, where the interactions are quite rare and ignorable.

In order to compute the integral in Equation (30), we use a summation approximation, based on discrete time points, $t_i = 0, t_1, t_2, ...t_n = t$. Denoting the

approximation for $\int_0^{t_i}[1-F(l_0,u)]du$ by $\widehat{\int}\bar{F}(t_i)$,

$$\widehat{\int}\bar{F}(t_n)=\widehat{\int}\bar{F}(t_{n-1})+\frac{(F(l_0,t_{n-1})-F(l_0,t_n))}{2}(t_n-t_{n-1})+F(l_0,t_n)(t_n-t_{n-1}),$$

for $n=1,2,...$ where $\widehat{\int}\bar{F}(0)=0$.

The approximation for Equation (30) is given by

$$E[I(t)]\approx\widehat{E}[I(t_n)]=\lambda_a\widehat{\int}\bar{F}(t_n)+I(0)(1-F(l_0,t_n)). \tag{31}$$

Note that we included the second term in the right-hand side of Equation (31) considering the possibility of having an initial set of CMTs present in the system at time t, i.e. $I(0)>0$.

In order to speed up our algorithm, we select intervals such that they get longer for larger t values, as the increment in $F(l_0,t)$ for subsequent time points gets quite negligible as the t value keeps increasing. More particularly, a CMT has a high disappearance probability early after its appearance as it initially has a tiny length. Given that it survives, its length grows quickly due to the positive average net velocity common to the parameter sets that we are considering, and probability of disappearance decreases rapidly. We will study some specific numeric examples in Section V.4; in summary, it is observed that the approximation works quite well compared to simulation results especially for early periods, where effects of interactions are relatively low. As interactions become more frequent (towards time T_1 in Figure 33) the estimates expectedly deviate from the simulation results. Therefore, we develop a method to adjust these estimates to account for the impacts of interactions. Before introducing this smoothing technique, we next describe the methodology that we use for estimating expected average length metric, $E(\bar{L}(t))$.

To estimate $E(\bar{L}(t))$, we do not use the fluid model for the length process, as

Equations (21) and (22) are no longer equivalent and would yield different distribution functions of $L(t)$. Instead, we employ a heuristic approach based on simplified simulations for a single CMT with no interactions. Let us denote the approximate expected average length based on these single CMT simulations by $\bar{L}^1(t)$ for different time points $t_i = 0, t_1, t_2..., t_n$ given that CMT is still in the system at time t. Note that we use thousands of simulations to estimate this average length, which is feasible as single CMT simulations are computationally inexpensive, as described above. Defining A_i as the appearance time of CMT i and D_i as its disappearance time, based on the relation

$$E[\bar{L}(t)] = E\left[\frac{\sum_{i=1}^{I(t)} L_i(t)}{I(t)}\right] = E\left[\frac{\sum_{i=1}^{I(t)} L_i(t)|D_i > t, A_i}{I(t)}\right],$$

$E(\bar{L}(t))$ is approximated using average of the following two estimates where expected average length and number of CMTs are treated as if independent:

$$\widehat{E}_1[\bar{L}(t_n)] = \frac{\sum_{i=1}^{n} \bar{L}^1(t_n - t_i)\lambda_a(t_i - t_{i-1})(1 - F(t_n - t_i)) + \bar{L}^1(t_n)I(0)(1 - F(t_n))}{\sum_{i=1}^{n} \lambda_a(t_i - t_{i-1})(1 - F(t_n - t_i)) + I(0)(1 - F(t_n))}, \tag{32}$$

and

$$\widehat{E}_2[\bar{L}(t_n)] = \frac{\sum_{i=1}^{n} \bar{L}^1(t_n - t_{i-1})\lambda_a(t_i - t_{i-1})(1 - F(t_n - t_{i-1})) + \bar{L}^1(t_n)I(0)(1 - F(t_n))}{\sum_{i=1}^{n} \lambda_a(t_i - t_{i-1})(1 - F(t_n - t_{i-1})) + I(0)(1 - F(t_n))}, \tag{33}$$

such that

$$E[\bar{L}(t)] \approx \widehat{E}[\bar{L}(t_n)] = \frac{\widehat{E}_1[\bar{L}(t_n)] + \widehat{E}_2[\bar{L}(t_n)]}{2}. \tag{34}$$

Note that according to Equation (32) CMTs arriving in $[t_i, t_{i+1})$ are assumed to appear in the beginning of the time period, t_i, whereas according to Equation (33) arrivals in $[t_i, t_{i+1})$ are moved to appear at the end of the time period, t_{i+1}. Both equations account for the initially existing CMTs similarly.

Having described the approximation techniques used for expected average length and number of CMTs, we continue to describe the algorithm we use to adjust those estimations to account for the effects of interactions. These effects are observed to be roughly proportionate to the total length reached in the system during organization, $\widehat{\sum L} \sim \sum L(T_2)$ among different settings with varying input parameters of simulations. As a result, we use simulation results for a baseline scenario with a single set of pre-determined parameters to determine weights for smoothing approximations of $E[\bar{L}(t)]$ and $E[I(t)]$. These weights are used for predictions of any scenario with a new set of parameters running only a single simulation of the new scenario. We first summarize steps used to determine weights for estimation based on a set of baseline simulations in Algorithm V.1, followed by further description of our predictive methodology.

Algorithm V.1. *(Determination of weights)*

0: Run R independent simulations of the baseline setting to obtain R realizations of both system metrics: $\bar{L}_r(t)$, $I_r(t)$, $r = 1, ..., R$, $t = 1, ..., T$. Calculate their minimum, maximum, and average values among independent runs, $\min_r \bar{L}_r(t)$, $\min_r I_r(t)$; $\max_r \bar{L}_r(t)$, $\max_r I_r(t)$; $\bar{\bar{L}}(t)$, $\bar{I}(t)$ *respectively for $t = 1, ..., T$. Note that the total length in the system reaches $\widehat{\sum L}$ at time T.*

1: Set the initial weight for $E[\bar{L}(t)]$, $\delta_1 = 1$ and the one for $E[I(t)]$, $\gamma_1 = 1$, and error check and control parameters for both metrics, $\rho_L^c, \rho_I^c, \rho_L^g, \rho_I^g$.

2: Initialize estimations $\widetilde{E}[\bar{L}(1)] = \widehat{E}[\bar{L}(1)]$, $\widetilde{E}[I(1)] = \widehat{E}[I(1)]$, and $\widetilde{\sum} L(1) = \widetilde{E}[\bar{L}(1)]\widetilde{E}[I(1)]$; and the vector used to store the total length values corresponding to the base weights calculated in this algorithm, $L_B(1) = 1$.

3: FOR $t = 1$ TO T

4: $\widetilde{E}[\bar{L}(t+1)] = \widetilde{E}[\bar{L}(t)] + \delta_t(\widehat{E}[\bar{L}(t+1)] - \widehat{E}[\bar{L}(t)])$

5: $\rho_L = \frac{\widetilde{E}[\bar{L}(t+1)]-\bar{\bar{L}}(t+1)}{\bar{\bar{L}}(t+1)}$ *//Calculate deviation from the average.*

6: *IF* $\rho_L < \rho_L^c$ *AND* $\min_r \bar{L}(t+1) < \widetilde{E}[\bar{L}(t+1)] < \max_r \bar{L}(t+1)$ *//Check if deviation is lower than the critical value and if the estimation is in the range between the minimum and maximum of realizations.*

7: $\delta_{t+1} = \delta_t$

8: *ELSE*

9: *WHILE* $(\rho_L > \rho_L^c$ *OR* $\widetilde{E}[\bar{L}(t+1)] > \max_r \bar{L}(t+1))$ *AND* $\delta_{t+1} > 0.05$

10: $\delta_{t+1} = \delta_{t+1} - 0.05$ *//Update weight.*

11: $\widetilde{E}[\bar{L}(t+1)] = \widetilde{E}[\bar{L}(t)]+\delta_{t+1}(\widehat{E}[\bar{L}(t+1)]-\widehat{E}[\bar{L}(t)])$ *//Update estimation.*

12: $\rho_L = \frac{\widetilde{E}[\bar{L}(t+1)]-\bar{\bar{L}}(t+1)}{\bar{\bar{L}}(t+1)}$ *//Update deviation from average.*

13: *END WHILE*

14: *END IF*

15: *Repeat similar cycle (steps 4-14) for estimating* $\widetilde{E}[I(t+1)]$ *and* γ_{t+1}.

16: $\widetilde{\sum} L(t+1) = \widetilde{E}[\bar{L}(t+1)]\widetilde{E}[I(t+1)]$ *//Calculate the estimated total length.*

17: $L_B(t+1) = \widetilde{\sum} L(t+1)$ *//Store the total length values corresponding to the weights.*

18: END FOR

Algorithm V.1 determines the weights to fit the estimations over the range of realizations of the baseline scenario, maintaining a certain deviation from the mean realization. Having explained computation of weights for the approximation methods and the corresponding total length values, we now discuss the proposed approach to estimate the expected system metrics for any given new scenario (in the parameter range for the organized case). For any problem with a new parameter set, only a single simulation is run to roughly determine the $\widehat{\sum L}$ value at which the system temporarily stabilizes, and its ratio to the corresponding value for the baseline scenario, $\widehat{\sum L}_B$.

According to this ratio, β, the weights are adjusted and estimations are calculated using the steps listed in the next algorithm.

Algorithm V.2. *(Prediction algorithm)*

0: Calculate $\beta = \frac{\widehat{\sum L}}{\widehat{\sum L_B}}$ *//Ratio of total length capacity to that of the baseline.*

1: Initialize estimations $\widetilde{E}[\bar{L}(1)] = \widehat{E}[\bar{L}(1)]$, $\widetilde{E}[I(1)] = \widehat{E}[I(1)]$, *and* $\widetilde{\sum} L(1) = \widetilde{E}[\bar{L}(1)]\widetilde{E}[I(1)]$*; weights for estimations* $w_L = w_I = 1$ *and positions for these weights* $p_L, p_I = 1$ *in the pre-determined weight vectors (see Algorithm V.1).*

2: FOR $t = 1$ *TO* T'*//A maximum time point for estimations.*

3: *IF* $\widetilde{\sum} L(t) < \widehat{\sum L}$ *//Total length cap not exceeded.*

4: $\widetilde{E}[\bar{L}(t+1)] = \widetilde{E}[\bar{L}(t)] + w_L(\widehat{E}[\bar{L}(t+1)] - \widehat{E}[\bar{L}(t)])$

5: $\widetilde{E}[I(t+1)] = \widetilde{E}[I(t)] + w_I(\widehat{E}[I(t+1)] - \widehat{E}[I(t)])$

6: *ELSE*

7: $\widetilde{E}[\bar{L}(t+1)] = \widetilde{E}[\bar{L}(t)]$; $\widetilde{E}[I(t+1)] = \widetilde{E}[I(t)]$.

8: *END IF*

9: $\widetilde{\sum} L(t+1) = \widetilde{E}[I(t+1)]\widetilde{E}[\bar{L}(t+1)]$

10: *FOR* $u = p_L : T_{max}$

11: *IF* $\widetilde{\sum} L(t+1) > \beta L_B(u)$ *//Updates weights if required comparing total length values to the pre-calculated base values (Algorithm V.1).*

12: $w_L = \delta(u), p_L = u$ *//Update weights and position in the base vector.*

13: $\widetilde{E}[\bar{L}(t+1)] = \widetilde{E}[\bar{L}(t)] + w_L(\widehat{E}[\bar{L}(t+1)] - \widehat{E}[\bar{L}(t)])$ *//Update estimation.*

14: *END IF*

15: *END FOR*

16: $\widetilde{E}[\bar{L}(t+1)] = \widetilde{E}[\bar{L}(t)] + w_L(\widehat{E}[\bar{L}(t+1)] - \widehat{E}[\bar{L}(t)])$

17: *Repeat Steps 10-15 similarly for* w_I, p_I *and* $\widetilde{E}[I(t+1)]$.

18: $\widetilde{E}[I(t+1)] = \widetilde{E}[I(t)] + w_I(\widehat{E}[I(t+1)] - \widehat{E}[I(t)])$

19: END FOR

In summary, Algorithm V.2 generates smoothed estimations with respect to the values obtained by Equations (31) and (34) employing weights calculated in Algorithm V.1. The total length parameters corresponding to the weights are adjusted according to the ratio of the total length capacity (around which the system stabilizes during organization) to that of the baseline. Note that our methodology requires just running one simulation for any new scenario with a given parameter set, which reduces computational time tremendously compared to running a large number of simulations. Having explained our methodology in detail, next we present some numerical examples.

V.4. Numerical Results

Having described our proposed methodology for estimation of expected system metrics, we first apply Algorithm V.1 on the baseline scenario (parameter set I), and determine weights to be used in Algorithm V.2 for other scenarios (Parameters sets II-IV). In order to test our methodology further, we consider three more problems where we generate input parameters with varying characteristics staying in the region of interest. The set of input parameters for all numerical examples are provided in Appendix A. Here, we list the parameters used for approximations and algorithms. For the approximations in Equations (31) and (34), we use time points $t = 0, 0.25, 0.5, 1, 2, ...$ Note that the intervals get larger for higher t values, as explained in Section V.3. For Algorithm V.1, we set $\rho_L^c = 0.02$, $\rho_L^g = 0.01$, $\rho_I^c = 0.04$, $\rho_I^g = 0.03$, based on our trials with various values. According to this, the plots of fitted values for the baseline scenario along with results of 10 independent simulation runs are plotted in Figure 34. Note that this case is used to estimate weights δ_t, γ_t and

corresponding total length ($L_B(t)$) values to be fed into Algorithm V.2 to calculate estimations for the rest of the scenarios.

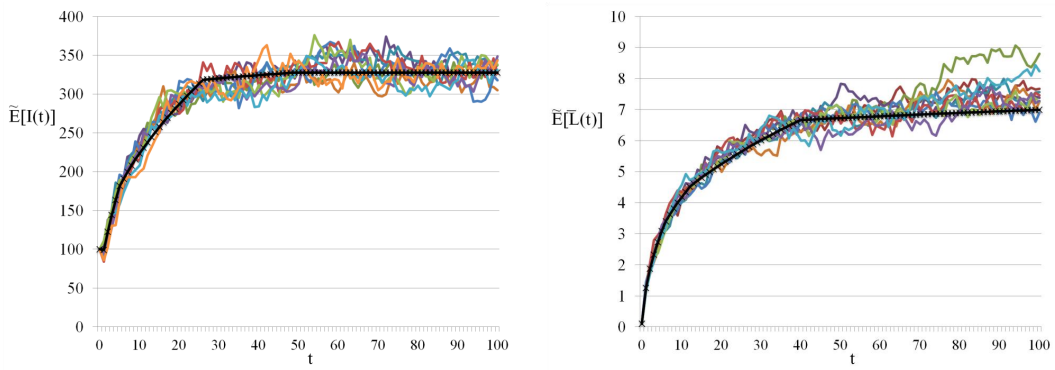

Fig. 34. 10 Independent Realizations of the Baseline Scenario with Fitted Values

Having calculated the weights (for estimation) using simulation results of the baseline scenario, we follow with implementation of prediction algorithm on the other parameter sets. Our first four examples are also based on data from biological experiments that were also used in previous chapters and listed in Appendix A with the rest of the parameters sets. Here, we present the corresponding β value for each set, which is an approximate ratio of the total length the system reaches during the time metrics stabilize to that of the baseline scenario. The β value is determined running a single simulation with the new parameter set, and is used to adjust the total length values corresponding to the pre-determined weights properly. It also gives an idea about how crowded the system is expected to get with respect to the baseline case.

Example 1: For this case (parameter set II), $\beta \approx 2.2$, which implies that the total system length is roughly 2.2 times that of the baseline case around the time organization settles. Implementing Algorithm V.2, the estimated system metrics are presented in Figure 35 together with realizations from simulations.

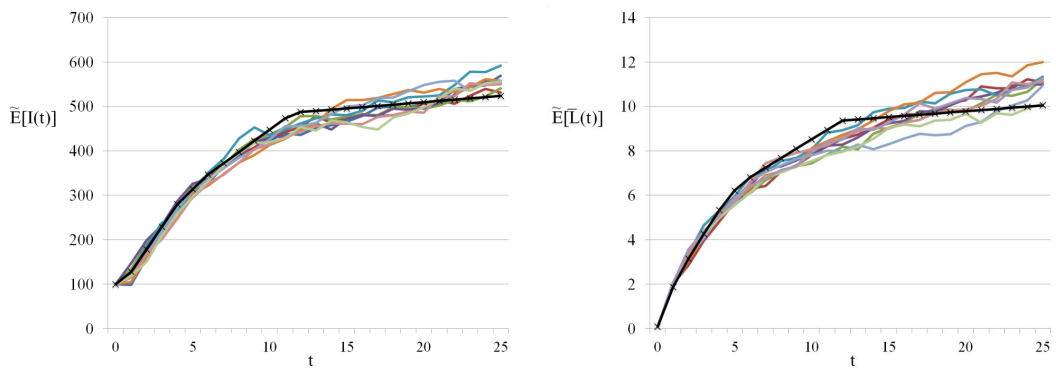

Fig. 35. Estimations for Example 1 with 10 Independent Realizations

Example 2: Next we consider a case (parameter set III) $\beta \approx 6.1$. Resulting estimations are presented in Figure 36.

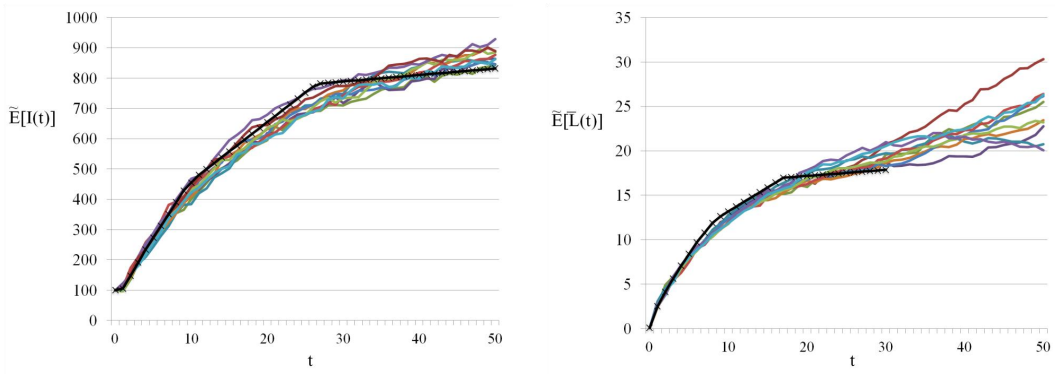

Fig. 36. Estimations for Example 2 with 10 Independent Realizations

The estimations of our proposed method seem to stay around the range of simulation results. It is worth noting that both examples correspond to parameter sets which cause highly dynamic behavior. As a result, organization occurs quite rapidly, and the pseudo-stabilization of system metrics last for a very short time. Further, as seen in Figures 35 and 36, metrics continue to slowly increase rather than stabilizing.

However, the proposed methodology still captures the average trend over time.

Example 3: In this example, we consider parameter set IV with an approximate β value of 2.1. The results are provided in Figure 37. Note that this is an organized scenario despite the fact that the parameter set does not satisfy the condition for organization derived in Chapter IV. Results suggest that our estimation method also works for such a case.

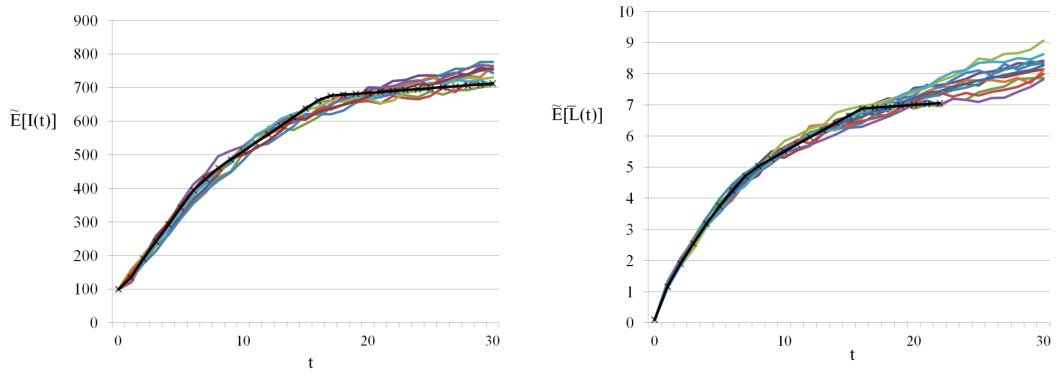

Fig. 37. Estimations for Example 3 with 10 Independent Realizations

We continue with two other numerical examples, where we derive the parameters to test some scenarios that complements our study. Two of the parameter sets that we generate correspond to relatively less dynamic settings with $\beta < 1$. Finally, we test a problem with different interaction parameters and appearance rate.

Example 4: The input parameters used in this example are given in the Appendix A (set VII) and are generated by reducing the dynamicity parameters and appearance rate of the baseline scenario (I) by half. This scenario corresponds to a β value of 0.95. The results are provided in Figure 38.

Note that the total length reached in this case (as well as the average length and total number values) is quite close to that of the baseline scenario although both the

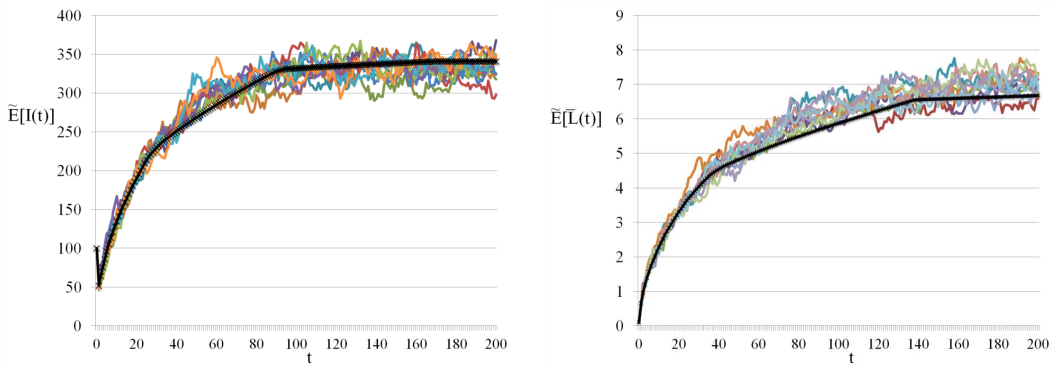

Fig. 38. Estimations for Example 4 with 10 Independent Realizations

average length change for a single CMT and the appearance rate of new CMTs are reduced by half. This is quite intuitive as the system stabilizes around a time where the arrival process and length dynamics balance each other. It is also worth noting that having a less dynamic system delays organization as observed in results. For the next example, we only reduce the appearance rate keeping other parameters constant to test a case where the β value is significantly reduced.

Example 5: For this case, we use the parameter set of the baseline scenario (I) with an appearance rate of $\lambda_a = 50$. The resulting β value is 0.6, which corresponds to a much less crowded system with respect to the baseline. Results are presented in Figure 39.

Finally, we present a case with different interaction parameters.

Example 6: In this example, we generate a setting with different interaction parameters and appearance rate with respect to the baseline scenario ($p_b = 0.5$, $p_c = 0.6$, $\theta^c = 60^0$). The resulting β value is around 0.95. Estimations are provided in Figure 40 together with sample simulation plots.

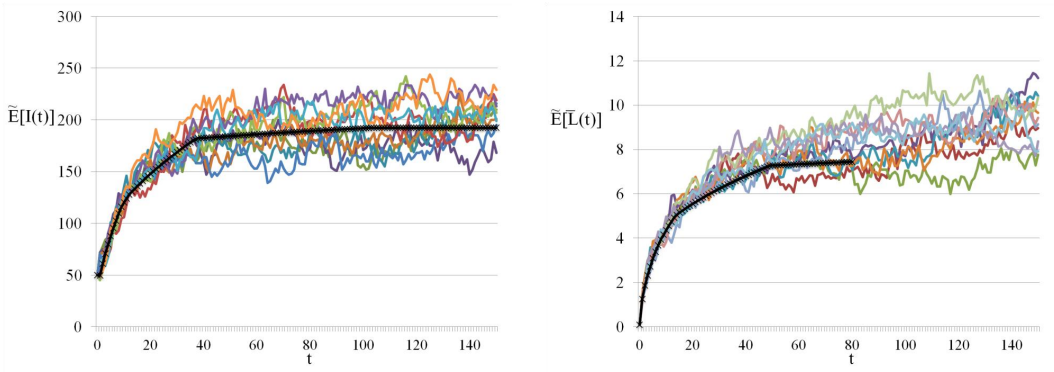

Fig. 39. Estimations for Example 5 with 10 Independent Realizations

V.5. Conclusions

In this chapter, we developed a methodology to estimate average length and number of CMTs in time for a given set of parameters. We first developed a fluid model for dynamics of a single CMT in the absence of interactions, and a method to calculate corresponding lifetime distribution using Laplace inversion techniques. We developed approximation algorithms for estimating expected system metrics based on lifetime distributions and data from single CMT simulations. For this, it is required to run an initial set of original simulation algorithm for a baseline scenario so that certain parameters used in the prediction algorithm can be determined. The sequential steps to predict system metrics for a given set of input parameters implementing the methodologies derived in this chapter and Chapter IV are outlined in Figure 41. For a given set, we first check if the condition for organization holds and accordingly continue to estimate expected average length and number values using related algorithms. This includes first calculating the lifetime distribution and expected average length values for a single CMT, and next expected values of average CMT length and number in the system in the absence of interactions. Finally, using the prediction algorithm

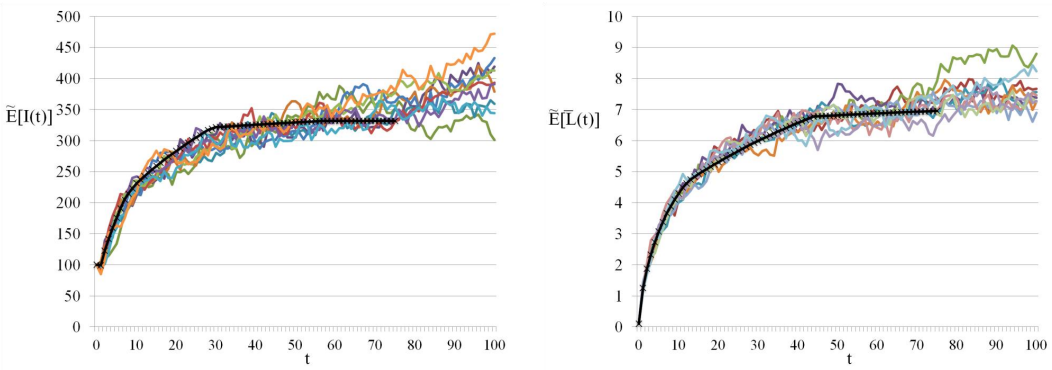

Fig. 40. Estimations for Example 6 with 10 Independent Realizations

and pre-determined weights, we smooth the estimations by approximating the impact of interactions. This requires running a single simulation of the system to adjust parameters related to the algorithms accordingly.

Numerical results suggests that our predictive methodology works well for cases with both different dynamicity and different interaction parameters, consequently varying characteristics. Although developed methodology requires applying a set of techniques in conjunction, it reduces computational complexity significantly compared to running a large number of simulations.

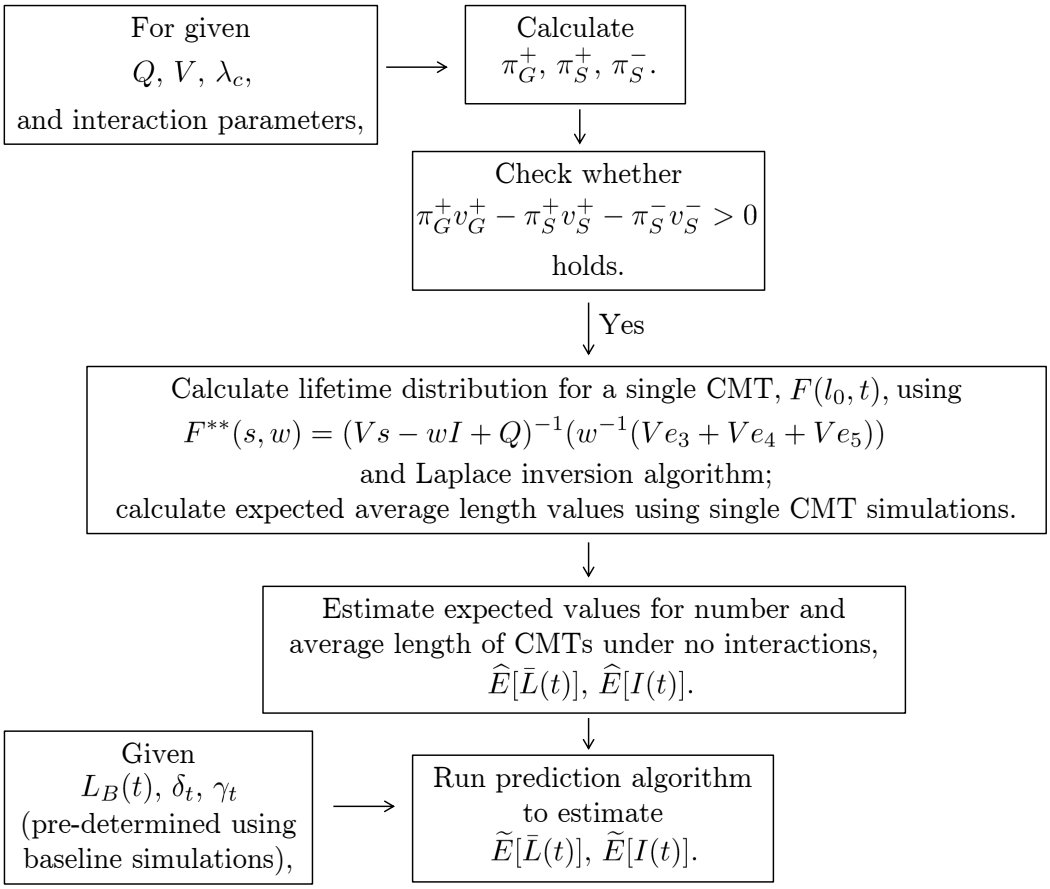

Fig. 41. Flowchart for Estimation of System Metrics for a Given Set of Input Parameters

CHAPTER VI

CONCLUSIONS AND FUTURE RESEARCH

In this dissertation, we studied a biological system inspired by cortical microtubules (CMTs) that serve as the skeleton of plant cells facilitating critical cellular processes. This system exhibits complex properties which are challenging to characterize, due to existence of both spatial and temporal dimensions as well as interactions among its components. Therefore, we used a wide range of methodologies in conjunction to model the system and conduct a thorough analysis. We began by simulating the system to model dynamics and interactions in detail based on data from biological experiments. We employed some quantitative metrics for comparing simulation results as well as using them in proposed analytical approaches. We used simulations to distinguish between different system characteristics, which we used to develop relevant analytical models. In particular, we developed a mean-field model and derived sufficient conditions for organization to be achieved employing Lyapunov stability concepts on a system of integro-differential equations. Finally, we developed a predictive methodology for estimating expected system metrics (expected number and average length of CMTs) in time based on a fluid model for single CMT dynamics. This approach uses a combination of tools including simulations, Laplace inversion techniques and approximation algorithms tailored to estimate effects of interactions on the expected average length and total number of CMTs.

This research provides an analysis of a complex biological system that would be infeasible relying on biological experiments. On the methodological side, it contributes to development of quantitative techniques for modeling complex stochastic systems with spatial and temporal properties. This research also has potential broader reaching impacts related to the fields of bio-energy, healthcare, and nanotechnology,

as explained in Chapter I. In this chapter, we summarize the conclusions of this study, followed by a discussion of future research directions.

VI.1. Conclusions

The simulation algorithm developed for the CMT system successfully replicated the organization seen in living cells using data from related literature. Our tests with different input parameters in Chapter III showed that interactions are necessary to achieve organization. In particular, bundling was found to contribute to organization directly by reorienting CMTs, whereas catastrophes facilitate elimination of misaligned CMTs and regulation of the density of CMTs in the system. In fact the catastrophe frequency per CMT changes in time parallel to the state of organization. Initially CMTs do not interact frequently; as they get long enough to interact, the frequency of catastrophes increases and peaks, followed by a continuous decrease as the system gets better organized.

We also investigated effects of other parameters on system organization and characteristics. Selecting a greater or lower critical interaction angle did not distort organization completely although both resulted in weaker organization, supporting the compatibility of naturally selected parameters. System organization was found to be robust to bundling and catastrophe probabilities as long as CMT dynamics guaranteed a positive net growth on average. We were also able to replicate system behavior seen in certain mutants and under varying conditions by altering the input parameters in accordance with the data from relevant literature.

We developed a quantification method based on entropy of angle distributions of CMTs in order to compare simulation results more reliably. In addition, we have also used this metric to measure the entropy values corresponding to live cell images, which

we observed to fall into similar ranges with simulation results. Hence, in addition to comparing the structure seen in living cells and our simulations qualitatively, we were also able to conduct a quantitative comparison by using entropy data and some other metrics (such as the average CMT length reported for living cells).

In addition to system organization, we also observed different characteristics for other system metrics such as average length and total number of CMTs and their evolution in time in simulations. Overall, in organized systems those metrics were observed to increase quickly at first until CMTs became long and crowded enough to interact, after which they stabilized around a constant value temporarily until organization is settled, and finally continued to increase indefinitely. In a way, the CMT system gets organized as a result of the balance between dynamics and interactions. Systems that fail to organize are roughly the ones that do not interact enough either due to lack of dynamics or interactions.

Having characterized different cases of system behavior and properties according to simulations, we developed two separate analytical methodologies in Chapters IV and V, to derive conditions for the organized (preferred) case, and estimate expected evolution of metrics related to CMT length and number in organized systems, in respective order. In Chapter IV, we modeled CMT dynamics and interactions based on a mean-field approach which led to a system of integro-differential equations. We conducted a stability analysis using entropy as a Lyapunov function and derived sufficient conditions for organization in terms of input parameters. This analysis also provided insights for convergence to an organized solution with a continuous decrease of entropy as seen in simulations, in addition to showing that is is possible to control system organization by regulating dynamicity parameters.

Finally, Chapter V contributes to prediction of performance measures such as expected total CMT number and average length in time for organized systems. We

developed an efficient methodology based on lifetime distribution and average expected length suggested by a fluid model of single CMT dynamics and single CMT simulations. The effect of interactions were estimated relying on a base set of simulations that are used to set certain weights for the predictive algorithm and running a single simulation for each problem with a new set of parameters.

It is worth noting that our models result in some intriguing insights in addition to agreeing well with experimental results and with each other. One property that we did not consider is that the building blocks for CMTs are kept at a roughly constant amount in the cell during organization, resulting in an upper-bound on the total system length, which seems to coincide with the total length capacity concept in our models. It is not currently feasible to determine the amount of this raw material in the plant cells relying on experimental methodologies. However as new measuring technologies emerge, if these parameters become available for modeling, our predictive approach can be improved to eliminate its reliance on a single simulation run for each scenario with a given parameter set. In general, the metrics that we extracted using simulations to characterize the system, provide biologists with measures that need to be tracked in living systems as well as new hypotheses to be tested.

VI.2. Future Research Directions

The methodologies and analysis presented in this dissertation can be extended to consider the following:

- *Other aspects of organization:* There are certain aspects seen in an organized system of CMTs other than being aligned in similar orientations to each other, such as the polarity which is defined as the dominant growth direction of CMTs in a system. Polarity is related to a different type of CMT appearance process,

where new CMTs are introduced into the system randomly on the already existing ones. Another property of interest is the overall orientation of the CMT array, which is observed to be specifically determined in most plant cells according to environmental and developmental cues. In fact, we have modeled both mechanisms using simulations (see Appendix B), where we were able to obtain some useful results and insights. However, incorporation of these into the analytical models requires consideration of system coordinates, which further complicates the tractability of formulations.

- *New quantification metrics:* The metric for organization can be improved to include other attributes of CMTs such as the density and bundling structure of arrays, in addition to their alignment. Such an extension would generalize it enough to distinguish cases such as a strongly-organized system with a very short and small number of CMTs, which is not a functionally preferred CMT structure. Techniques from data envelopment analysis are potential tools for combining multiple attributes of the CMT system to obtain a unified measure.

- *Improvement of methods based on experimental data:* Acquisition of more data on real CMT dynamics may result in improvement of developed methodologies, particularly reducing the reliance of predictive algorithms on simulations as discussed in Section VI.1. In fact, those types of models bring insights and new hypotheses to be tested on living systems and are bound to be updated iteratively as new experimental data are revealed, and vice versa.

- *Microtubule systems in animal cells:* Finally, this research can be applied on certain microtubule systems in specialized animal cells (such as neurons and muscle cells) that lack a central control mechanism similar to CMT systems.

REFERENCES

Abate, J. and Whitt, W. (1992) The Fourier-Series Method for Inverting Transforms of Probability Distributions. *Queueing Systems*, **10**(1), 5–88.

Abate, J. and Whitt, W. (2006) A Unified Framework for Numerically Inverting Laplace Transforms. *INFORMS Journal on Computing*, **18**(4), 408–421.

Allard, J.F. (2010) Mathematics and Biophysics of Cortical Microtubules in Plants, Ph.D. thesis, University of British Columbia, Vancouver, Canada.

Allard, J.F., Wasteneys, G.O. and Cytrynbaum, E.N. (2010a) A Mechanochemical Model Explains Interactions Between Cortical Microtubules in Plants. *Biophysical Journal*, **99**(4), 1082–1090.

Allard, J.F., Wasteneys, G.O. and Cytrynbaum, E.N. (2010b) Mechanisms of Self-organization of Cortical Microtubules in Plants Revealed by Computational Simulations. *Molecular Biology of the Cell*, **21**(2), 278–286.

Ambrose, J.C., Allard, J.F., Cytrynbaum, E.N. and Wasteneys, G.O. (2011) A CLASP-Modulated Cell Edge Barrier Mechanism Drives Cell-Wide Cortical Microtubule Organization in Arabidopsis. *Nature Communications*, **2**, 430.

Ambrose, J.C. and Wasteneys, G.O. (2008) CLASP Modulates Microtubule-Cortex Interaction During Self-Organization of Acentrosomal Microtubules. *Molecular Biology of the Cell*, **19**(11), 4730–4737.

Avdis, E. and Whitt, W. (2007) Power Algorithms for Inverting Laplace Transforms. *INFORMS Journal on Computing*, **19**(3), 341–355.

Bar-Yam, Y. (1997) *Dynamics of Complex Systems*, Perseus Press, Cambridge, MA.

Baulin, V.A., Marques, C.M. and Thalmann, F. (2007) Collision Induced Spatial Organization of Microtubules. *Biophysical Chemistry*, **128**(2-3), 231–244.

Burk, D.H., Liu, B., Zhong, R., Morrison, W.H. and Ye, Z.H. (2001) A Katanin-Like Protein Regulates Normal Cell Wall Biosynthesis and Cell Elongation. *Plant Cell*, **13**(4), 807–827.

Burk, D.H. and Ye, Z.H. (2002) Alteration of Oriented Deposition of Cellulose Microfibrils by Mutation of a Katanin-Like Microtubule-Severing Protein. *Plant Cell*, **14**(9), 2145–2160.

Canny, J. (1986) A Computational Approach to Edge Detection. *IEEE Transactions on Pattern Analysis and Machine Intelligence*, **8**(6), 679–698.

Cantrell, R.S. and Cosner, C. (2003) *Spatial Ecology via Reaction-Diffusion Equations*, John Wiley & Sons, West Sussex, England.

Chaikin, P.M. and Lubensky, T.C. (1995) *Principles of Condensed Matter Physics*, Cambridge University Press, New York.

Chan, J., Calder, G., Fox, S. and Lloyd, C. (2007) Cortical Microtubule Arrays Undergo Rotary Movements in Arabidopsis Hypocotyl Epidermal Cells. *Nature Cell Biology*, **9**(2), 171–175.

Chan, J., Sambade, A., Calder, G. and Lloyd, C. (2009) Arabidopsis Cortical Microtubules are Initiated along, as Well as Branching from, Existing Microtubules. *Plant Cell*, **21**(8), 2298–2306.

Chaplain, M.A.J. and Anderson, A.R.A. (1999) Modelling the Growth and Form of Capillary Networks, in *On Growth and Form: Spatio-temporal Pattern Formation*

in Biology, edited by Chaplain, M.A.J., Singh, G.D. and Mclachlan, J.C., Chapter 13, John Wiley & Sons, West Sussex, England, pp. 225–249.

Chaplain, M.A.J., Singh, G.D. and Mclachlan, J.C. (eds.) (1999) *On Growth and Form: Spatio-temporal Pattern Formation in Biology*, John Wiley & Sons, West Sussex, England.

Choudhury, G.L., Lucantoni, D. and Whitt, W. (1994) Multidimensional Transform Inversion with Applications to the Transient $M/G/1$ Queue. *The Annals of Applied Probability*, **4**(3), 719–740.

Crauel, H. and Gundlach, M. (eds.) (1999) *Stochastic Dynamics*, Springer-Verlag, New York.

Curry, G.L. and Feldman, R.M. (1987) *Mathematical Foundations of Population Dynamics*, Texas A&M University Press, College Station, TX.

Cytrynbaum, E.N., Rodionov, V. and Mogilner, A. (2003) Computational Model of Dynein-Dependent Self-Organization of Microtubule Asters. *Journal of Cell Science*, **117**(8), 1381–1397.

Cytrynbaum, E.N., Rodionov, V. and Mogilner, A. (2006) Nonlocal Mechanism of Self-Organization and Centering of Microtubule Asters. *Bulletin of Mathematical Biology*, **68**(5), 1053–1072.

Deinum, E.E., Tindemans, S.H. and Mulder, B.M. (2011) Taking Directions: The Role of Microtubule-Bound Nucleation in the Self-Organization of the Plant Cortical Array. *Physical Biology*, **8**(5), 056002.

Desai, R.C. and Kapral, R. (2009) *Dynamics of Self-Organized and Self-Assembled Structures*, Cambridge University Press, New York.

Dixit, R., Chang, E. and Cyr, R. (2006) Establishment of Polarity During Organization of the Acentrosomal Plant Cortical Microtubule Array. *Molecular Biology of the Cell*, **17**(3), 1298–1305.

Dixit, R. and Cyr, R. (2004) Encounters Between Dynamic Cortical Microtubules Promote Ordering of the Cortical Array through Angle-Dependent Modifications of Microtubule Behavior. *Plant Cell*, **16**(12), 3274–3284.

Dogterom, M. and Leibler, S. (1993) Physical Aspects of the Growth and Regulation of Microtubule Structures. *Physical Review Letters*, **70**(9), 1347–1350.

Eren, E.C., Dixit, R. and Gautam, N. (2010) A Three-Dimensional Computer Simulation Model Reveals the Mechanisms for Self-Organization of Plant Cortical Microtubules into Oblique Arrays. *Molecular Biology of the Cell*, **21**(15), 2674–2684.

Eren, E.C., Gautam, N. and Dixit, R. (2012) Computer Simulation and Mathematical Models of the Noncentrosomal Plant Cortical Microtubule Cytoskeleton. *Cytoskeleton*, 10.1002/cm.21009.

Ghosh, A., Miller, D., Zou, R., Sokhansanj, B. and Kriete, A. (2006) Spatiotemporal Systems Biology, in *Computational Systems Biology*, edited by Kriete, A. and Eils, R., Chapter 15, Elsevier Academic Press, Burlington, MA, pp. 327–362.

Goel, A. and Vogel, V. (2008) Harnessing Biological Motors to Engineer Systems for Nanoscale Transport and Assembly. *Nature Nanotechnology*, **3**(8), 465–475.

Gray, R.M. (1990) *Entropy and Information Theory*, Springer-Verlag, New York.

Hawkins, R.J., Tindemans, S.H. and Mulder, B.M. (2010) Model for the Orientational Ordering of the Plant Microtubule Cortical Array. *Physical Review E*, **82**(1 Pt 1), 011911.

Hoyle, R. (2006) *Pattern Formation: An Introduction to Methods*, Cambridge University Press, Cambridge, UK.

Ishida, T., Kaneko, Y., Iwano, M. and Hashimoto, T. (2007a) Helical Microtubule Arrays in a Collection of Twisting Tubulin Mutants of Arabidopsis Thaliana. *Proceedings of the National Academy of Sciences of the United States of America*, **104**(20), 8544–8549.

Ishida, T., Thitamadee, S. and Hashimoto, T. (2007b) Twisted Growth and Organization of Cortical Microtubules. *Journal of Plant Research*, **120**(1), 61–70.

Kaneko, K. and Tsuda, I. (2001) *Chaos and Beyond: A Constructive Approach with Applications in Life Sciences*, Springer-Verlag, New York.

Kawamura, E. and Wasteneys, G.O. (2008) MOR1, the Arabidopsis Thaliana Homologue of Xenopus MAP215, Promotes Rapid Growth and Shrinkage, and Suppresses the Pausing of Microtubules in Vivo. *Journal of Cell Science*, **121**(24), 4114–4123.

Kharoufeh, J.P. and Gautam, N. (2004) Deriving Link Travel-Time Distributions Via Stochastic Speed Processes. *Transportation Science*, **38**(1), 97–106.

Kriete, A. and Eils, R. (eds.) (2006) *Computational Systems Biology*, Elsevier Academic Press, Burlington, MA.

Lagomarsino, M.C., Tanase, C., Vos, J.W., Emons, A.M., Mulder, B.M. and Dogterom, M. (2007) Microtubule Organization in Three-Dimensional Confined Geometries: Evaluating the Role of Elasticity Through a Combined In Vitro and Modeling Approach. *Biophysical Journal*, **92**(3), 1046–1057.

Long, E.F., Vaidya, N.K. and Brandeau, M.L. (2008) Controlling Co-Epidemics:

Analysis of HIV and Tuberclosis Infection Dynamics. *Operations Research*, **56**(6), 1366–1381.

Lu, J.L., Valois, F., Dohler, M. and Barthel, D. (2008) Quantifying Organization by Means of Entropy. *IEEE Communications Letters*, **12**(3), 185–187.

MacDonald, J.R. (1964) Accelerated Convergence, Divergence, Iteration, Extrapolation, and Curve Fitting. *Journal of Applied Physics*, **35**(10), 3034–3041.

Maini, P.K. (1999) Some Mathematical Models for Biological Pattern Formation, in *On Growth and Form: Spatio-temporal Pattern Formation in Biology*, edited by Chaplain, M.A.J., Singh, G.D. and Mclachlan, J.C., Chapter 7, John Wiley & Sons, West Sussex, England, pp. 111–128.

Maly, I. (2002) Diffusion Approximation of the Stochastic Process of Microtubule Assembly. *Bulletin of Mathematical Biology*, **64**(2), 213–238.

Martin, M.T., Plastinoa, A. and Rossob, O.A. (2006) Generalized Statistical Complexity Measures: Geometrical and Analytical Properties. *Physica A*, **369**(2), 439–462.

Mikhailov, A.S. and Calenbuhr, V. (2002) *From Cells to Societies: Models of Complex Coherent Action*, Springer-Verlag, Berlin, Germany.

Moorthy, M.V. (1995) Numerical Inversion of Two-Dimensional Laplace Transforms–Fourier Series Representation. *Applied Numerical Mathematics*, **17**(2), 119–127.

Murata, T., Sonobe, S., Baskin, T.I., Hyodo, S., Hasezawa, S., Nagata, T., Horio, T. and Hasebe, M. (2005) Microtubule-Dependent Microtubule Nucleation Based on Recruitment of Gamma-Tubulin in Higher Plants. *Nature Cell Biology*, **7**(10), 961–968.

Murray, J.D. (1993) *Mathematical Biology*, Springer-Verlag, New York.

Nagorcka, B.N. and Adelson, D.A. (1999) Pattern Formation Mechanisms in Skin and Hair: Some Experimental Tests, in *On Growth and Form: Spatio-temporal Pattern Formation in Biology*, edited by Chaplain, M.A.J., Singh, G.D. and Mclachlan, J.C., Chapter 6, John Wiley & Sons, West Sussex, England, pp. 89–110.

Ott, E. (1993) *Chaos in Dynamical Systems*, Cambridge University Press, Cambridge, UK.

Palsson, B.Q. (2006) *Systems Biology: Properties of Reconstructed Networks*, Cambridge University Press, New York.

Schieve, W.C. and Allen, P.M. (1982) *Self-Organization and Dissipative Structures: Applications in the Physical and Social Sciences*, University of Texas Press, Austin, TX.

Shannon, C.E. (1948) A Mathematical Theory of Communication. *The Bell System Technical Journal*, **27**, 379–423.

Shapiro, L.G. and Stockman, G.C. (2001) *Computer Vision*, Prentice-Hall, Inc., Upper Saddle River, NJ.

Shaw, S.L., Kamyar, R. and Ehrhardt, D.W. (2003) Sustained Microtubule Treadmilling in Arabidopsis Cortical Arrays. *Science*, **300**(5626), 1715–1718.

Shaw, S.L. and Lucas, J. (2011) Intrabundle Microtubule Dynamics in the Arabidopsis Cortical Array. *Cytoskeleton*, **68**(1), 56–67.

Sherratt, J.A., Perumpanani, A.J. and Owen, M.R. (1999) Pattern Formation in Cancer, in *On Growth and Form: Spatio-temporal Pattern Formation in Biology*,

edited by Chaplain, M.A.J., Singh, G.D. and Mclachlan, J.C., Chapter 4, John Wiley & Sons, West Sussex, England, pp. 47–73.

Shi, X. and Ma, Y. (2010) Understanding Phase Behavior of Plant Cell Cortex Microtubule Organization. *Proceedings of the National Academy of Sciences*, **107**(26), 11709–11714.

Skjeltrop, A.T. and Belushkin, A.V. (2005) *Dynamics of Complex Interconnected Systems: Networks and Bioprocesses*, Springer, The Netherlands.

Sugimoto, K., Williamson, R.E. and Wasteneys, G.O. (2000) New Techniques Enable Comparative Analysis of Microtubule Orientation, Wall Texture, and Growth Rate in Intact Roots of Arabidopsis. *Plant Physiology*, **124**(4), 1493–1506.

Sun, J.Q. and Luo, A.C.J. (eds.) (2006) *Bifurcation and Chaos in Complex Systems*, Elsevier, The Netherlands.

Thitamadee, S., Tuchihara, K. and Hashimoto, T. (2002) Microtubule Basis for Left-handed Helical Growth in Arabidopsis. *Nature*, **417**(6885), 193–196.

Tindemans, S.H., Hawkins, R.J. and Mulder, B.M. (2010) Survival of the Aligned: Ordering of the Plant Cortical Microtubule Array. *Physical Review Letters*, **104**(5), 058103.

Wasteneys, G.O. and Ambrose, J.C. (2009) Spatial Organization of Plant Cortical Microtubules: Close Encounters of the 2D Kind. *Trends in Cell Biology*, **19**(2), 62–71.

Waterman, M.S. (1995) *Introduction to Computational Biology: Maps, Sequences and Genomes*, Chapman & Hall, London, UK.

Wolff, R.W. (1989) *Stochastic Modeling and the Theory of Queues*, Prentice Hall, New Jersey.

Wynn, P. (1966) On the Convergence and Stability of the Epsilon Algorithm. *SIAM Journal on Numerical Analysis*, **3**(1), 91–122.

Yarahmadian, S., Barker, B., Zumbrun, K. and Shaw, S.L. (2011) Existence and Stability of Steady States of a Reaction Convection Diffusion Equation Modeling Microtubule Formation. *Journal of Mathematical Biology*, **63**(3), 459–492.

APPENDIX A

INPUT PARAMETER SETS (DYNAMICS)

Parameter Set II:

$$Q = \begin{bmatrix} -7.234 & 6.72 & 0.236 & 0 & 0.278 & 0 \\ 2.427 & -2.941 & 0 & 0.236 & 0 & 0.278 \\ 5 & 0 & -13.27 & 6.72 & 1.55 & 0 \\ 0 & 5 & 2.427 & -8.977 & 0 & 1.55 \\ 25.125 & 0 & 12.75 & 0 & -44.595 & 6.72 \\ 0 & 25.125 & 0 & 12.75 & 2.427 & -40.302 \end{bmatrix}$$

$$V = diag(0.72, 3.5, -11.78, -9, -2.78, 0)$$

Parameter Set III:

$$Q = \begin{bmatrix} -9.617 & 6.72 & 2.338 & 0 & 0.559 & 0 \\ 2.427 & -5.324 & 0 & 2.338 & 0 & 0.559 \\ 12.438 & 0 & -21.908 & 6.72 & 2.75 & 0 \\ 0 & 12.438 & 2.427 & -17.614 & 0 & 2.75 \\ 8.75 & 0 & 4.375 & 0 & -19.845 & 6.72 \\ 0 & 8.75 & 0 & 4.375 & 2.427 & -15.552 \end{bmatrix}$$

$$V = diag(3.72, 6.5, -15.18, -12.4, -2.78, 0)$$

Parameter Set IV:

$$Q = \begin{bmatrix} -7.537 & 6.72 & 0.535 & 0 & 0.282 & 0 \\ 2.427 & -3.244 & 0 & 0.53521 & 0 & 0.282 \\ 6.211 & 0 & -16.036 & 6.72 & 3.105 & 0 \\ 0 & 6.211 & 2.427 & -11.742 & 0 & 3.105 \\ 15.6 & 0 & 5.6 & 0 & -27.92 & 6.72 \\ 0 & 15.6 & 0 & 5.6 & 2.427 & -23.627 \end{bmatrix}$$

$$V = diag(-0.28, 2.5, -8.98, -6.2, -2.78, 0)$$

Parameter Set V:

$$Q = \begin{bmatrix} -11.806 & 6.72 & 2.343 & 0 & 2.743 & 0 \\ 2.427 & -7.512 & 0 & 2.343 & 0 & 2.743 \\ 3.05 & 0 & -15.82 & 6.72 & 6.05 & 0 \\ 0 & 3.05 & 2.427 & -11.527 & 0 & 6.05 \\ 1.556 & 0 & 1.378 & 0 & -9.653 & 6.72 \\ 0 & 1.556 & 0 & 1.378 & 2.427 & -5.36 \end{bmatrix}$$

$$V = diag(-0.78, 2, -6.58, -3.8, -2.78, 0)$$

APPENDIX B

ADDITIONAL SIMULATION RESULTS AND DISCUSSION

In this appendix, we present the results from our simulation study that were not included in Chapter III. While introducing our conclusions, we also discuss some relations to the other literature that were reviewed in Chapter II.

Microtubule-Dependent Appearance (Nucleation) of New CMTs and Array Organization

In our simulations, we also tested the impact of microtubule-dependent nucleation, where a new CMT appears on an already existing one, which is called the mother CMT, rather than an arbitrary location overall the cell surface, as defined in Section II.3.1.5. The new CMT either grows along its mother CMT or at an acute angle to it, which is called the *branch angle*. The relative probabilities along with the distribution for branch angle are determined based on experimental data from Murata *et al.* (2005) and Chan *et al.* (2009). According to this, a new CMT grows along its mother CMT with a 0.38 probability; or it grows at an angle that is sampled from a distribution with a mean of 40^o. Branching to the left or right side of the mother CMT is equally likely and the new CMTs originate with their leading ends facing toward the leading end of the mother CMT. The location of appearance is uniformly distributed among the existing growing segments of CMTs. We have incorporated microtubule-dependent nucleation together with the regular appearance process at an equal average rate, keeping the total arrival rate of new CMTs into the system same as the baseline rate. Our results show that incorporation of microtubule-dependent nucleation in simulations does not have a significant effect on the degree and rate of

CMT organization, in line with the results of Allard *et al.* (2010b) as discussed in Section II.3 (see Figure 42). However it has a remarkable impact on array polarity, which will be discussed next.

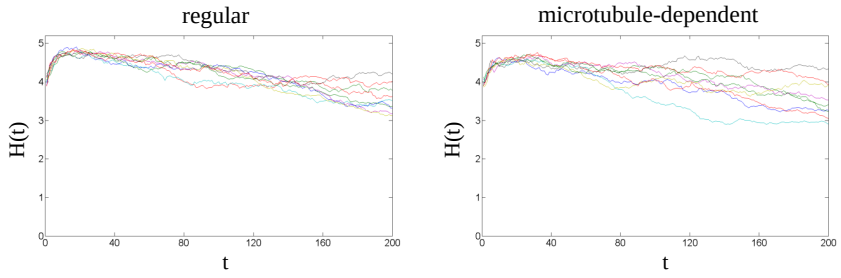

Fig. 42. Comparison of Entropy Plots for Simulations with and without Microtubule-Dependent Nucleation

Factors that Affect Array Polarity

In addition to ordering into parallel arrays and the overall orientation of CMTs, another characteristic of CMT organization is polarity, which is a measure of similarity of the growth direction of CMTs. Certain recent studies based on live-cell imaging of plant cells revealed that well-ordered CMT arrays can have one or more domains of net polarity, with the bulk of the CMTs facing one direction within these domains (Chan *et al.*, 2007; Dixit *et al.*, 2006); whereas other researchers have found little net polarity in CMT arrays (Shaw and Lucas, 2011). In our simulations, we observed that it is not possible to obtain such polarity with only regular appearance process (i.e., CMTs originating from randomly assigned nucleation sites (points) over the cell surface). However, incorporating microtubule-dependent CMT nucleation together with regular appearance process, the frequency of observing net polarity in ordered CMT arrays increased significantly. A sample plot of angular distributions for a

simulation with microtubule-dependent nucleation that shows net polarity compared to its counterpart with the baseline setting are presented in Figure 43.

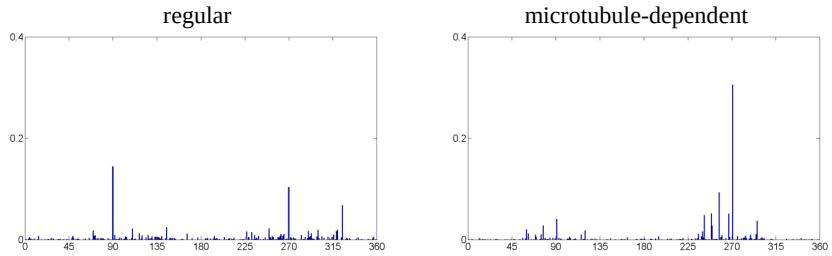

Fig. 43. Sample Angle Distribution Plots for Simulations with and without Microtubule-Dependent Nucleation

Factors that Result in CMT Array Skewing

In our 3D simulations with catastrophe inducing edges on the top and bottom of the cylindrical cell surface as described in Section III.3, CMTs are organized roughly parallel to these edges, so that they form shallow helical arrays along the planar surface of the cylinder (Figure 24) similar to the helical arrangements of CMTs observed in many plant cell types (Sugimoto *et al.*, 2000). The helical CMT arrays are observed irrespective of whether microtubule-dependent nucleation is included or not in our simulations.

Certain CMT arrays are observed to organize in an oblique manner, as described in some experimental studies with mutants that twist the growth dynamics of CMTs in plant cells (Ishida *et al.*, 2007a; Thitamadee *et al.*, 2002). It is not known whether the changes in CMT dynamics contribute to the formation of an oblique CMT array. To determine if defective CMT dynamics can change the overall pitch of the CMT array, we simulated the parameters from related mutants that, respectively, show

right- and left-handed skewed CMT arrays (Ishida *et al.*, 2007a). Our results show that the CMT dynamics of these mutants result in either short CMTs that fail to become organized or relatively poorly organized CMT arrays that do not exhibit skewing. Thus, in line with our results in Chapter III, the defective CMT dynamics cannot explain overall orientation of the CMT array, particularly how oblique CMT arrays are formed in this case.

To explore possible mechanisms that are responsible for oblique CMT arrays, we simulated the following scenarios, inspired by the conceptual framework for the role of CMT appearance, particularly branch-form nucleation, in CMT array orientation (Wasteneys and Ambrose, 2009):

- an increase or decrease in the mean branch angle on both sides of the mother CMT during microtubule-dependent CMT nucleation;
- introducing a bias for one side of the mother CMT (i.e., nucleation on either the left or the right of the mother CMT);
- an increase or decrease in the mean branch angle on only one side of the mother CMT;
- assigning only one of the end walls of the cylinder as a catastrophe-inducing edge.

Note that microtubule-dependent CMT nucleation is included in all of these scenarios. In these experiments, we defined an oblique array as one that shows at least a 20^o shift from the transverse orientation. This is a conservative definition based on the average skewing angle of 10^o reported in experimental studies of twisted growth mutants (Ishida *et al.*, 2007a). Our results show that all of the tested mechanisms increase the frequency of observing oblique CMT array formation compared with control experi-

Table 5. Skewing of CMT Arrays under Different Conditions

	Condition	Runs (Skewed)	Ave. Skew. Angle
	Baseline case	0%	-
(i)	60^o mean branch angle	40%	32^o
(ii)	20^o mean branch angle	30%	23^o
(iii)	Left-side branching	20%	30^o
(iv)	60^o mean branch angle on the left	20%	35^o
(v)	20^o mean branch angle on the left	40%	31^o
(vi)	Only one catastrophe-inducing edge	50%	21^o

ments without these modifications (Table 5; Figure 44). Table 5 lists the percentage of runs that showed skewed arrays for each mechanism along with the average skewing angle. Note that plots in Figure 44 are numbered in line with the conditions listed in Table 5. Our results regarding CMT skewing are in line with the conjectures that different mechanisms might be operational in the different mutants and experimental treatments that lead to twisting of CMT arrays (Ishida *et al.*, 2007b). Among the conditions that we tested, changing the edge properties and the mean branch angle on either one side or both sides of a mother CMT were found to be particularly effective in changing the pitch of the CMT array. These conditions however did not skew CMT arrays with a fixed handedness. We tested if the extent and timing of branch-form CMT nucleation can confer fixed handedness during skewing of CMT arrays based on a concept proposed by Wasteneys and Ambrose (2009). The scenario that worked best involved first allowing CMTs to organize into a transverse array in the absence of any microtubule-dependent nucleation followed by a switch to 100% branch-form CMT nucleation. Under these conditions, we obtained oblique arrays that consistently skewed in the same direction (Figure 45). We note that inclusion of CMT nucleation along the mother CMT (38% of the total microtubule-dependent nucleation) in this scenario disrupted the formation of oblique CMT arrays.

As mentioned in Section II.3, Deinum *et al.* (2011) simulated a related situation

in which CMT appearance process continuously transitions from exclusively regular to more frequent microtubule-dependent nucleation with increasing CMT density. This scenario did not result in consistent array skewing in their simulations. However, it is not easy to exactly compare this study with ours, as the nucleation scenarios, modeling of edges, and parameter ranges differ significantly between the two.

Other Analysis Regarding the CMT Lifetime, Length, Number and Orientation

In this section, we present some other analysis and results regarding the relations between certain attributes of CMTs in simulated systems, such as their lifetime, length, number and orientation. A graph of the lifetimes of individual CMTs from a sample simulation plotted against their appearance (birth) time and orientation (at the time of disappearance) is given in Figure 46. As seen in the figure, most of the CMTs have a relatively short lifetime, whereas a small number of them have an extremely long lifetime. The relatively longer lifetime values are clustered around the dominant angles that appear during simulations as expected. The overall character of the lifetime distribution (see Figure 47 for a sample histogram) is roughly similar to the one derived for single CMTs in Chapter V, where there is a high probability for small time values that decreases quickly as the values keep increasing. It is worth noting that this distribution is a multimodal one with more than one local maxima, although not noticeable from the figure.

We also analyzed the relations between length and number of CMTs based on simulation results. As seen in Figures 48 and 49, there is a roughly linear relation between the number of CMTs, $I(t)$, and the average CMT length, $\bar{L}(t)$, and accordingly a quadratic relation between the number of CMTs, $I(t)$, and the total CMT length in the system, $\sum L(t)$. In Figure 48, three lines for different trends in the data

(similar to the three-phase behavior seen in the course of organization as discussed in Section V.1) are fitted using linear regression.

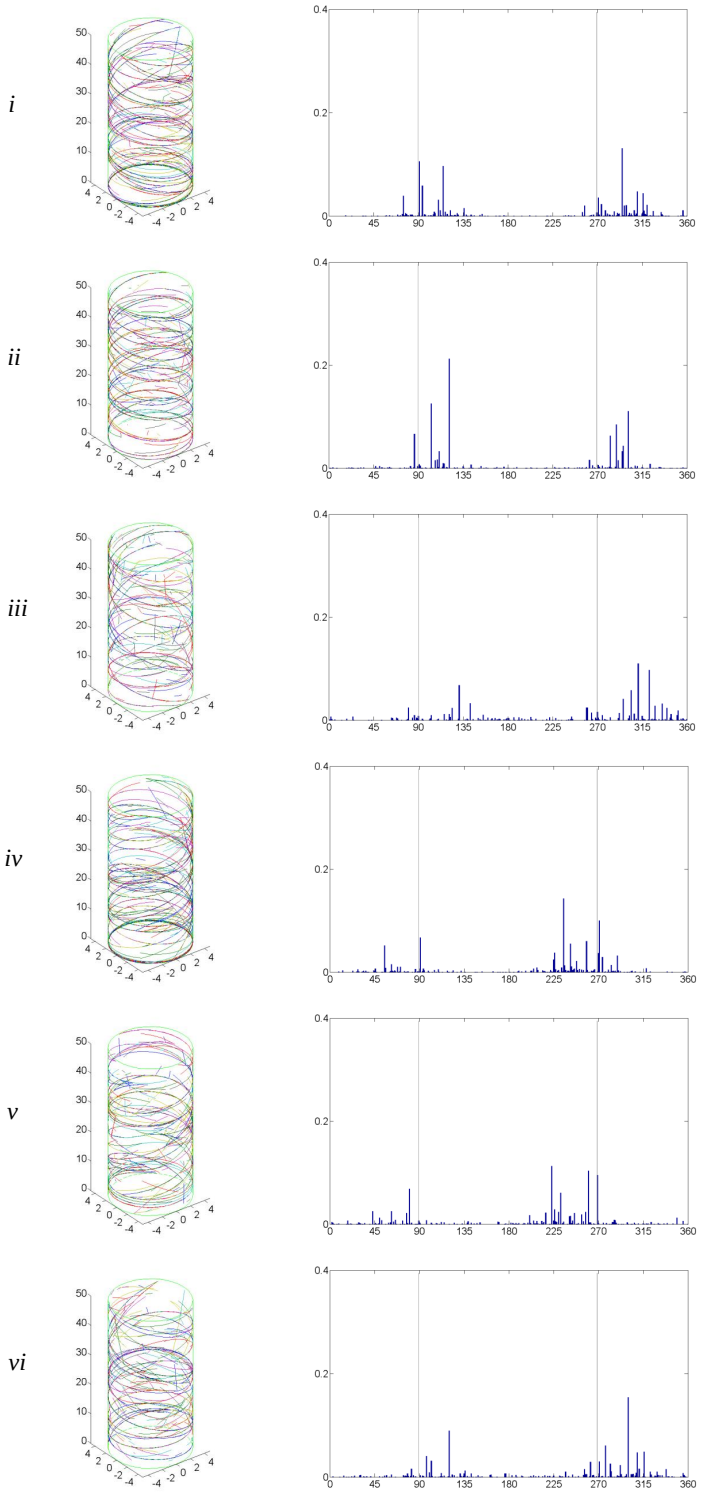

Fig. 44. Sample Angle Distribution Plots and 3D Snapshots of Simulations with Different Scenarios for CMT Array Twisting

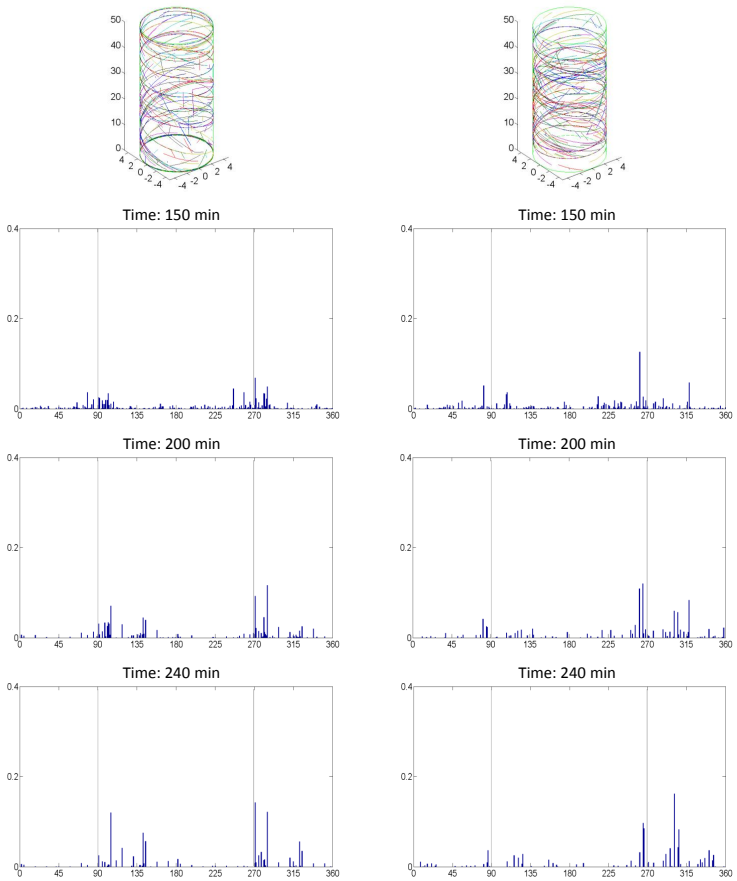

Fig. 45. Sample Angle Distribution Plots and 3D Snapshots of Simulations for Fixed-Handed CMT Array Twisting

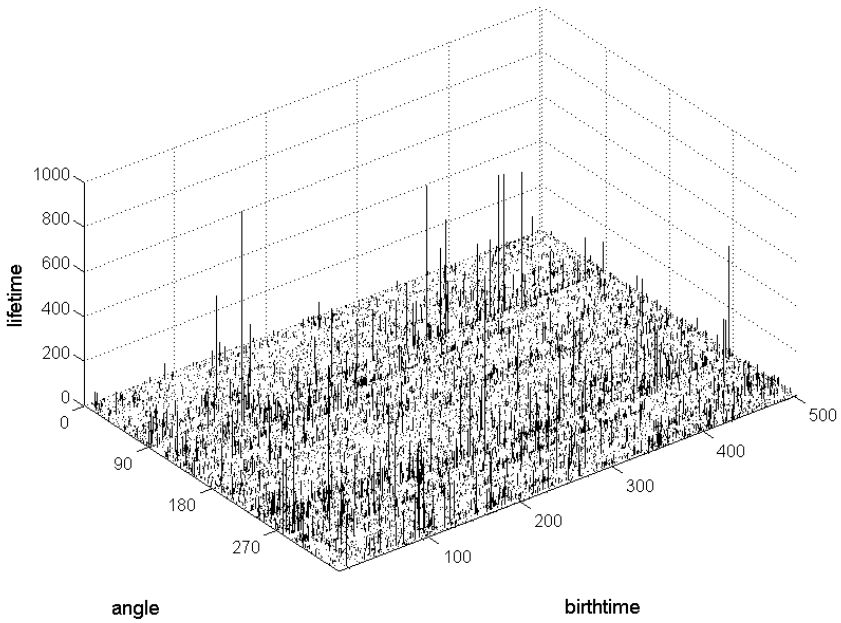

Fig. 46. Lifetimes of CMTs Plotted against Their Birthtime and Angle Values

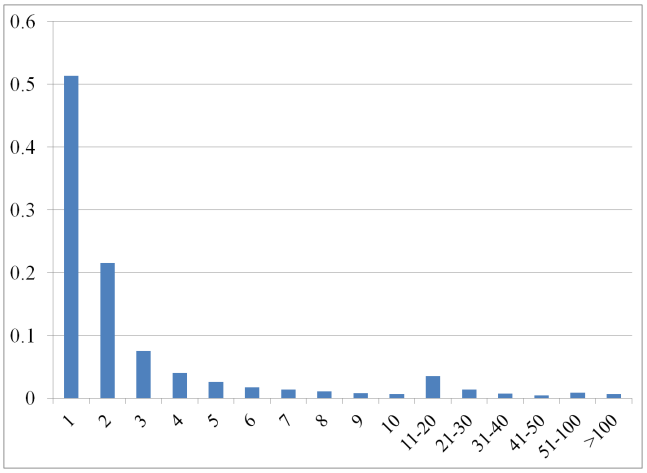

Fig. 47. Histogram of Lifetime Distribution for CMTs Based on a Sample Simulation

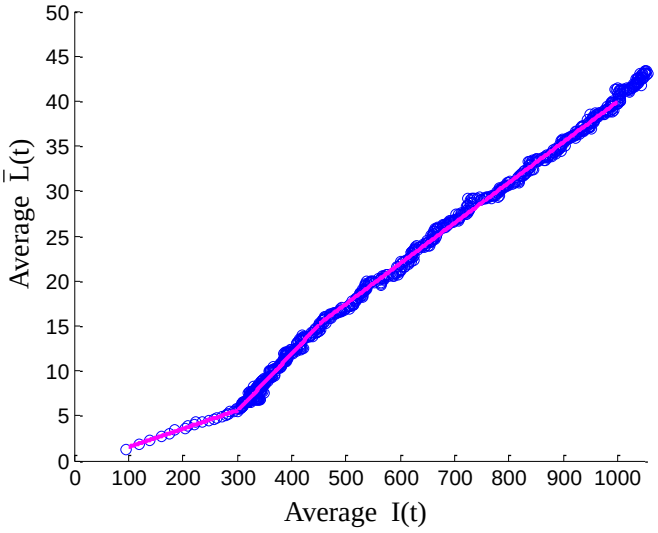

Fig. 48. Average Length vs. Total Number of CMTs Averaged over Multiple Independent Simulation Runs

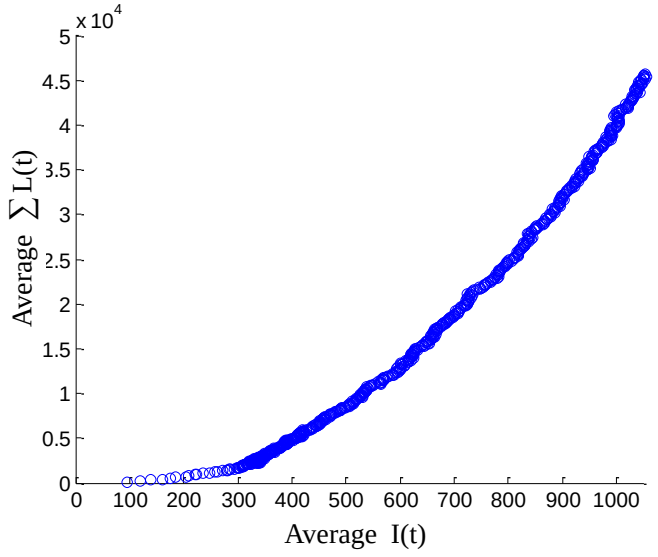

Fig. 49. Total Length vs. Total Number of CMTs Averaged over Multiple Independent Simulation Runs

VITA

Ezgi Can Eren received her B.S. degree in Industrial Engineering from Bogazici University, Istanbul, Turkey; and joined the Department of Industrial and Systems Engineering at Texas A&M University in the same year for her Ph.D. studies. Her research interests lie in development and application of stochastic and quantitative models for emerging domains such as bio-systems, spatial and temporal processes, complex systems and energy efficiency.

She may be reached at her department address: Department of Industrial and Systems Engineering, Texas A&M University, 3131 TAMU, College Station, TX 77843-3131. Her email address is ezgi@tamu.edu; or alternatively, ezgicaneren@gmail.com.

This document was typeset in LaTeX by the author.